学位申請論文

汪 発武

AN EXPERIMENTAL STUDY ON GRAIN CRUSHING AND EXCESS PORE PRESSURE GENERATION DURING SHEARING OF SANDY SOILS

– A KEY FACTOR FOR RAPID LANDSLIDE MOTION –

by

Fawu Wang

A thesis submitted to the Graduate School of Science
Kyoto University
in partial fulfillment of the requirements
for the degree of Doctor of Science
in the Division of Earth and Planetary Science

August, 1998

ABSTRACT

The disaster mitigation by refuge from rapid landslides is very difficult, and the prediction of rapid landslide motion is an extremely important subject for society. There are many factors affecting the moving speed of landslide. Among them, the most important factor is the decrease of soil strength induced by excess pore pressure generation under undrained condition after the beginning of landslide motion. According to "sliding-surface liquefaction" proposed by Sassa et al (1996), the grain crushing character of sandy soils has great effect on the excess pore pressure behavior. By means of the ring shear apparatuses, the fundamental and application tests on the key factors — grain crushing character and excess pore pressure generation behavior, were performed.

In the fundamental experiments, three-type samples were used. They are: Toyoura standard sand consisting of rounded quartz sands, silica sand consisting of angular and sub-angular quartz sands, and Osaka-group coarse sandy soil consisting of angular quartz sands, feldspar and mica that is liable to grain crushing. The consolidated-drained ring shear test method was used to investigate the grain crushing susceptibility of samples, while the consolidated-undrained ring shear test (constant-speed test and cyclic-loading test) were used to investigate the excess pore pressure generation properties of samples. It was observed that, under the undrained shear, excess pore pressure is generated fast and reaches high value at steady state on the sample that has high grain crushing susceptibility.

According to test results of sample height change in the drained tests and excess pore pressure ratio in the undrained tests, along with shear displacement, dilatancy character of sandy soils can be divided to three phases. They are "initial negative dilatancy", "initial positive dilatancy" and "negative dilatancy due to grain crushing" The first two phases are affected by initial structure, and the last one is affected by grain crushing susceptibility.

The Nikawa landslide in Nishinomiya City, which was induced by the January 17,

1995 Hyogoken-Nambu earthquake, and the July 10, 1997 Harihara debris slide–debris flow in Izumi City, Kagoshima Prefecture, which was induced by a heavy rainfall, because both of them have a similar character of rapid landslide motion, were chosen as the study cases in this thesis.

In the geotechnical simulation test on the Nikawa landslide loaded with the real seismic wave of the Hyogoken-Nambu earthquake, it was observed that, after the very short time of the main shock, shear displacement also continued, and "sliding-surface liquefaction" was achieved through the accumulation of residual excess pore pressure, which was caused by grain crushing. In the other experiment on the andesitic sample taken from the Harihara debris slide–debris flow, it was observed that the andesitic sample is even easier to take grain crushing than Osaka-group coarse sandy soil. During shearing, because of the "sliding-surface liquefaction" in the shear zone and the decrease of the permeability coefficient, a new structure of soil formed. With this structure, excess pore pressure is generated and accumulated easily, while difficult to dissipate.

Based on the study results, according to the grain crushing character of soils and the generation behavior of (residual) excess pore pressure, the mechanisms of the rapid landslide motion in the two landslides, i.e., the Nikawa landslide induced by earthquake and the Harihara debris slide–debris flow induced by rainfall, were explained respectively. Then, the mechanism of rapid landslides is supposed as follows: for a slope at a stress condition near critical state, with an external force, such as earthquake and rainfall, the soil at the potential sliding surface fails at first. This failure makes the soil mass move for a certain displacement. If the soil at the sliding surface is fully saturated, under the undrained (even at localized undrained) condition, initial loose structure collapse and/or grain crushing caused by shearing will result in the generation of excess pore pressure, and in turn, make a landslide travel rapidly.

Table of Contents

Chapter Page

ABSTRACT i
1. INTRODUCTION 1
1.1 Background for This Study 2
1.2 Aim and Major Works of This Study 3
1.3 Definitions and Restrictions 4
2. RING SHEAR APPARATUS 8
2.1 Stress Control and Gap Control System 9
2.2 Structure 9
3. PROPERTIES OF SAMPLES 12
4. GRAIN CRUSHING CHARACTER OF SANDY SOILS AND EXCESS PORE PRESSURE GENERATION DURING SHEARING 14
4.1 Test Program and Procedure 15
4.1.1 Consolidated-Drained Constant-Speed Ring Shear Tests 15
4.1.2 Consolidated-Undrained Constant-Speed Ring Shear Tests 16
4.1.3 Consolidated-Undrained Cyclic-Loading Ring Shear Tests 17
4.2 Test Results 18
4.2.1 Consolidated-Drained Constant-Speed Ring Shear Tests 19
4.2.2 Consolidated-Undrained Constant-Speed Ring Shear Tests 21
4.2.3 Consolidated-Undrained Cyclic-Loading Ring Shear Tests 23
4.3 Possibility of Excess Pore Pressure Prediction in Undrained Condition by Drained ring shear Tests 26
5. A GEOTECHNICAL SIMULATION STUDY ON THE NIKAWA LANDSLIDE INDUCED BY THE JANUARY 17, 1995 HYOGOKEN-NAMBU EARTHQUAKE IN JAPAN 29
5.1 The Nikawa Landslide 30
5.2 Input of Seismic Loading 31

5.3 Sample Preparation and Test Procedure 35
5.4 Test Results....36
5.5 Grain Crushing Property of the Tested Sample 38
5.6 Analysis 39
6. A SIMULATION STUDY ON THE JULY 10, 1997 HARIHARA DEBRIS SLIDE–DEBRIS FLOW INDUCED BY A RAINFALL IN KAGOSHIMA PREFECTURE, JAPAN 41
6.1 Investigation and Sampling at the Initial Landslide 42
6.2 Simulation Test under Undrained Condition 42
6.3 Simulation Test under Drained Condition 44
6.4 Analysis 46
7. CONCLUSIONS 47
ACKNOWLEDGEMENTS....50
BIBLIOGRAPHY 51
CAPTION: TABLES AND FIGURES....57
APPENDIX 109

1. INTRODUCTION

Landslides almost occur every year in the world, because of earthquake, rainfall and other factors, such as engineering activities, and so on. Those rapidly moving landslides often cause serious disasters because they are so rapid that people have no enough time to evacuate from the landslide site or take their property out. The disasters caused by landslides are being enlarged by the urbanization and population growth. Rapid landslides often travel long distance, and affect not only their source areas, but also the travel areas and deposition areas. For this reason, the rapid and long run-out landslides are well known. There are many examples in Japan. The Nikawa landslide, which was induced by the January 17, 1995 Hyogoken-Nambu earthquake, killed 34 persons (Sassa et al. 1995). The December 6, 1996 Otari landslide-triggered-debris flow, killed 6 persons (Marui et al. 1996, Sassa et al. 1997). The July 10, 1997 Harihara debris slide–debris flow in Kagoshima Prefecture induced by rainfall, killed 21 persons (Sassa et al. 1998a). There are also many rapid landslides occurred in my motherland, China, in these years. For example, the Xintan landslide, which occurred on June 12, 1985 in the Three-Gorge area, although a successful failure-time-prediction made nobody be injured, the landslide also cut the navigation in the Yangtze River for one week (Wang et al. 1991). The Salashan landslide, which occurred on March 7, 1983 in Gansu Province, destroyed three villages near the toe of this landslide and killed 227 persons (Cao 1986, Zhang et al. 1992). The disaster caused by landslide is cruel, but the mechanism of the rapid landslide is not yet completely understood. Therefore, for disaster predication and

mitigation, it is very important to study the mechanism of rapid landslide.

1.1 BACKGROUND FOR THIS STUDY

Generally, landslides with high gravitational potential always move rapidly, while those with low gravitational potential move slowly. In spite of that, some landslides occurred on very gentle slopes also moved rapidly. For instance, some loess landslides induced by Haiyuan earthquake in 1920 in China (Zhang 1996), and the Nikawa landslide (Sassa et al. 1996), took place in gentle slopes. It is well known that whether a landslide can move rapidly is affected by many factors. The most important factor is, during landslide motion, whether the sliding surface is in undrained condition or in drained condition. Hutchinson et al. (1971) pointed out that undrained loading is a fundamental mechanism of mudflows and other mass movements, based on the observation made in mudslides with electrical piezometers. Seed (1968) concluded that landslide during earthquake was caused by liquefaction of sandy soil layer under the undrained condition.

Sassa et al (1996) proposed a concept of "sliding-surface liquefaction" to interpret the rapid landslide occurred in medium dense and dense Osaka-group coarse sandy soils of the Nikawa landslide. Figure 1.1 illustrates the difference between liquefaction and "sliding-surface liquefaction" It was described as: "Liquefaction is normally caused by destruction of the meta-stable soil structure in loose sandy soil mass, that the failure will occur before stress path reaches the failure line, while, "sliding-surface liquefaction" takes place only along a sliding surface, that need not destruction of the structure. It can take place even in medium or dense soil structure because grain crushing along the sliding surface results in volume shrinkage and pore pressure generation"

The concept proposed by Sassa is just estimation, and there are two defects in it. The first one is, the property of grain crushing was estimated from Shirakawa sand in Kyoto based on Fukuoka (1991), combining with the obtained effective stress path in the undrained ring shear test. Measurement of grain crushing property on the sandy soil

taken from the Nikawa landslide was not performed. The second is, the cyclic-loading was assumed as a sine wave with increasing amplitude cycle by cycle, with frequency of 0.1 Hz. In the current situation, whether excess pore pressure generation depends on the frequency of cyclic-loading or not, and how the amplitude of cyclic-loading affect excess pore pressure generation are unclear. Therefore, if possible, it is necessary to conduct a geotechnical simulation test with a real seismic record on a real case.

Since 1995, two new undrained ring shear apparatuses have been developed in the Disaster Prevention Research Institute, Kyoto University by Sassa and his colleagues, which are able to load a real seismic-record. Therefore, it becomes possible to carry out a geotechnical simulation test on the Nikawa landslide with a real seismic loading of the Hyogoken-Nambu earthquake, and to perform a fundamental study on the grain crushing and pore pressure generation during shearing of sandy soils.

1.2 AIM AND MAJOR WORKS OF THIS STUDY

The aim of this study is to confirm the concept of "sliding-surface liquefaction" and study the relationship between grain crushing and excess pore pressure generation. Drained ring shear tests is used to investigate the grain crushing susceptibility of different sandy soils, while undrained ring shear tests is used to investigate their excess pore pressure generation behavior.

The major works are as follows.

At first, the fundamental study on the grain crushing properties in the drained condition and excess pore pressure generation in the undrained condition, during constant-speed shearing and cyclic-loading was performed. The relationship between grain crushing properties of sandy soils and excess pore pressure generation behaviors was analyzed.

Moreover, a trial was made on the geotechnical simulation test loaded with a real seismic record of Hyogoken-Nambu earthquake on the sandy soil taken from the

Nikawa landslide. The excess pore pressure generation behavior under a real seismic record was analyzed.

Finally, to verify the effectiveness of the concept of "sliding-surface liquefaction" in the rainfall-induced landslide type, another series of simulation tests on the Harihara debris slide–debris flow was carried out. The grain crushing property of the andesitic deposit in drained ring shear test and the excess pore-pressure generation behavior in undrained condition and drained condition were analyzed.

1.3 DEFINITIONS AND RESTRICTIONS

The followings give some definitions and restrictions used in this thesis.

Landslide and Slide: According to Cruden (1991), the term "landslide" is used to denote "the movement of a mass of rock, debris or earth down a slope" The movements have been divided into five types: falls, topples, slides, spreads, and flows. A slide is a down-slope movement of a soil or rock mass occurring dominantly on surfaces of rupture or on relatively thin zones of intense shear strain (Cruden et al. 1996).

Grain crushing: A process of soil grain size becoming smaller and smaller when stresses imposed on soil grains exceed their strength. It is also called as particle breakage (Lade et al. 1996).

Particle breakage factor, *B* (Marsal 1967): Marsal (1967) developed a measure of particle breakage concerning the design and construction of earth and rockfill dams. While performing large-scale triaxial compression tests, he noticed significant amounts of particle breakage. He subsequently developed a breakage index, *B*, to quantify this breakage. His method involves the change in individual particle sizes between the initial and final grain size distributions. The difference in the percentage retained is computed for each sieve size. This difference will be either positive or negative. Marsal's breakage factor, *B*, as shown in Figure 1.2, is the sum of the difference having the same sign (Equation1.1). The lower limit of Marsal's index is zero percent, and has a

theoretical upper limit of 100%.

$$B = b_1 + b_2 + b_3 + b_4 = B_1 + B_2 + B_3 + B_4 + B_5 \tag{1.1}$$

Relative density (D_r): This term is defined as

$$Dr = \frac{e_{max} - e}{e_{max} - e_{min}} \times 100\% \tag{1.2}$$

where e_{max} = viod ratio of soil in the loosest condition; e = void ratio of soil; e_{min} = void ratio of soil in the densest condition. In this study, D_{ri} is the initial relative density of a sample set in shear box before application of any load, while D_r is relative density after normal consolidation.

Sample height change: During shearing in the drained condition, the sample in the shear box will change its volume. This phenomenon is termed as "dilatancy" Because the area of shear zone in the ring shear apparatus is constant in the ring shear apparatus, and the deformation is not uniformly distributed in sample height, but mainly takes place at the shear zone, the volume change is represented as sample height change. The initial value of sample height change is zero at the beginning of shearing after sample is consolidated.

Pore pressure coefficient in direct-shear state, B_D: A parameter to check the degree of saturation of sample in the direct shear condition. It was proposed by Sassa (1985) based on the pore pressure coefficient, B, proposed by Skempton (1954). It is a ratio of pore pressure response to the normal stress increment of sample under undrained condition. When B_D is greater than 0.95, the sample is considered to be fully saturated.

Seismic coefficient, K: The ratio of seismic acceleration to gravity acceleration, g.

Critical seismic coefficient, Kc: The critical value of seismic coefficient that makes the factor of safety for a slope equal unity in drained condition. It depends on the engineering geology conditions of a specific slope, such as slope angle, groundwater

table, friction angle of the sliding surface and so on.

Seismic coefficient ratio, K/K_c: The ratio of seismic coefficient to the critical seismic coefficient for a specific slope. It is used as a parameter of seismic intensity in this study. When $K/K_c = 1$, it means that an earthquake makes a slope to the critical state in the drained condition.

Excess pore pressure: It is the pore pressure generated in soils under the undrained condition during soil deformation. The pore pressure change caused by the change of normal stress under the undrained condition is not included in the excess pore pressure.

Excess pore pressure ratio (r_u): It is the ratio of excess pore pressure to the initial effective normal stress. It is used as the index to evaluate the degree of high-mobility and liquefaction. Theoretically, when $r_u = 1$, it means a fully liquefaction.

Liquefaction: The basic mechanism of onset of liquefaction is elucidated from the observation on behavior of a sand sample undergoing cyclic stress application in the laboratory triaxial test apparatus. It is generally observed that the pore pressure was built-up steadily as the cyclic axial stress is applied, and eventually approaches a value equal to the initially applied confining pressure, thereby producing an axial strain of about 5% in double amplitude. Such a state has been referred to as "initial liquefaction" or simply "liquefaction" (Terzaghi et al. 1948, Ishihara 1993). It was defined by Sladen et al. (1985) based on the definition given by Castro (1969) as follows: Liquefaction is a phenomenon wherein a mass of soil loses a large percentage of its shear resistance, when subjected to monotonic, cyclic, or shock loading, and flows in a manner resembling a liquid until the shear stress acting on the mass is as low as the reduced shear resistance.

Sliding-surface liquefaction: This concept was proposed by Sassa et al (1996) when they were in studies of some landslides triggered by the January 17, 1995 Hyogoken-Nambu earthquake through the undrained ring shear tests. Even with medium dense and dense sandy soils, excess pore pressure can be built-up because of the grain crushing

during shearing. It is a localized liquefaction phenomenon in an actual landslide.

Steady state of deformation: The steady state of deformation for any mass of particles is that state in which the mass is continuously deforming at constant volume, constant normal effective stress, constant shear stress, and constant velocity. The steady state of deformation is achieved only after all particle orientation has reached a statistically steady state condition and after all particles breakage, if any, is complete, so that the shear stress needed to continue deformation and the velocity of deformation remain constant (Poulos 1981).

2. RING SHEAR APPARATUS

The undrained cyclic-loading ring shear apparatus DPRI Ver.5 and Ver.6 developed by Sassa and his colleagues in Disaster Prevention Research Institute (abbreviated as DPRI), Kyoto University in 1995 (Sassa 1997) were used in this study. They are the improved types in ring-shear apparatus series.

Initially, modern ring-shear apparatus was developed by Bishop et al. (1971) to study the residual strength of soils. Without limit of shear displacement, it is widely used to study the mechanical behavior of landslide motion (Tika et al. 1996). Bromhead (1979) and Gibo (1994) made ring-shear apparatuses to study residual strength of soils. A series of ring-shear apparatuses were developed and improved in DPRI, Kyoto University by Sassa et al. (Sassa et al. 1984, Sassa et al. 1989, Sassa 1995, Sassa 1998). From DPRI Ver.3, the basic principle for the ring-shear apparatuses is the same, and undrained ring-shear test can be conducted. The new intelligent type dynamic-loading ring-shear apparatuses (DPRI Ver.5 and Ver.6) can conduct geotechnical simulation test of landslide induced by earthquake.

Figure 2.1 is a photograph of the DPRI Ver.6 ring-shear apparatus. The most important features of both apparatuses, DPRI Ver.5 and Ver.6, are listed in Table 2.1. During test, normal stress, shear resistance, pore pressure, shear displacement and vertical displacement are measured and recorded automatically by an acquisition system.

2.1 STRESS CONTROL AND GAP CONTROL SYSTEM

Figure 2.2 shows the electronic control system of the DPRI Ver.5 apparatus. This system is composed of stress control and gap control. Stress control includes normal stress-control and shear stress-control. When a normal stress is applied, the control signal passes from the computer through a servo-oil valve, and the load cell N_1 exerts a vertical load, N_1, on the sample. Friction generated between the sample and shear box at the inner and outer rings is measured as N_2 by load cell N_2. The feedback N_1-N_2 then becomes to control signal and controls the normal stress. Shear stress is applied as shear torque T by servomotor (DPRI ver.6 has two servomotors, T_1 and T_2). Load cells S_1 and S_2 measure the shearing resistance at the shear surface.

Gap control is used to keep the upper and lower parts of the shear box in undrained condition. The upper ring is fixed to the center axis, which is controlled by a servo-oil-piston. With high precision of 0.001 mm, the gap-control system keeps the upper part of the shear box pressing the rubber edges in the lower part of the shear box under a compression pressure of 1.5 kN or so (controlled by gap sensor GS). The friction between the rubber edge and the upper rings during shearing is measured, and the value is subtracted from the monitored shear resistance in data processing.

2.2 STRUCTURE

Figure 2.3 is the schematic structure of the DPRI Ver.6 ring shear apparatus. The circular sample is in the shear box at the middle of the apparatus. The lower half is rotated by servomotors (marked as rotating parts in the figure), while the upper half (marked as a movable parts in the figure) is restrained by two load cell S_1 and S_2 to measure shear resistance. The axial is moveable part for gap control. Through oil piston OP_2 and measured by load cell N_2, a pressure acting on rubber edges inserted in the lower rings was applied to keep upper ring and lower ring contact tightly. Before normal stress is applied, load cell N_2 is reset to zero. When normal stress is applied through oil piston OP_1 and measured by load cell N_1, the side friction N_2 between

sample and upper ring will generate because of the compression of sample. The actual normal stress acting on the sample will be N_1-N_2.

During test, VD measures the vertical displacement, i.e., the sample height change, and SD measures the shear displacement corresponding to the center of the circular sample at shear zone.

Pore pressure is measured by pore-pressure transducer P_1 and P_2. Pore pressure sealing and measurement are about the same as those were introduced by Shoaei et al. (1994). Figure 2.4 is a half section of the undrained shear box and the pore pressure gauge. At the bottom of the shear box, there is a porous metal. Through the lower drainage line, CO_2 and de-aired water are supplied in the process of sample saturation. After a filter paper is set, sample is set in the shear box, with different sample-making methods depending on the test purpose. Then another filter paper is putted on the sample, and then loading plate is located. Before consolidation, space exists between the upper filter paper and porous metal of the loading plate. The "O"-rings keep the sample in the undrained condition. Upper drainage line is used to drain air and water in saturation and consolidation process, and is also used to supply initial pore pressure on the sample when it is necessary. Rubber edge is fixed in the lower ring, before a test, it is cleaned and covered by teflon and silicone grease to decrease the friction between the rubber edge and the upper ring, and also to prevent water leakage. Pore pressure transducer is inserted in the upper ring. Through a water path in the upper ring and a felt cloth filter sandwiched by two metal filters, it measures the pore pressure near the shear zone. In a test, after sample is saturated, the knob in the pore pressure gauge is opened to drain air and water. This secures that there is no air in the water path. The results of undrained check on the ring shear apparatus have been presented by Wang et al. (1997a).

For the following reasons, ring shear apparatus was used in this study.

1) It can simulate the stress and deformation situation of soils in the sliding zone of a landslide.

2) As a simulation test apparatus, because the stress and deformation parameters can be measured precisely, it is better than other types model tests.
3) When comparing to the triaxial test, its unlimited shear displacement makes the study possible on the post-failure behavior of landslides.
4) The sample in the shear zone is enough for the grain size distribution analysis when studying the susceptibility of grain crushing of sandy soils.

3. PROPERTIES OF SAMPLES

Toyoura standard sand, silica sand and Osaka-group coarse sandy soil were used in this study.

Toyoura standard sand (T-sample) is one kind of Japanese standard sand extensively studied by several researches (Tatsuoka et al. 1986, Ishihara 1993, Bellotti et al. 1997). These researches indicated that the mechanical properties of dry and saturated sand are nearly identical. It is predominantly a uniform sub-angular to rounded fine sand with approximately 90% of quartz and 4% of chert.

Silica sand (S-sample) is construction material for industrial use. It is made of weathered silica sand, and has a uniform grain size distribution. The grain is almost angular. It consists of 92 ~ 98% of quartz, and a little amount of feldspar. In this study, the silica sand no.7, with a mean grain size of 0.16 mm, was used.

Osaka-group coarse sandy soil (O-sample) was taken from the source area in the Takarazuka landslide, which was also triggered by the January 17, 1995 Hyogoken-Nambu earthquake (Sassa et al. 1996). It is located in the Takarazuka Golf Club. The deposit of Osaka-group is a limnetic and marine deposit of the Pliocene to the Mid-Pleistocene distributed around the Osaka area, Japan (Itihara 1996). It is an angular sandy soil consisting of weathered granite and is composed of 77 percent of quartz and 23 percent of feldspar and mica.

Some classification and index properties of the employed samples are listed in

Table 3.1. It needs to mention that the measurements of these properties followed the Japanese Geotechnical Society Standard (the Japanese Geotechnical Society, 1990). In the test for maximum and minimum density of sand, because O-sample is not suitable to use the test method for maximum and minimum densities of sands, which is restricted by the standard No. JSF T 161-1990, these values for O-sample are just for reference.

To get residual friction angle of the three types of sandy soils that will be used in the cyclic-loading ring shear tests, speed-controlled ring shear tests were conducted with dry sample. The procedure is as follows.

① Set oven-dried sample in the ring shear box with free-fall deposition method. This method is described in section 4.1 later.

② Consolidate the sample under 490 kPa.

③ Shear the sample at 3 mm/sec.

④ After the residual state was reached, decrease the normal stress to about 0 during shearing gradually. The obtained failure line and residual friction angle for the three samples were presented in Figure 3.1 and Table 3.1.

4. GRAIN CRUSHING CHARACTER OF SANDY SOILS AND EXCESS PORE PRESSURE GENERATION DURING SHEARING

Grain crushing initially used to evaluate and predict the possibility of erosion, and was mainly studied with triaxial test and compression test (Marsal 1967, Lade et al. 1996). Fukuoka (1991) used ring shear apparatus to study grain-crushing property of sandy soil in the sliding zone of the Zentoku landslide. Vankov et al. (1998) found that grain crushing depends on the energy that applied on the sample during test. Generally, larger energy will result in more grain crushing. Moreover, Wang et al. (1998a) investigated grain crushing susceptibility of different sandy soils and found that, grain shape and hardness of minerals have great effects on the grain crushing susceptibility. The investigation results of the grain crushing property of different sandy soils will be reported here. Wang et al. (1997b) presented that sandy soil type greatly affect the behaviors of excess pore pressure generation in the undrained cyclic-loading, and according to the concept of "sliding-surface liquefaction", it must have some relation with the grain crushing. Therefore, in this chapter, grain crushing properties of sandy soils are studied by consolidated-drained constant-speed ring shear test. The effects of the type of sandy soils and initial density are discussed. Then, at about the same initial density of the same samples, the generation process of excess pore pressure is investigated by the consolidated-undrained constant-speed ring shear tests. Based on the results of both series tests, the relationship between grain crushing and pore pressure generation was analyzed, and the possibility of prediction of pore pressure generation

based on sample height change in drained tests was discussed. Moreover, to investigate the effect of grain crushing susceptibility on pore pressure generation in cyclic-loading, a series of undrained cyclic-loading ring shear test was performed. Besides the sandy type, the effects caused by other factors such as frequency of cyclic-loading and the initial density of sample were also discussed.

4.1 TEST PROGRAM AND PROCEDURE

The three types of sandy soils, O-sample, S-sample and T-sample were used in this test program. Free-fall deposition method was used for preparing loose samples, while dry tamping method was used to make O-sample (dense). With free-fall deposition method, oven-dry sample is poured with a cup or plastic bottle from the top of upper shear box. While, with dry tamping method, after oven-dry sample is poured with a cup from the top of upper shear box and a thin layer is formed, tamping is applied lightly with a rubber flat-bottom tamper. At the mean time, the compression index, C_c, for them was obtained by consolidating the sample under normal stress of p_1 = 98 kPa and p_2 = 196 kPa, respectively, and calculating the corresponding void ratio, e_1 and e_2. The compression index C_c is expressed as Equation (4.1).

$$C_c = \frac{e_1 - e_2}{\log p_2 - \log p_1} \tag{4.1}$$

The relative densities of the samples and the compression index are listed in Table 4.1. D_{ri} is initial relative density of a sample before application of any load, while D_r is relative density after normal consolidation.

4.1.1 Consolidated-Drained Constant-Speed Ring Shear Tests

The consolidated-drained constant-speed ring shear tests on wet samples were conducted to investigate the sample height change during shearing process. After shearing for a long shear displacement, grain crushing may occur at the shear zone.

Thereafter, the sample at shear zone was taken out, then grain size distribution was analyzed and the grain crushing susceptibility was investigated.

In these series tests, after the sample set in the shear box, water was supplied through the lower drainage line until water flowed out of the upper drainage line. It is believed that, the fine particle caused by grain crushing can be kept at the shear zone, and does not fall down to the bottom of the shear box in wet condition.

At first, the samples were normally consolidated under the normal stress of 196 kPa. The shear speed was 3 mm/sec. The shear displacement was 42 m considering the sample quantity for grain size distribution analysis.

It need to mention that, to evaluate the grain crushing susceptibility caused by shearing only, samples of the same relative density with that in the drained ring shear tests were prepared, and consolidated under normal stress of 196 kPa. Then grain size distribution analyses were performed on the consolidated samples.

4.1.2 Consolidated-Undrained Constant-Speed Ring Shear Tests

The consolidated-undrained constant-speed ring shear tests on the fully saturated samples were conducted to investigate the pore pressure generation in different samples under the undrained condition.

The following procedure is adopted in the saturated undrained ring shear tests.

① Weigh dry sample and set it in the shear box with free-fall deposition method for loose sample and dry tamping method for dense sample.

② Pass CO_2 gas through the sample from the bottom drainage line to the top drainage line.

③ Under a minimal pressure, slowly infiltrate de-aired water into the sample from the lower drainage line, to replace the CO_2 in the sample pores, until the water flows out of the upper drainage line.

④ Consolidate the sample under 50 kPa normal stress.

⑤ Confirm the degree of saturation. Apply a normal stress increment, $\Delta\sigma$ = 50

kPa, in the undrained condition, and measure the increment of the excess pore pressure, Δu. Calculate B_D (= $\Delta u / \Delta\sigma$), the pore pressure parameter in the direct-shear state. A high B_D value indicates a high degree of saturation.

⑥ Consolidate the samples normally under the normal stress of 196 kPa or so.

⑦ Shear the sample at the shear speed of 3 mm/sec. Final shear displacement was determined as 500 mm considering that excess pore pressure will have no great change after sample is sheared for so much shear displacement.

4.1.3 Consolidated-Undrained Cyclic-Loading Ring Shear Tests

The undrained cyclic-loading ring shear tests on the saturated samples, which conducted by Wang et al. (1998b, c), are referred here to show two results: (1) how the pore pressure generate with the shear displacement under cyclic-loading, and (2) the effects of frequency of cyclic-loading, initial void ratio on the generation behavior of excess pore pressure under cyclic-loading.

The undrained cyclic-loading ring shear test simulates the stress condition of a soil element in the sliding zone of an infinitely long slope subjected to a horizontal seismic force. Among the many cited examples of landslides induced by earthquakes (Sassa et al. 1996, Zhang 1996), landslide thickness generally ranges from 15 to 40 m, with occasional large landslides have thickness exceeding 100 m. Most of these landslides occurred on slopes of 15 ~ 40° before failure. To represent an "ideal" slope, and considering the capability of the ring shear apparatus, slope height is assumed to be 30 m and slope angle to be 25°

Figure 4.1 shows a schematic diagram of the undrained cyclic-loading ring shear test. The unit weight γ_t =20 kN/m^3 is taken as the unit weight. Thus, the weight of the soil element is W = 544 kN/m^2 The seismic force is assumed to act from the back of the landslide in horizontal direction. The critical horizontal seismic coefficient in a drained condition case, K_c, is given by Equation (4.2)

$$K_c = \tan(\phi - \theta) - [\tan\theta + \tan(\phi - \theta)]\frac{u_0 \cos\theta}{W} \quad (4.2)$$

Where, ϕ is the angle of internal friction of the sample (in degrees), u_0 is the initial pore pressure, because groundwater often exists above the sliding surface in earthquake-induced landslides with high-mobility. An example is the Nikawa landslide. The initial pore pressure for the "ideal" landslide is assumed 20 kPa in the saturated condition.

The seismic coefficient ratio, K/K_c, is designated as the cyclic stress-magnitude parameter. Cyclic-loading of constant magnitude lasted for 10 cycles with frequency of 0.02 Hz, 0.1 Hz or 0.5 Hz (Figure 4.2). The cycle number at which failure occurring can be detected from the monitored data of shear resistance and shear displacement.

The test condition, including the sample name, initial density state, frequency of cyclic-loading, initial slope angle, and the amplitude of cyclic-loading are listed in Table 4.2. For example, O(Dense)-F(0.1)-25° means this test is to simulate a 25° slope consisted of dense O-sample subjected to a cyclic-loading of 0.1 Hz. Except O(Dense)-F(0.1)-25° (K/K_c = 2), the K/K_c value for the other tests is 1.5.

The following procedure is adopted in the cyclic-loading ring shear tests.

① Set, saturate the sample and confirm the degree of saturation as described in the previous section.

② Consolidate the sample under the planned initial normal stress, σ_0.

③ Apply the planned initial shear stress, τ_0, under the drained condition as slowly as possible, avoiding generation of excess pore pressure.

④ Apply the initial pore pressure u_0 through the upper drainage line.

⑤ Close all the drainage valves, change the shear box to the undrained condition.

⑥ Simultaneously apply the planned cyclic normal-stress increment, $\Delta\sigma$, and cyclic shear-stress increment, $\Delta\tau$.

4.2 TEST RESULTS

4.2.1 Consolidated-Drained Constant-Speed Ring Shear Tests

Grain crushing properties of four samples were investigated. The results include the grain size distribution analyses, and the sample height change during shearing.

After the drained shearing was over, the shear box was opened. It was observed that, in the tests on the O-sample (loose) and O-sample (dense), grain crushing mainly generated in the shear zone of 10 ~ 20 mm thick. Figure 4.3 shows the results of the grain-size distribution analysis of samples after consolidation and samples taken from the shear zone after shearing. Then, Marsal's breakage factor, B, was calculated to quantify the grain crushing susceptibility. The B value for T-sample is 2.8%, for S-sample is 4.3 %, for O-sample (loose) is 9.0% and for O-sample (dense) is 9.0%. It can be concluded that, the O-sample is the easiest sample to be crushed, while the T-sample is the difficult one to be crushed.

The relationship between sample height change versus shear displacement is presented in Figure 4.4. In contraction (shrinkage), sample height decreased; while in dilatancy, sample height increased. In the four samples, the O-sample (dense) shows a typical curve. The sample height change along with shear displacement can be divided to three "dilatancy" phases — "initial negative dilatancy", "initial positive dilatancy" and "negative dilatancy due to grain crushing" by the border point "A" and "B" During the "initial negative dilatancy", when the shear displacement is small, it is volume shrinkage caused by the position adjustment of soil grains. The other three samples also show the "initial negative dilatancy" after the onset of shearing. During the "initial positive dilatancy", when the shear displacement increases, until the peak strength of soil is reached and the soil fails. This part is volume dilation caused by shearing in a medium dense or dense soil. A loose sample like O-sample (loose) does not show "initial positive dilatancy" The word "initial" used in the two phrases above means that the two phases of dilatancy are mainly affected by the initial density (initial structure) of soils. It is believed that, for extremely dense soils, the "initial negative dilatancy" would not exist, while, in extremely loose soils, the "initial positive dilatancy" would not exist.

During the "negative dilatancy due to grain crushing", after the initial dilatancy that mainly affected by the initial density completed, the sample height changes dominantly decided by the grain crushing susceptibility of soil. In Figure 4.4, although it is difficult to extract exactly the part caused by grain crushing, combining with the result in Figure 4.3, it can be estimated that the last part in the curve of sample height change is mainly caused by grain crushing.

The Marsal's breakage factors, B, as well as the compression index, C_c, of samples at a certain relative density, against the final sample height changes, are plotted in Figure 4.5. It is indicated that a relationship exists among the sample height change with the particle breakage factor, B, and the compression index, C_c. The sample, which has a large compression index and can be easily crushed, will generate large change in sample height during shearing. From this figure, it is also found that, after a rather long shear displacement, the Marsal's breakage factors, B, for O-sample (loose) and O-sample (dense) become to a certain value. It indicates that the initial density of sample has not obvious effect on the Marsal's breakage factors for long shear displacement. The difference of the final sample height changes between O-sample (loose) and O-sample (dense) is caused by the initial density of sample. Therefore, it is reasonable to use the sample height change as a relative index to evaluate the grain crushing susceptibility, while considering the effect of initial density of sample in mind.

According to the previous study (Lade et al. 1996), grain crushing is affected by 1) the stress level (proximity to failure), the stress magnitude and the stress path, 2) grain size, 3) particle angularity, 4) uniform coefficient, 5) mineral hardness, and 6) introduction of water. In this test result, it is confirmed that, under the same stress condition, the internal affecting factors on grain crushing are: 1) mineral hardness. Sands consisting of hard minerals such as quartz are difficult to be subjected to the grain crushing than those consisting of feldspar and mica. 2) particle angularity. Sands with angular shape are easier to be crushed than those with rounded grains. S-sample and T-sample are mainly composed of quartz, but S-sample was easily crushed. It is probably

because S-sample is angular, while T-sample is sub-rounded.

4.2.2 Consolidated-Undrained Constant-Speed Ring Shear Tests

The initial relative densities of samples in undrained ring shear tests were tried to keep as the same with drained ring shear tests (see Table 4.1). Excess pore pressure ratio, $r_u(t)$, is expressed as the ratio of excess pore pressure increment to initial effective normal stress in this test condition (Equation 4.3) (Popescu et al. 1997).

$$r_u(t) = \frac{u(t) - u_0}{\sigma_0'} \tag{4.3}$$

In Figure 4.6, the excess pore pressure ratios during tests are presented. Effective stress paths for all four tests are shown in Figure 4.7. Let us analyze the excess pore pressure curve of O-sample (dense) in Figure 4.6. At the beginning, when sample was sheared for 0.3 mm, the sample began to be contractive due to the position adjustment of grains. Under the undrained condition, it resulted in the excess pore pressure generation. Therefore, the excess pore pressure ratio increased until a peak point "A", in correspondence to the drained test, this phase is also called "initial negative dilatancy". After the shear displacement reached 4 mm at point "A", because of the positive dilatancy character of dense soil, excess pore pressure dissipates and excess pore pressure ratio decreases to -0.16. Obviously, this phase was affected by the initial density, and is correspondingly termed "initial positive dilatancy". For S-sample and T-sample, because of relatively loose initial state, excess pore pressure ratios just decreased a bit. For loose sample of the O-sample (loose), there is no negative excess pore pressure generated. When excess pore pressure ratio reached the lowest value, noted as point "B", it means the end of the "initial positive dilatancy". After the "initial positive dilatancy" is over, because excess pore pressure ratio decreases to the lowest value, effective stress would reach its maximum value. It means that, the shearing energy acting on the grain particles during shearing reaches the maximum value. It is

liable to perform grain crushing for the sample at the shear zone. Therefore, along with the grain crushing taking place at the shear zone, there is a tendency of volume shrinkage, and results in the generation of excess pore pressure. This process will continue until the effective stress is small enough that no grain crushing will take place, i.e., until the steady state of deformation is reached. The phase from point "B" is named "Negative dilatancy due to grain crushing". At this phase, the sample difficult to be crushed like T-sample will show no change in excess pore pressure ratio. S-sample shows a little increasing tendency, because it is also difficult to be crushed. O-sample (loose) does not show a positive dilatancy, but at the last phase, because of grain crushing, the excess pore pressure ratio also increased. The curves of O-sample (loose) and O-sample (dense) nearly reach to a same value at the end of tests. This result indicates that, for a long shear displacement, the initial structure of sample has no obvious effect on the pore pressure generation in the steady state.

Figures 4.7 show the effective stress paths for all these tests. The shear displacements at some points were plotted in them. Figure 4.7(a) shows effective stress path of O-sample (loose). From beginning, because of the generation of pore pressure caused by negative dilatancy, the effective stress began to decrease after sheared for 5.0 mm. Then, because of the grain crushing, the stress path decreased to a very low level along the failure line. Figure 4.7(b) shows the effective stress path of O-sample (dense). Because of the generation of pore pressure caused by the negative dilatancy, the effective stress began to decrease until point "A". Then due to positive dilatancy, negative excess pore pressure generated from point "A" to point "B". Thereafter, because of grain crushing, stress path decreased to a low level about the same with that for O-sample (loose) along the failure line. Figure 4.7(c) is effective stress path of S-sample, after generation of pore pressure caused by the negative dilatancy, the effective stress began to decrease until sheared for 5.0 mm. Then due to the positive dilatancy, negative excess pore pressure was generated until sheared for 97 mm. Thereafter, because grain crushing is difficult to take place in S-sample, the stress path decreased a

bit along the failure line. Figure 4.7(d) is effective stress path of T-sample, because of the same mechanism as the previous ones, the effective stress path began to decrease until sheared for 4.23 mm. Then due to positive dilatancy, negative excess pore pressure generated until sheared for 124.7 mm, this phase is very large when compared with S-sample. Because T-sample is the most difficult one to generate grain crushing in all of the samples used in this study, the stress path just decreased a very little bit.

Comparing the results of consolidated-undrained ring shear tests with the consolidated-drained ring shear tests, the process of pore pressure generation with shear displacement in consolidated-undrained ring shear test, is similar to the process of the sample height change with shear displacement in the consolidated-drained ring shear tests. Although it will be affected by some other factors, both shear processes can be divided to three phases. They are "initial negative dilatancy", "initial positive dilatancy", and "negative dilatancy due to grain crushing" In "initial negative dilatancy", the sample is contractive in the drained condition, and positive pore pressure is generated in the undrained condition. If the initial density is large enough, the contraction of soil grain will not occur. In "initial positive dilatancy", the sample is dilative in the drained condition. When the sample is not so loose, a negative pore pressure will be generated in the undrained condition. In "negative dilatancy duo to grain crushing", because of the grain crushing, the sample is contractive in the drained condition and positive pore pressure will be generated in the undrained condition.

4.2.3 Consolidated-Undrained Cyclic-Loading Ring Shear Tests

The time series data and the stress paths were listed in the Appendix 1. The detail description can be referred to Wang et al. (1998b, 1998c). Only the relationship between pore pressure generation and shear displacement at different test conditions were analyzed in this thesis.

In the time-series data of O-F(0.1)-25° described in Wang et al. (1997b) (Figure A-1 in Appendix 1), after the sample reached the steady state, pore pressure varied in the

same phase with normal stress, and large pore pressure is always generated when large shear displacement occurs. According to Sassa et al. (1998b), under the undrained cyclic-loading, the measured pore pressure can be divided into two components: cyclic component and residual component. The cyclic component is mainly caused by variation of normal stress increment. It is almost equal to the increment of normal stress under fully saturated condition. The residual component is mainly due to deformation. As an example, Figure 4.8 shows that the measured excess pore pressure is separated to the two parts with test result of O-F(0.1)-25° The residual components refined from the measured pore pressure for cyclic-loading ring shear tests were then used to calculate the residual excess pore pressure ratio, $r_{ur}(t)$, which is defined as Equation (4.4). The residual excess pore pressure ratio is an index to evaluate the "sliding-surface liquefaction" susceptibility of sandy soils with shear displacement under cyclic-loading.

$$r_{ur}(t)=\frac{u(t)-u_0-B_D\Delta\sigma(t)}{\sigma_0'} \tag{4.4}$$

Where, $r_{ur}(t)$ is residual excess pore pressure ratio. $u(t)$ is measured excess pore pressure. u_0 is initial pore pressure. $\Delta\sigma(t)$ is the applied normal stress increment. $\sigma_0' = \sigma_0 - u_0$ is initial effective stress. B_D is pore pressure coefficient in direct-shear state. In this series test, $B_D \geq 0.95$ for all of the saturated samples, and in the calculation of the residual excess pore pressure ratio, B_D was dealt with as 1.0 for simplicity.

1) Residual excess pore pressure ratio of various samples in the undrained cyclic-loading ring shear tests at the same K/K_c value and the same frequency

To show the different behavior of excess pore pressure generation affected by samples themselves, the residual excess pore pressure generated in test O-F(0.1)-25°, T-F(0.1)-25°, and S-F(0.1)-25°, the undrained cyclic-loading ring shear tests on O-sample, T-sample and S-sample at $K/K_c = 1.5$ with cyclic frequency = 0.1 Hz, are presented in Figure 4.9.

The pattern of the residual excess pore pressure generation with shear displacement

is almost the same as that in the consolidated-undrained constant-speed ring shear tests. At the end of cyclic-loading, the residual excess pore pressure ratio of O-F(0.1)-25° was 0.87, of T-F(0.1)-25° was 0.2 and of S-F(0.1)-25° was 0.6. It is in the same order as that of grain crushing susceptibility. It is indicated that, in cyclic-loading, grain crushing also strongly affects the residual excess pore pressure behavior of sandy soils.

2) Excess pore pressure ratio of O-samples at various frequencies of cyclic-loading at the same K/K_c value

Frequency is an important index of seismic wave. To investigate how the frequency affect the pore pressure behavior under the undrained condition, frequencies of 0.02 Hz and 0.5 Hz were used in the undrained cyclic-loading ring shear tests on O-sample. The results were compared with that of O-F (0.1)-25° and shown in Figure 4.10. Despite different frequencies, O-sample reached the steady state of deformation at 100 mm of shear displacement for all tests. Before that, although test data with 0.5 Hz can not be clarified because of possible measurement lag of pore pressure in high frequency, the residual excess pore pressure ratio of 0.1 Hz is larger than that of 0.02. However, in the whole process, the effect of frequency is not so obvious, and only the shear displacement affects the residual excess pore pressure ratio.

3) Residual excess pore pressure ratio of O-sample at different initial relative densities

Figure 4.11 shows the residual excess pore pressure ratios of O-sample (loose) at K/K_c = 1.5, 0.1 Hz and O-sample (dense) at K/K_c = 2, 0.1 Hz (The test with O-sample (dense) did not fail when K/K_c = 1.5). The loose sample almost had no pore pressure dissipation in the whole shearing process. It went to "sliding-surface liquefaction" directly. While, O-sample (dense) generated negative residual excess pore pressure before 10 mm of shear displacement, due to the positive dilatancy resulting from the initial dense state. Thereafter, the residual excess pore pressure was generated rapidly from 10 mm to 100 mm of shear displacement. This phenomenon is similar to the O-sample (dense) in the consolidated-undrained constant-speed ring shear test. It is indicated that, on the soils susceptible to grain crushing, "sliding-surface liquefaction"

could generate even at a relatively dense state, and for a long shear displacement, the effect of initial density is not so obvious.

The residual excess pore pressure generation in the undrained cyclic-loading ring shear tests on various samples shows the same trend with that in consolidated-undrained constant-speed ring shear tests. The soils susceptible to grain crushing are prone to the "sliding-surface liquefaction" in the saturated-undrained condition. The residual excess pore pressure behavior obviously depends on the grain crushing characters during shearing. For different frequency, higher frequency causes excess pore pressure generation a bit quickly, but the effect of frequency is not so obvious. "Sliding-surface liquefaction" can generate in soils susceptible to grain crushing, even at a relatively dense state. For a long shear displacement, the initial density has no obvious effect on the final residual excess pore pressure ratio.

4.3 POSSIBILITY OF EXCESS PORE PRESSURE PREDICTION IN UNDRAINED CONDITION BY DRAINED RING SHEAR TESTS

From the results obtained in the ring shear tests with different sands and sandy soils, it is found that grain crushing can be evaluated with the sample height change in the consolidated-drained ring shear test for a certain shear displacement. The sample height change provides a good relationship with Marsal's particle breakage factor, B. Although the initial density of sample will affect the final sample height change, those sandy soils with high particle breakage factor, B, will achieve a high final sample height change. Moreover, the excess pore pressure generation behavior of sandy soils in the undrained condition has a similar tendency with the sample height change in the drained condition. Both (sample height change in the drained condition and excess pore pressure ratio in the undrained condition) of them can be mainly divided to three phases: "initial negative dilatancy", "initial positive dilatancy" and "negative dilatancy due to grain crushing" (see Figure 4.12). Therefore, it is supposed that the pore pressure generation behavior in the undrained condition can be estimated based on the results of consolidated-drained

ring shear tests.

By means of triaxial compression tests, some achievements were carried out. For example, Groot et al. (1997) presented a mathematical description of the "dry" properties and used it to predict the specific stress path found in undrained triaxial tests for loose sand. The theoretical foundation is that, the constitute properties of soil skeleton of loose sand most relevant for predicting liquefaction flow-slides are contraction and elastic compressibility. In the drained and undrained ring shear tests presented above, it also shows that, along with the shear displacement for sandy soils at the same density, when the contraction happened in the drained test, positive pore pressure generated in the undrained test; while, when the dilation happened in the drained test, negative pore pressure generated in the undrained test. The volumetric change of undrained sand, if it is fully saturated, can be considered to be zero, because the volumetric change of water can be ignored when the stress level changes in a small range. This means that the decrease in volume due to grain crushing and compressibility etc, will be compensated by the increasing of volume due to a decreasing mean effective stress and generation of excess pore pressure.

Grain crushing will affect the soil property. Assuming that the effect of grain crushing on the soil property can be ignored during a small range of shear displacement (such as 500 mm), it is believed that a relationship could be constructed between the sample height change in the drained ring shear test and the pore pressure generation in the undrained ring shear test. As discussed in Section 4.2.1, in the consolidated-drained ring shear test, the sample height change mainly consists of two parts: one caused by grain crushing; the other caused by compressibility. There is a near linear relationship between them. In addition, both of them have a linear relation with the normal effective stress. Therefore, the sample height change in the drained ring shear test can be presented as a function of normal stress. Because all of the drained ring shear tests were conducted under a constant normal stress, the assumption above can not be verified.

There is a test program in planning to compare the results of consolidated-drained

ring shear test with the consolidated-undrained ring shear test. In this program, we will make two samples with the same relative density. On one of them, perform the undrained constant normal stress constant-speed ring shear test at first, then take the effective stress in this test and use it as a control signal of normal stress to conduct a consolidated-drained constant-speed ring shear test on the other sample. So, the excess pore pressure generation of sandy soils could be estimated by the sample height change behavior in drained ring shear tests. This makes possible the prediction of "sliding-surface liquefaction" behavior of failure even by means of drained ring shear test which can be done by the conventional ring shear apparatus (Bishop et al. 1971), even at a landslide field. Because this program can not be achieved in the current control system of the ring shear test, it is recommended to conduct later.

5. A GEOTECHNICAL SIMULATION STUDY ON THE NIKAWA LANDSLIDE INDUCED BY THE JANUARY 17, 1995 HYOGOKEN-NAMBU EARTHQUAKE IN JAPAN

The January 17, 1995 Hyogoken-Nambu earthquake in Japan killed more than 5,500 persons, destroyed about 200,000 houses, and induced some disasters of landslides. The Nikawa landslide is one of the largest geo-disasters of the earthquake. It destroyed 11 houses and killed 34 persons. According to Sassa et al. (1995, 1996), the landslide volume was 110,000~120,000 m^3 The moving distance was 175 m. No observation data of the sliding speed is available. However, it is believed that it was a high-speed landslide, because no one could evacuate from the destroyed houses and all 34 residents were killed.

As an example of rapid landslide induced by earthquakes, the Nikawa landslide was studied by Sassa et al. (1996), with an undrained ring shear apparatus, DPRI Ver.3. In that study, normal stress was kept as constant, and shear stress was applied as a sine wave at 0.1 Hz that the amplitude increased cycle by cycle. In undrained condition, sample was sheared and effective stress path was obtained. Basing on the study, Sassa et al (Sassa et al. 1996) proposed a concept termed "sliding-surface liquefaction" Sliding-surface liquefaction can take place even in medium and dense soil layer because grain crushing in the shear zone results in volume reduction and generation of pore pressure.

It was confirmed that in the undrained condition, frequency of cyclic loading has no obvious effect on the pore pressure generation (Peacock et al. 1968, Yoshimi et al. 1975,

Tatsuoka et al. 1986). Loading frequency between 0.05 Hz and 1 Hz were generally used as the frequency of cyclic loading in the undrained triaxial test (Tatsuoka et al. 1986), simple shear test (Peacock et al. 1968) and ring-shear test (Yoshimi et al. 1975). However, according to Newmark's "sliding-block theory" (Newmark 1965) and Arias intensity measure (also termed accelerogram energy, is the sum of the energy absorbed by a population of simple oscillators evenly spaced in frequency) (Arias 1970, Kayen et al. 1997), a cycle of cyclic-loading with low frequency means high energy. Tests in lower frequency correspond to greater energy to the soil than those given by an actual earthquake. Therefore, a controversy was arisen. To clarify the question and investigate the dynamic behavior of landslide during earthquakes, it is necessary to perform a test using a real earthquake record. To study landslide induced by earthquake, an improved undrained ring-shear apparatus, DPRI Ver.5, which is possible to load real seismic wave was developed in 1995 (Sassa 1997). This apparatus was used in this study.

This simulation test will be the first one to reproduce shear failure in direct shear state under a real seismic record by ring-shear apparatus. The objective of this study is, through the simulation test loaded with the seismic record monitored in January 17, 1995 Hyogoken-Nambu earthquake, to examine the mechanism of the Nikawa landslide induced by the earthquake, and through the drained ring-shear test to investigate the grain crushing property of the tested sample, which will be the key factor of pore pressure generation in the sliding zone of an actual landslide.

5.1 THE NIKAWA LANDSLIDE

The details of the Nikawa landslide were introduced by Sassa et al. (1996). Figure 5.1 is a photograph showing the whole area of the Nikawa landslide. The landslide occurred on a gentle slope, and moved for a long distance to the nearby residential area. Figure 5.2 shows the plan of the landslide area before the landslide occurred. The sliding direction of this landslide is about N60°E. Location of borings and excavation pits P1 and P2 for observation and sampling point S1 are plotted. Standing ground water

was observed at secondarily moved debris. Although January in this area was very dry, the Osaka-group layer composing the slope retained ground water. The table of ground water was confirmed later by ground water level monitored in them, because the ground water takes a very important role in landslide motion.

Figure 5.3 is the A-A' section shown in Figure 5.2. It is drawn based on the ground surface survey, boring investigation and the ground water monitoring at the boreholes. The average angle of the sliding surface was about 20 degrees. The base rock of the slope was granite. The Osaka-group layer, a terrace deposit distributing on the slope, overlaid on it. In this section, the Osaka-group layer is shown as a single layer. In fact, three sub-layers were observed in field. They are rocky sub-layer at the base (O_b sub-layer), sandy soil sub-layer (O_{s1}, O_{s2} and O_{s3}), and clayey sub-layer (O_{c2}). In the upper part and lower part of the slope, the Osaka group layer was overlaid by the terrace deposit. On the old slope surface, landfill consisted of the distributed Osaka-group layer. The landslide is believed to have occurred in the landfill. According to the standard penetration test, the N value at the landfill was smaller than 10, which showed a relatively small resistance. Test sample was taken from the landslide mass just above the sliding surface by excavating the landslide debris, namely the same materials (Osaka-group coarse sandy soil) in which the sliding surface was formed.

The ground water was observed to flow out from the headscarp of the landslide. To investigate the depth of groundwater table, some boreholes were drilled immediately after the landslide. The ground water table existed in 6~7m below the ground surface near and outside of the landslide area in three boreholes from February to March 1995 (Sassa et al. 1996).

5.2 INPUT OF SEISMIC LOADING

There are many earthquake records of the Hyogoken-Nambu earthquake observed at different locations. Unfortunately, there was no one located at the Nikawa landslide area. Theoretically, it would be best to use a seismic record monitored at the landslide

site, but it did not exist. Among these seismic records, the seismometer at the JR Takarazuka Station is the nearest one from the Nikawa landslide. Therefore, the real seismic wave monitored at the JR Takarazuka Station was used in this study by courtesy of Japan Railway Technical Research Institute.

There are two important elements in the input seismic wave. One is the peak ground acceleration, and the other is wave shape. Concerning the peak ground acceleration, an attenuation equation (Equation 5.1) proposed by Fukushima & Tanaka (1992) was employed.

$$\log A = 0.42Mw - \log(R + 0.025\times 10^{0.42Mw}) - 0.0033R + 1.22 \qquad (5.1)$$

Where A is the average of two peak horizontal acceleration in cm/s^2, Mw the moment magnitude and R the distance from an observatory station to the fault rupture in km. Although this equation is for the horizontal acceleration, because vertical acceleration also attenuates following the same law, the correction of the vertical acceleration is also processed with this equation.

According to the Active Fault Map in Urban Area published by Geographical Survey Institute of Japan (1996) and Irikura et al. (1995), the distance from the active fault, the Koyo active fault, to the JR Takarazuka Station and the Nikawa landslide are about 7 km and 0.5 km, respectively. The peak acceleration for the moment magnitude *(Mw)* value for the Hyogoken-Nambu earthquake was 7.0. By calculation, the peak ground acceleration at the Nikawa landslide was about 1.4 times to that at the JR Takarazuka Station.

Fukushima & Tanaka (1990) also found that, in general, the mean curve of the peak ground acceleration for loose soil was 140% times of the average curve. The seismic measurement system was set in stiff layer at the JR Takarazuka Station. While, as mentioned above, the Nikawa landslide mass was consisted of landfill of the Osaka-

group coarse sandy soil that had a low standard penetration number in the standard penetration test, i.e., a low N value. So the peak acceleration in the landslide consisted of landfill was assumed to be 1.4 times of that measured by seismometers at the JR Takarazuka Station. Considering the two factors, 2.0 (1.4×140% ≈ 2.0) was selected as the amplifying coefficient of the peak ground acceleration. It means the applied peak ground acceleration is 2.0 times of that monitored at the JR Takarazuka Station.

Concerning the wave shape and loading magnitude, through the following procedure (Based on Fukuoka et al. 1998), the seismic wave acting on the soil element in the sliding surface was obtained.

(1) Determine the horizontal seismic acceleration ($a_{HR}(t)$) in the sliding direction of the landslide. By means of NS components ($a_{NS}(t)$) and EW components ($a_{EW}(t)$) of the earthquake (Figure 5.4(a)) (Equation 5.2).

$$a_{HR}(t) = (a_{NS}{}^2(t) + a_{EW}{}^2(t))^{1/2} \cos\delta \tag{5.2}$$

(2) Determine the two components in parallel direction and normal direction to the sliding surface, by summing the horizontal component $a_{HR}(t)$ and the vertical component $a_{UD}(t)$ (Figure 5.4(b)). The component in the normal direction to the sliding surface, a_{NR} (t), and the component in the shear direction of the sliding surface, $a_{SH}(t)$, are obtained as:

$$a_{NR}(t) = a_{UD}(t)\cos\theta - a_{HR}(t)\sin\theta \tag{5.3}$$

$$a_{SH}(t) = a_{UD}(t)\sin\theta + a_{HR}(t)\cos\theta \tag{5.4}$$

(3) The three components of the earthquake, i.e., UD, EW and SN monitored at the JR Takarazuka Station were used to calculate $a_{NR}(t)$ and $a_{SH}(t)$, the acceleration parallel and normal to the sliding surface of the Nikawa landslide. Then, considering the

distance effect and the difference caused by bedrock and landfill, these two components were timed by 2.0, and then two acceleration components, i.e., the component in the normal direction to the sliding surface, A_{NR} (t), and the component in the shear direction of the sliding surface, $A_{SH}(t)$, are obtained as:

$$A_{NR}(t) = 2.0 \times a_{NR}(t),\ A_{SH}(t) = 2.0 \times a_{SH}(t) \tag{5.5}$$

(4) Calculate the initial stress and the seismic stress on the sliding surface. A soil column with a unit width along the slope was considered in Figure 5.4(c). So, the self-weight of a unit column is:

$$W = (\gamma_1(H - h_w) + \gamma_2 h_w)\cos\theta,\quad m = W / g \tag{5.6}$$

The initial stress condition can be determined by:

$$\sigma_0 = W\cos\theta, \tau_0 = W\sin\theta \tag{5.7}$$

Moreover, the seismic stresses can be determined by:.

$$\Delta\sigma(t) = mA_{NR}(t), \Delta\tau(t) = mA_{SH}(t) \tag{5.8}$$

(5) Calculate the test stress parameters. Here, we use the following values based on the field investigation. H = 14m, θ = 20°, γ_1 = 17.6 kN/m^3, γ_2 = 20.6 kN/m^3, respectively (Kawasaki Geology Corporation 1995). The pore pressure table above the sliding surface was assumed to be about 5m (at least), because the ground water table outside the landslide area was 6~7m below the ground surface. Accordingly, the initial normal stress σ_0 was 231.0 kPa, the initial shear stress τ_0 was 84.0 kPa, and the initial pore pressure u_0 was 49.0 kPa.

Eventually, the dynamic-loading stress input was obtained as shown in Figure 5.5. The seismic wave lasts for 40 seconds. The main shock distributed between 3 second and 7 second. After the seismic wave is over, the stress state of the soil element returns to the initial total stress state. Figure 5.6 is the stress path obtained from control signal of the normal stress and shear stress. The failure line drawn in this figure was the residual failure line obtained from the following simulation test. Some points locating above the failure line means that the earthquake loading gave the greater stress over the failure line.

5.3 SAMPLE PREPARATION AND TEST PROCEDURE

Grains greater than 4.75 mm are about 7% of the sample. They were eliminated after dried in oven, considering the size of the shear box. The physical properties of the sample are shown in Table 5.1. It needs to mention that the measurements of these properties followed the Japanese Geotechnical Society Standard (the Japanese Geotechnical Society, 1990). In the test for maximum and minimum density of sand, because the sample is not suitable to use the test method for maximum and minimum densities of sands, which is restricted by the standard No. JSF T 161-1990, these values for the sample are just for reference.

The seismic loading simulation test on the Nikawa landslide was performed by following procedures:

① Weigh and set the dry sample in the shear box with free-fall deposition method, and then saturate it. The degree of saturation is then confirmed by B_D value, a pore pressure coefficient in direct shear state (Sassa 1985). The B_D value at this test was 0.98. It means a high degree of saturation was achieved.

② Consolidate the sample at the initial normal stress, σ_0 and then apply the initial shear stress, τ_0 at drained condition.

③ Apply the initial pore pressure u_0 from the upper drainage line to simulate the ground water condition. The relative density of the sample then was 147.2 percent.

Following this procedure, the test sample was a bit over-consolidated.

④ Change the shear box to undrained condition, because the soil element at sliding surface will be under the undrained condition during earthquake loading. Load the dynamic wave of normal stress and shear stress simultaneously, as shown in Figure 5.5.

During the test, the data acquisition rate was set as 200 readings/sec, the maximal data acquisition rate.

5.4 TEST RESULTS

Figure 5.7 shows the time-series data of monitored parameters of normal stress σ, pore pressure u, shear resistance τ and shear displacement. In Figure 5.7(a), the normal stress monitored is almost the same as the control signal. Figure 5.7(b) shows the variation of pore pressure. During the main shock (3~7 sec), the excess pore pressure changed rapidly in response with the loading stresses. The bottom of pore pressure value indicated the pore pressure built-up during the main shock. It is noticed that pore pressure is increasing to a certain value after the cease of main shock. Figure 5.7(c) shows the variation of shear resistance and shear displacement. During the main shock, the sample failed because the loaded shear stress exceeded the shear strength of the soil. Shear displacement was observed. However, it was so small during the main shock that can not be visible in this figure. The mobilized shear resistance changes rapidly, but the maximum value did not decrease so much during the main shock. It is quite remarkable that the shear displacement accelerates. It is apparently resulted from the decrease of shear resistance to a certain low value, reasonably corresponding to the tendency of pore pressure built-up after the main shock. This is the same phenomenon observed in the previous research in the 0.1 Hz cyclic-loading ring shear test for the same soil sample (Sassa et al. 1995). It would be a localized liquefaction in the shear zone.

To check the monitored data more precise, the time series data from the start to 10 seconds were presented in Figure 5.8. Pore pressure varied with the same phase with the

normal stress with an increasing tendency. From 3.5 second, the shear displacement was generated, it means that the sample failed. From about 4 second, the shear displacement increased rapidly. However, the shear displacement was only 5 mm when the main shock was over (at about 7 second). A very important phenomenon is that, the shear displacement continued to increase after the main shock, and the excess pore pressure continued to be built-up as clearly found in Figure 5.8(b). This naturally resulted in the reduction of shear resistance, and caused the rapid landslide with high-mobility. Considering the susceptibility of the Osaka-group (weathered granitic coarse sands) to grain crushing during shearing under a certain normal stress, it is believed that the grain crushing occurred in this process. Grain crushing causes the volume reduction of the sample; in turn, it causes the excess pore pressure generation under the undrained condition.

Figure 5.9 shows the stress path obtained in the simulation test. ESP means the effective stress path, while TSP means the total stress path. Because of possible delay of pore pressure measurement during the period of high frequency, some stress points distributed above the failure line. Although it is difficult to follow the process of each stress path with this figure, referring to the time series data, it is reasonable described the stress path as following. At first, the stress path reached the peak strength failure line (ϕ_p = 38.3°) and the soil failed. The state of shear zone became to residual one. During the progress of shearing after the failure, the effective stress path turned to the residual failure line (ϕ_r = 36.2°). Shearing under a high effective stress should cause the grain crushing and then result in the generation of excess pore pressure. Thereafter, with the generation of great excess pore pressure, the effective stress path descended along the residual failure line to a very low effective stress level. The grain crushing process goes to close, until the effective stress became small enough that grain crushing can not take place any more. This is somewhat different from the usual liquefaction, in which the stress path instantaneously reduces to a very low stress level without reaching the peak strength failure line. It is consistent with the phenomenon of "sliding-surface

liquefaction" In it, the excess pore pressure, which caused by grain crushing in the shear zone during shearing is emphasized. The grain crushing makes volume reduction, and results in the built-up of excess pore pressure. To examine the concept, the built-up of residual excess pore pressure with shear displacement is presented here, and the grain crushing property of the sample is investigated later.

Figure 5.10 shows the built-up process of residual excess pore pressure ratio with shear displacement. Here, the residual excess pore pressure ratio ($r_{ur}(t)$) was obtained by Equation (4.4). It is shown that, although there is some noise between 0.2 mm and 3 mm, the increase trend of $r_{ur}(t)$ with shear displacement is clearly observed. Especially, after 10 mm, it is convinced that, the excess pore pressure is generated with the increasing of shear displacement. When the shear displacement exceeds 1000 mm, the excess pore pressure ratio becomes greater than 0.8. It means that the liquefaction phenomenon occurred with the progress of shear displacement. The process between the shear displacement and the liquefaction in the shear zone was further confirmed.

5.5 GRAIN CRUSHING PROPERTY OF THE TESTED SAMPLE

After the simulation test, the drained constant-speed ring-shear test was carried out on the same kinds of sample to investigate the grain crushing property of the tested sample.

Under a normal stress of 196 kPa, and shear speed of 3 mm/sec, the sample was sheared for 42 m in drained condition. Figure 5.11 is the sample height change during the shearing. During the shear displacement from the start to 10 mm, the change of the sample height is very small. From 10 mm, the sample height reduced with the shear displacement at a direct logarithm relation. Volume reduction may occur without grain crushing, however, it will soon terminate within a small shear displacement as proved by triaxial tests and shear box tests. The volume change presented in Figure 5.11 seems to be great different from that, such large volume reduction is unlikely caused without grain crushing. Wang et al. (1998) conducted a series test to compare the grain crushing

susceptibility of Toyoura standard sand, silica sand and Osaka-group coarse sandy soil taken from the Takarazuka Golf Club landslide, which was also induced by the January 17, 1995 Hyogoken-Nambu earthquake. It is found that the Osaka-group coarse sandy soil taken from the Takarazuka Golf Club landslide is easily crushable. Comparing the result in this study with those results, it is indicated that the Osaka-group coarse sandy soil taken from the Nikawa landslide is also with high grain crushing susceptibility.

In order to investigate the state of grain crushing in the shear zone, the sheared sample after the drained test was excavated and the cross section was exposed. Figure 5.12 is the photograph showing the cross section of the sample in the shear box. It is clearly that a grain-crushing zone was formed at the shear zone. The pins show the upper and lower boundary of the grain-crushing zone. Then, the samples in the shear zone, and that at the upper part and lower part of the shear box were taken out, and grain size distribution analyses were conducted on them. Figure 5.13 is the result comparing to the original sample. The samples at the upper part and lower part have just the same grain size distribution with the original one, while that in the shear zone was much finer. It is indicated that grain crushing only took place in the shear zone, and the sample height change dominantly resulted from the grain crushing in the shear zone. Based on this result, it is reasonable to interpret that the built-up of pore pressure is resulted from the grain crushing in the shear zone. Therefore, the liquefaction proposed as "sliding-surface liquefaction" can be distinguished from the usual liquefaction.

5.6 ANALYSIS

The mechanism of the Nikawa landslide was investigated. The landslide showed high-mobility even it took place in a very dry period. Sassa et al (1996) explored its high-mobility from the localized liquefaction phenomenon in the shear zone based on the undrained ring shear test of 0.1 Hz sine wave. Questions raised as that loading of 0.1 Hz corresponding to greater earthquake energy. Then, earthquake loading using the real seismic record was loaded in this research. Test results presented that shear

displacement started during the main shock, but it was very small. The major phenomenon representing the rapid motion of the landslide occurred after the main shock. Shear displacement increased rapidly, pore pressure was built-up continually and shear resistance reduced to a very low value after the main shock is over. The grain crushing process was estimated from the sample height change in progress with shear displacement and confirmed carefully by grain size distribution analysis of the soils taken from the shear zone after test.

This study provided a reasonable interpretation of the highly mobile Nikawa landslide in a very dry period, also presented an objective experimental data of grain crushing and sample height change in the shear zone.

6. A SIMULATION STUDY ON THE JULY 10, 1997 HARIHARA SLIDE–DEBRIS FLOW INDUCED BY A RAINFALL IN KAGOSHIMA PREFECTURE, JAPAN

During the rainy season in July 1997, heavy rainfall occurred in Kagoshima Prefecture, Japan. This rainfall caused many landslides and debris flows. The most catastrophic disaster was a rapid debris slide–debris flow at the Harihara torrent, Izumi City that occurred at about midnight on July 9 and the early morning on July 10.

The name of the Harihara debris slide–debris flow is given according to Cruden et al. (1996). To identify the multiple types of material and movement involved in the complex landslide, and provide clarity in the description, a dash known as "en dash" is used to link the two stages. The "debris slide–debris flow" means a slide takes place at first, and then it changes to a debris flow.

Figure 6.1 shows the location and the outline of the debris slide–debris flow (Shimokawa, 1997). A slide with a volume of about 2×10^5 m^3 moved into the Harihara torrent and spread over an alluvial fan and overtopped an almost completed check dam. The debris mass destroyed 19 houses and 11 non-residential buildings on the alluvial fan. 21 residents were killed and 13 were injured. The total precipitation from July 7 to 10 at Izumi City was 613.5 mm, and precipitation in 24 hrs before the failure was very heavy (Sassa et al. 1998).

Figure 6.2 is an oblique aerial view of the rapid debris slide–debris flow. As seen in

this photo, an initial landslide moved down the valley. In the middle of the course, a check dam (14 m high, 85 m wide, and 22,000 m^3 in storage volume) had been almost completed. The moving mass filled the storage area, overtopped the dam, and flooded the channeled small stream on the alluvial fan. Through field investigation, Sassa et al. (1998a) confirmed that it was properly called a rapid long run-out landslide. The collision with the dam apparently caused the mass to break, after which it was transformed into much more of a fluid.

6.1 INVESTIGATION AND SAMPLING AT THE INITIAL LANDSLIDE

The investigation team from DPRI, Kyoto University investigated the initial landslide. After the landslide mass went out from the slope, a valley, which smoothly continued to the main stream of the Harihara torrent, appeared like a tributary. The concave bedrock surface formed a subsurface valley; and it was recognized that the landslide was caused in the rock debris by pore pressure increase in this subsurface valley (Figure 6.3) (Sassa et al. 1998a). To investigate the initiation mechanism of this landslide by means of ring shear apparatus, a sample was taken from the sidewall of this valley (location marked as "Sampling point" in Figure 6.4). The sidewall included large boulders, gravel and fine soil. Sample excluding grains larger that 9.5 mm was taken in the field. The sliding surface was formed along the ground water path connecting the Harihara torrent as imagined from the contour map on Figure 6.3. Figure 6.4 shows a longitudinal section through the initial landslide and the resulting path of the movement. The section of source area is drawn by field survey, while the section of the deposit area is based on the topographical map. The initial stress condition of the soil element at the sliding surface then was estimated according to the field survey in the source area.

6.2 SIMULATION TEST UNDER UNDRAINED CONDITION

The ring shear apparatus used in testing was DPRI Ver.6, and the medium-speed gear was used (maximum speed using this gear was 33 cm/sec). The Harihara debris

slide–debris flow was initiated by heavy rainfall. Grains smaller that 0.074 mm were removed in the laboratory by sieving because fine soils are eroded from the torrent deposits and from the parts of slope in the ground-water paths of subsurface valleys (Hiura et al. 1985). To simulate this landslide by means of the ring shear apparatus, the following procedures were followed:

① Apply the initial normal stress and shear stress corresponding to the initial stress state at the sliding surface in the slope to the saturated sample which was set in the shear box with free-fall deposition method.

② Increase the pore pressure at a slow constant rate (100 kPa/1300 sec) corresponding to the rise of ground-water level caused by the rainfall in the field.

③ Change the shear box from the drained state to the undrained state soon after the shearing begins in order to measure effective stress path.

④ After reaching steady state motion, change the shear box to the drained state again to examine the speed of pore pressure dissipation.

Figure 6.5 shows the stress path (A) and the time series data (B, C) of the test, "Start" in (A) shows the initial stress corresponding to the stress along the potential sliding surface in the slope. The horizontal shift of stress path is due to pore pressure increase corresponding to the rise of ground-water table. The increase of normal stress and shear stress caused by the rise of groundwater table was ignored for simplification. When the shear displacement began to increase, the shear box was changed to the undrained state, as indicated. The effect of closing the pore pressure supply appeared as slight decrease in pore pressure, because the average pore pressure in the shear box was a bit smaller than the supplied pore pressure. However, excess pore pressure was generated rapidly with the progress of shear displacement. Then, a rapid shearing began with the drop of shear resistance, as shown in Figures 6.5 (B, C). The mobilized apparent friction angle in the steady state was only 2.0° as shown in (A). After sufficient shearing at the steady state, the shear box was changed to the drained state. The stress

path shows that excess pore pressure dissipated. However, the mobilized shear resistance remained at a very low level. This indicates the pore pressure maintained in the shear zone although drainage from the shear zone should have occurred. When the pore pressure dissipates and the effective stress thus tends to increase, further grain crushing and comminution will take place, until a certain critical effective normal stress is reached. Under the critical effective stress, grain crushing does not occur. The volume (sample height) reduction after the change to the drained condition found in Figure 6.5(C) supports this interpretation.

Figure 6.6 shows the variation of excess pore pressure ratio and shear resistance with shear displacement. For the beginning to 10 mm of shear displacement, excess pore pressure ratio increased as the result of the simulation of the rise of groundwater table. Because of creep deformation, shear displacement of 10 mm was generated. After the shear box was switched to the undrained condition, because the "initial negative dilatancy" was completed, the excess pore pressure ratio decreased at once and shear resistance increased showing a behavior of "initial positive dilatancy" Thereafter, because of grain crushing, excess pore pressure was generated and shear resistance decreased rapidly with the progress of the shear displacement. When the shear displacement reached 1000 mm, the excess pore pressure ratio reached 0.85 and then became a constant. It is believed a "sliding-surface liquefaction" phenomenon took place.

6.3 SIMULATION TEST UNDER DRAINED CONDITION

To investigate the effect of grain crushing at the shear zone in this andesitic debris, another test using the original sample without sieving out grains smaller than 0.074 mm was performed, as shown in Figure 6.7. In this test, the pore pressure was gradually increased from the initial stress state of point "A" until the stress reached the failure line at point "B", at which point the shear displacement began to increase. However, the drained state of the shear box (upper drainage line was open) was still maintained after

the initiation of post-failure shear displacement (B-C), and the extent of decrease of the apparent friction angle after failure was observed. As seen in the stress path, the apparent friction angle decreased to 5.3°, even though it was slightly greater than the value of 2.0° determined in the undrained test of Figure 6.5. The upper drainage line was closed to measure the excess pore pressure after point "C" (bottom of the stress path) was reached, and the stress path reached the failure line at point "D" The excess pore pressure generated in the shear zone seemed to be distributed throughout the entire box. Because the effective stress should be the point "E" corresponding to the total stress point C, this estimation will need further examination. Permeability was measured before and after the test by supplying water from the bottom of shear box and monitoring the water discharge from the top of shear box. Therefore, this measured value of permeability was an average value that included the shear zone. The value changed from 1.0×10^{-4} cm/sec before the shear test to 4.8×10^{-7} cm/sec after the test.

In the drained condition, it is impossible to measure the pore pressure at the shear zone. Figure 6.8 shows the shear resistance and sample height change with the shear displacement during the drained period. The decrease of shear resistance can be looked as the increase of pore pressure. However, in the drained condition, the generated pore pressure would dissipate. If the rate of dissipation equals the rate of generation, the shear resistance would keep as a constant. From the beginning to 2 mm shear displacement, the sample height change shows a dilatancy, and in this phase, the shear resistance increased. From 2 mm to 15 mm, although the sample height change shows a contractive tendency, the shear resistance does not show so much change. It is estimated that the dissipation rate of pore pressure in this phase equals to the generation rate of excess pore pressure. From 15 mm, the shear resistance decreased rapidly to a very low value, about 27 kPa, and at the mean time, the sample height shrank rapidly also. It is verified that, grain crushing happened in the shear zone and it has two important functions. One is resulting in the pore pressure generation, another is to decrease the permeability of soil. Therefore, even in the drained condition, if the pore pressure

generation rate is faster than the dissipation rate of pore pressure, a localized "undrained condition" can be formed, and this will result in the "localized liquefaction" at the sliding surface.

After the test described above, the sample in the shear box was sheared for other purpose (including measurement of the friction angle, and so on) and the total shear displacement reached 113 m. Then the shear zone was exposed and carefully observed (Figure 6.9). The shear zone was very silty, while the samples above and below this layer were in their original states. Then, the sample from the shear zone was taken out to perform the grain size distribution analysis. Figure 6.10 shows the results in comparing with the original sample. It is obvious that remarkable grain crushing took place. The Marsal's particle breakage factor, *B*, for the andesitic sample sheared for 113 m is 74.8%, showing the andesitic soil has high susceptibility for grain crushing.

6.4 ANALYSIS

In the two experiments on the andesitic sample taken from the Harihara debris slide–debris flow, it was observed that it is even easier to develop grain crushing in the andesitic sample than in the Osaka-group coarse sandy soil. During the shearing, grain crushing happened, and it caused localized liquefaction in the shear zone and the decrease of the permeability. The formation of the soil structure, in which excess pore pressure is generated easily and is difficult to dissipate, was observed.

7. CONCLUSIONS

1. Comparing the results of the consolidated-drained ring shear tests and the consolidated-undrained ring shear tests on the three types samples: Toyoura standard sand, Silica sand, and Osaka-group coarse sandy soil, it was observed that, in sandy soils with higher grain crushing susceptibility, excess pore pressure generates easier in the undrained condition.

2. Along with the shear displacement, for dense crushable sandy soil, like Osaka-group coarse sandy soil, sample height change in drained condition and excess pore pressure generation in undrained condition can be divided to three phases. They are "initial negative dilatancy", "initial positive dilatancy" and "negative dilatancy due to grain crushing". The sample height change in the drained condition has a good correspondence to the excess pore pressure generation in the undrained condition. Based on this observation, the prediction of excess pore pressure generation based on sample height change result in the drained ring shear test becomes possible.

3. Study on the cyclic-loading behavior of sandy soils shows that: It is the grain crushing susceptibility of sandy soils that affects the residual excess pore pressure generation behavior after failure; the frequency of cyclic-loading has not so much obvious effect on the residual pore pressure generation with the shear displacement, but some small localized tendencies were observed; and the initial density state has some effects on the residual excess pore pressure

generation at the beginning period of shearing process. For a very long shear displacement until steady state is reached, only the sandy type (grain crushing susceptibility) mainly affects the pore pressure generation behavior.

4. In the geotechnical simulation test on the Nikawa landslide loaded with the real seismic wave of Hyogoken-Nambu earthquake, it was observed that, after the very short time of main shock, shear displacement also continued, and the "sliding-surface liquefaction" was achieved through the accumulation of the residual excess pore pressure caused by the grain crushing during shearing. In the other geotechnical simulation tests on the andesitic sample taken from the Harihara debris slide–debris flow, it was observed that it is even easier to take grain crushing than Osaka-group coarse sandy soil. During shearing, because of the localized liquefaction in the shear zone and the decrease of the permeability, the formation of a soil structure, in which excess pore pressure is generated easily and is difficult to dissipate, was observed.

5. It is confirmed that "sliding-surface liquefaction" is a localized liquefaction phenomenon. It depends on the behavior of grain crushing susceptibility of sandy soil when the soils are sheared for a long shear displacement. When the initial structure of sandy soils is medium or dense, it is impossible for the "sliding-surface liquefaction" to take place in those samples that are difficult to be crushed.

6. The mechanism of rapid landslide is proposed as: for a slope at a stress condition near critical state, with an external disturbance, such as earthquake or rainfall, the soil at the potential sliding surface would fail at first. This failure makes the soil mass move for a certain displacement. If the soil at the sliding surface is with high susceptibility for grain crushing, under the saturated undrained (even at localized undrained) condition, grain crushing caused by shearing will result in the generation of excess pore pressure, and in turn, cause a rapid landslide.

Contents of this thesis are based on papers as follows:

1. Wang, F. W. and Sassa, K. (1998): Experimental study on the factors affecting high-mobility of landslides by ring shear tests. Proceedings Eighth International IAEG (International Association of Engineering Geology and the Environment) Congress, Vancouver, Canada, 1998, pp. 1819-1826. (Chapter 4).
2. Wang, F. W., Sassa, K. and Fukuoka, H. (1998): Geotechnical simulation test for the Nikawa landslide induced by January 17, 1995 Hyogoken-Nambu earthquake. Soils and Foundations (submitted). (Chapter 5).
3. Sassa, K., Fukuoka, H. and Wang, F. W. (1998): Mechanism of rapid long run-out motion in the May 1997 Sumikawa reactivated landslide in Akita Prefecture and the July 1997 the Harihara debris slide–debris flow, Kagoshima Prefecture, Japan. Journal of Japan Landslide Society, Vol. 35, No. 2, pp. 29-37 (In Japanese with English abstract). (Chapter 6).

ACKNOWLEDGEMENTS

The author is deeply grateful to Professor Kyoji Sassa for his continuous encouragement and many suggestions that vitally contributed to the research.

A very sincere thanks is extended to Associate Professor Hiroshi Fukuoka for his assistance during testing.

The lectures on Landslides Dynamics by Professor Kyoji Sassa, Exploration Method in Landslide by Associate Professor Akira Suemine, and Dr. Atsuo Takeuchi, Geology by Professor Masahiro Chigira, Geomorphology by Professor Kazuo Okunishi, and Soil Dynamics by Professor Hideo Sekiuchi provided an important background for this investigation.

Deeply appreciate the encouragement given by Ashok Chugh of the US Bureau of Reclamation, Engineering and Research Division, Denver, Colorado.

Deep thanks are put forwards to the former and present post graduate students in the Landslide Section, Disaster Prevention Research Institute, Kyoto University.

Finally, the author wishes to acknowledge, with his most sincere gratitude, his family. His wife Shuzhen LI and his son Yang WANG are his sunshine in a foreign country.

BIBLIOGRAPHY

1. Arias, A. (1970): A measure of earthquake intensity. *Seismic Design for Nuclear Plants* (Hansen R. J. ed.), MIT Press, Cambridge, Mass., pp. 438-483.
2. Bellotti, R., Benoit, J., Fretti, C. and Jamiolkowshi, M. (1997): Stiffness of Toyoura sand from dilatometer tests. *ASCE Journal of Geotechnical and Geoenvironmental Engineering*, Vol. 123, No. 9, pp. 836-846.
3. Bishop, A. W., Green, G. E., Garga, V. K., Anderson, A. and Brown, J. D. (1971): A new ring shear apparatus and its application to the measurement of the residual strength. *Géotechnique*, Vol. 21, No. 4, pp. 273-328.
4. Bromhead, E. N. (1979): A simple ring shear apparatus. *Ground Engineering*, Vol. 12, No. 5, pp. 40-44.
5. Cao, B. L. (1986): The geologic characteristics of the Saleshan type of super-landslide and a model for spatial prediction. *Proc. of Fifth International Association of Engineering Geology International Congress*, Vol. 3, pp. 1989-1997.
6. Castro, G. (1969): *Liquefaction of Sands*. Harvard University, Cambridge, Harvard Soil Mechanics Series, No. 81.
7. Cruden, D. M. (1991): A simple definition of a landslide. *Bulletin of the International Association of Engineering Geology*, No. 43, pp. 27-29.
8. Cruden, D. M. and Varnes, D. J. (1996): Landslide types and processes. In Special Report 247: *Landslides -- Investigation and Mitigation.* (A.K. Turner and R.L. Schuster, eds.), TRB, National Research Council, Washington, D.C., Chap. 3, pp. 36-75.
9. Fukuoka, H. (1991): Variation of the friction angle of granular materials in the high-speed high-stress ring shear apparatus, -Influence of re-orientation, alignment and crushing of grains during shear-. *Disaster Prevention Research Institute Annuals*, Kyoto University, Vol.41, No.4, pp. 243-279.
10. Fukuoka, H., Wang, F. W. and Sassa, K. (1998): Ring shear test with real seismic

loading. *Proc. 1998 Annual Conference of the Japan Society of Erosion Control Engineering*, JSECE Publication No. 25. Sapporo, pp. 98-99 (in Japanese).

11. Fukushima, Y. and Tanaka, T. (1990): A new attenuation relation for peak horizontal acceleration of strong earthquake ground motion in Japan. *Bulletin of the Seismological Society of America*, Vol. 80, No. 4, pp. 757-783.
12. Fukushima, Y. and Tanaka, T. (1992): Revised attenuation relation for peak horizontal acceleration using a new data base. Programme and Abstracts of Seism. Soc, Japan, No.2, pp. 116 (in Japanese).
13. Geographical Survey Institute of Japan (1996): *Active Fault Map in Urban Area: Northwest Part of Osaka* (in Japanese).
14. Gibo, S. (1994): Ring shear apparatus for measuring residual strengths and its measurement accuracy. *Journal of Japan Landslide Society*, Vol. 31, No.3, pp. 24-30.
15. Groot, M. B. D. and Stoutjesdijk, T. P. (1997): Undrained stress path of loose sand predicted from dry tests. *Canadian Geotechnical Journal,* Vol. 34, pp. 131-138.
16. Hiura, H., Sassa, K., Kitera, N. and Ohte, K. (1985): Case study of the Nakaba liquefied landslide. *Proc. 4th Int. Conf. and Field Workshop on Landslides*, Tokyo, pp. 299-304.
17. Hutchinson, J. N. and Bhandari, R. K. (1971): Undrained loading, a fundamental mechanism of mudslide and other mass movements. *Géotechnique*, Vol. 21, No. 4, pp. 353-358.
18. Irikura, K. and Fukushima, Y. (1995): Attention characteristics of peak amplitude in the Hyogoken-Nambu earthquake, Journal of Natural Disaster Science, Vol. 16, No. 3, pp. 39-46.
19. Ishihara, K. (1993): Liquefaction and flow failure during earthquakes. *Géotechnique*, Vol. 43, No. 3, pp. 351-415.
20. Itihara, M. (1996): *The Osaka group layer and Chinese loess layer* (in Japanese). Tokyo: Chikuji-Shokan.

21. Kawasaki Geology Corporation (1995): *Field Investigation Report on the Nikawa Landslide.*

22. Kayen, R. E. and Mitchell, J. K. (1997): Assessment of liquefaction potential during earthquakes by Arias intensity. ASCE *Journal of Geotechnical and Geoenvironmental Engineering*, Vol. 123, No. 12, pp. 1162-1174.

23. Lade, P. V., Yamamura J. A. and Bopp, P. A. (1996): Significance of particle crushing in granular materials. *ASCE Journal of Geotechnical Engineering*, Vol. 122, No. 4, pp. 309-316.

24. Marsal, R. J. (1967): Large scale testing of rockfill materials. *ASCE Journal of Soil Mechanics and Foundations Division,* Vol. 93, No. SM2, pp. 27-43.

25. Marui, H., Sato, O. and Watanabe, N. (1996): Preliminary report on the Gamahara torrent debris flow of December 6, 1996, Japan. *Journal of Natural Disaster Science*, Vol. 18, No. 2, pp. 89-97.

26. Newmark, N. M. (1965): Effects of earthquakes on dams and embankments. *Géotechnique*, Vol. 15, No. 2, pp. 139-160.

27. Peacock, W. H. and Seed, H. B. (1968): Sand liquefaction under cyclic loading simple shear conditions. *ASCE Journal of Soil Mechanics and Foundations Division*, Vol. 94, No. SM3, pp. 689-708.

28. Popescu, R., Prevost J. H. and Deodatis, G. (1997): Effects of spatial variability on soil liquefaction: some design recommendations. *Géotechnique*, Vol. 47, No. 5, pp. 1019-1036.

29. Poulos, S. J. (1981): The steady state of deformation. *ASCE Journal of the Geotechnical Engineering Division*, Vol. 107, No. GT5, pp. 553-562.

30. Sassa, K., Shima, M., Hiura, H., Nakagawa, A. and Suemine, A. (1984): *Development of Ring Shear Type Debris Flow Apparatus*, Report of Grant-in-Aid for Scientific Research by Japanese Ministry of Education, Science and Culture (No. 57860028).

31. Sassa, K. (1985): The mechanism of debris flows. *Proceedings of XI Int'l*

Conference on Soil Mechanics and Foundation Engineering, Vol. 3, pp. 1173-1176. San Francisco.

32. Sassa, K., Fukuoka, H. and Vibert, C. (1989): A new high-speed high-stress ring shear apparatus and the undrained shear strength during motion, *Proc. The Japan-China Symposium on Landslides and Debris Flows*, Niigata and Tokyo, pp. 93-97.
33. Sassa, K. (1995): Keynote Paper: Access to the dynamics of landslides during earthquakes by a new cyclic loading ring shear apparatus. *Proceedings of 6th International Symposium on Landslide*, 1992, in "*Landslides*", Vol. 3, Rotterdam: Balkema, pp. 1919-1939.
34. Sassa, K., Fukuoka, H. and Sakamoto, T. (1995): The rapid and disastrous Nikawa landslide. *Landslide News* (Japan Landslide Society), No.9, pp. 6-9.
35. Sassa, K. (1996): Prediction of earthquake induced landslides, Special Lecture of 7th International Symposium on Landslides, "*Landslides*", Balkema, Vol. 1, pp. 115-132.
36. Sassa, K., Fukuoka, H., Scarascia-Mugnozza, G. and Evans, S. (1996): Earthquake-induced-landslides: Distribution, motion and mechanisms. Special Issue for the great Hanshin Earthquake Disasters, *Soil and Foundations*, pp. 53-64.
37. Sassa, K. (1997): A new intelligent type dynamic loading ring shear apparatus. *Landslide News* (Japanese Landslide Society), No. 10, pp. 33.
38. Sassa, K., Fukuoka, H. and Wang, F. W. (1997): Mechanism and risk assessment of landslide-triggered-debris flows: Lesson from the 1996.12.6 Otari debris flow disaster, Nagano, Japan. *Landslide Risk Assessment* (ed. Cruden and Fell), *Proceedings of the Int'l Workshop on Landslide Risk Assessment*, pp. 347-356. Rotterdam: Balkema.
39. Sassa, K. (1998): Mechanisms of landslide triggered debris flow. *Environmental Forest Science* (Sassa, K. ed.), *Proceedings of IUFRO Div. 8 Conference*, Kyoto, Kluwer Academic Publisher, pp. 471-490.
40. Sassa, K., Fukuoka, H. and Wang, F. W. (1998a): A rapid landslide-debris flow at

Izumi City, Kagoshima, Japan, 1997. *Landslide News* (Japanese Landslide Society), No. 11, pp.1-6.

41. Sassa, S. and Sekiguchi, H. (1998b): Wave-induced liquefaction of beds of sand in a centrifuge. *Géotechnique*, in press.
42. Seed, H. B. (1968): Landslides during earthquakes due to soil liquefaction. *ASCE Journal of Geotechnical Engineering Division*, Vol. 94, No. SM5, pp. 1055-1122.
43. Shimokawa, E. (1997): The Harihara river debris flow disaster, Izumi City. *Proceedings of 35th Mountain Conservation Symposium,* pp. 29-37 (in Japanese).
44. Shoaei, Z. and Sassa, K. (1994): Basic study on the shear behavior of landslides during earthquakes: Excess pore pressure generation in the undrained cyclic loading ring shear tests. *Bulletin of the Disaster Prevention Research Institute, Kyoto University*, Vol. 44, Part 1, pp. 1-44.
45. Skempton, A. W. (1954): The pore-pressure coefficient A and B. *Géotechnique*, Vol. 4, No. 4, pp. 143-147.
46. Sladen, J. A., D'Hollander, R. D. and Krahn, J. (1985): The liquefaction of sands, a collapse surface approach. *Canadian Geotechnical Journal,* Vol. 22, pp. 564-578.
47. Tatsuoka, F., Toki, S., Miura, S., Kato, H., Okamoto, M., Yamada, S., Yasuda, S. and Tanizawa, F. (1986): Some factors affecting cyclic undrained triaxial strength of sand. *Soils and Foundations*, Vol. 26, No. 3, pp. 99-116.
48. Terzaghi, K. and Peck, R. B. (1948): *Soil Mechanics in Engineering Practice.* 2nd edn, pp. 108-115. Chichester: Wiley.
49. The Japanese Geotechnical Society (1990): *Standard Methods for the Geotechnical Tests*, pp. 43-115.
50. Tika, T. E., Vaughan, P. R. and Lemos, L. J. L. J. (1996): Fast shearing of pre-existing shear zones in soil. *Géotechnique*, Vol. 46, No. 2, pp. 197-223.
51. Vankov, D. A. and Sassa, K. (1998): Energy approach to evaluation of grain crushing. *Environmental Forest Science* (Sassa, K. ed.), *Proceedings of IUFRO Div. 8 Conference*, Kyoto, Kluwer Academic Publisher, pp. 615-622.

52. Wang, F. W. and Tan, Z. D. (1991): The forming mechanism and sliding character of the 1985.6.12 Xintan landslide, Three-gorge area, China. *Journal of Yangtze River Scientific Research Institute*, Vol. 8, No.3, pp. 28-34 (in Chinese).

53. Wang, F. W. and Sassa, K. (1997a): Experimental study on the earthquake induced landslide displacement: effects of saturated condition and sand type. *Proceedings International Symposium on Landslide Hazard Assessment*, Xian, pp. 225-240.

54. Wang, F. W. and Sassa, K. (1997b): Shear displacement behavior of sandy soils in different states of saturation and the seismic coefficient in cyclic-loading ring shear tests. *Journal of Natural Disaster Science,* Vol. 19, No. 1, pp. 31-45.

55. Wang, F. W. and Sassa, K. (1998a): Experimental study on the factors affecting high-mobility of landslides by ring shear tests. *Proceedings 8th International Association of Engineering Geology and the Environment International Congress*, Rotterdam: Balkema, Vol.3, pp. 1819-1826.

56. Wang, F. W. and Sassa, K. (1998b): Ring shear tests on sliding-surface liquefaction behavior of sandy soils, *Disaster Prevention Research Institute Annuals*, Kyoto University, No. 41, B-2, 16p (in Press).

57. Wang, F. W., Sassa, K. and Fukuoka, H. (1998c): Cyclic-loading ring shear tests to study high-mobility of earthquake-induced-landslides. *Environmental Forest Science* (Sassa, K. ed.), *Proceedings of IUFRO Div. 8 Conference*, Kyoto, Kluwer Academic Publisher, pp. 575-582.

58. Yoshimi, Y. and Oh-oka, H. (1975): Influence of degree of shear stress reversal on the liquefaction potential of saturated sand. *Soils and Foundations*, Vol. 15, No. 3, pp. 27-40.

59. Zhang, D. X. and Sassa, K. (1992): The mechanism of movement in the Saleshan landslide 1983 in China. *Disaster Prevention Research Institute Annuals*, Kyoto University, No. 35 B-1, pp. 95-112 (in Japanese).

60. Zhang, D. X. (1996): A study on the mechanism of loess landslides induced by earthquakes. *Journal of Natural Disaster Science*, Vol. 18, No. 1, pp. 27-41.

CAPTIONS

Tables

Table 2.1 The most important features of the DPRI Ver.5 and Ver.6 ring shear apparatus.

Table 3.1 Classification and index properties of the employed samples.

Table 4.1 Relative density and compression index C_c of test samples in the drained ring shear tests and the undrained ring shear tests.

Table 4.2 Sample relative densities and amplitude of cyclic-loading for the consolidated undrained cyclic-loading ring shear tests.

Table 5.1 Physical properties of the test sample of the Osaka-group coarse sandy soil.

Figures

Figure 1.1 Stress path and illustration of (mass) liquefaction and "sliding-surface liquefaction" (modified from Sassa et al. 1996).
P.F.L.: Peak failure line, R.F.L.: Residual failure line.

Figure 1.2 Definition of Marsal's breakage factor, *B*. It is a sum of the difference having the same sign based on the grain size distribution analysis results of original sample and tested sample (modified from Vankov et al. 1998).

Figure 2.1 Photograph of the DPRI Ver.6 ring shear apparatus.

Figure 2.2 Electronic control system for the ring shear apparatus.

Figure 2.3 Schematic structure of the DPRI Ver.6 ring shear apparatus.

Figure 2.4 A half section of the undrained shear box and the pore pressure measurement.

Figure 3.1 Ring shear test results for residual friction angle on three samples (shear speed = 3 mm/sec). a) O-sample, D_r = 117.6%; b) T-sample, D_r = 34.8% and c) S-sample, D_r = 59.3%.

Figure 4.1 Schematic diagram of the cyclic-loading ring shear tests.

A_0: Initial stress state in dry condition. $\sigma_0 = W\cos\theta$, $\tau_0 = W\sin\theta$;

P_0: Initial stress state when initial pore pressure, u_0, exists;

Critical stress increment K_cW: $\triangle\sigma_c = -K_cW\sin\theta$, $\Delta\tau_c = K_cW\cos\theta$.

Figure 4.2 Stress pattern used in the cyclic-loading tests (case of frequency = 0.1 Hz).

Figure 4.3 Grain-size distribution of samples after consolidation and samples taken from shear zone after shear finished.

Dotted line: sample after consolidation; solid line: sample from shear zone after shearing.

Figure 4.4 Sample height change during consolidated drained constant speed ring shear tests. D_r for T-sample was 39.7%, for S-sample was 60.8%, for O-sample (loose) was 87.1% and for O-sample (dense) was 100.8%. The numbers in bracket show the sample height at the beginning of shearing.

Figure 4.5 Relationships between final sample height change and Marsal's breakage factors, B, as well as the compression index, C_c of samples at a certain relative density.

Figure 4.6 Excess pore pressure ratio of various samples in consolidated-undrained constant-speed ring shear test.

Shear speed = 3 mm/sec. D_r for T-sample was 45.9%, for S-sample was 63.6%, for O-sample (loose) was 93.5% and for O-sample (dense) was 98.0%.

Figure 4.7 Stress path of various samples in consolidated undrained constant speed ring shear test.

Shear speed = 3 mm/sec. (a) O-sample (loose), (b) O-sample(dense), (c) T-sample and (d) S-sample.

Figure 4.8 Process showing pore pressure divided to cyclic component and residual component, and the definition of "residual excess pore pressure ratio" (with the data of O-F(0.1)-25°).

Figure 4.9 Residual excess pore pressure ratio generated in the consolidated undrained cyclic-loading tests on O-sample (loose), T-sample and S-sample at K/K_c = 1.5 with cyclic frequency = 0.1 Hz.

Figure 4.10 Residual excess pore pressure ratio generated in the undrained cyclic-loading tests on O-sample (loose) at frequencies of 0.02 Hz, 0.1 Hz and 0.5 Hz at K/K_c = 1.5.

Figure 4.11 Residual excess pore pressure ratio generated in the consolidated undrained cyclic-loading tests on loose O-sample (loose) at K/K_c = 1.5, 0.1 Hz and O-sample (dense) at K/K_c = 2.0, 0.1 Hz.

Figure 4.12 Comparison of sample height change in the consolidated drained ring shear test and excess pore pressure ratio in the consolidated undrained ring shear test on O-sample (dense).

Figure 5.1 Photo of the Nikawa landslide (Taken by K. Sassa, 1995.1.21).

Figure 5.2 Plan of the slope before the Nikawa landslide occurred and the outline of the landslide area (from Sassa et al. 1996).

Figure 5.3 Geological section of the Nikawa landslide along A-A' line in Fig. 5.2 (from Sassa et al. 1995).

Figure 5. 4 The synthesizing procedure from seismic loading to normal stress and shear stress.

(a): Transfer the horizontal (EW and NS) components to the horizontal slope direction.

(b): Transfer the horizontal component along the slope direction and the vertical component (UD) to the component along the sliding surface.

(c): Sum up the initial stress (W) and the increments of normal stress ($\Delta\sigma$) and shear stress ($\Delta\tau$) acting on the sliding surface by multiplying acceleration and mass of the soil columns.

Figure 5.5 Loading stresses on the sample of the simulation test on the Nikawa

landslide.

(a): Normal stress, (b): Shear stress

Figure 5.6 Stress path of the control signal in the simulation test on the Nikawa landslide.

The residual failure line obtained from the geotechnical simulation test.

Figure 5.7 Time-series data of the simulation test on the Nikawa landslide.

$B_D = 0.97$, $D_r = 147.2$ percent

(a): Normal stress; (b): Pore pressure; (c): Shear resistance and shear displacement

Figure 5.8 Time series data during the main shock in the simulation test on the Nikawa landslide.

$B_D = 0.97$, $D_r = 147.2$ percent

(a): Normal stress; (b): Pore pressure; (c): Shear resistance and shear displacement

Figure 5.9 The stress path for the simulation test on the Nikawa landslide.

ESP: Effective stress path, TSP: Total stress path

$B_D = 0.97$, $D_r = 147.2$ percent

Figure 5.10 The relation of residual excess pore pressure ratio with the shear displacement in the simulation test on the Nikawa landslide.

Figure 5.11 Sample height change with the shear displacement of Osaka-group coarse sandy soil taken from the Nikawa landslide under the drained ring shear test. Normal stress = 196 kPa, shear speed = 3 mm/sec. Initial relative density = 152.8 percent

Figure 5.12 Photograph of the sample after sheared for 42 m in the drained test.

A trench cut in the shear box. Pins show the upper and lower boundary of the grain crushing zone

Figure 5.13 Grain size distribution analysis results for the original sample, sample at the shear zone, at the upper part and the lower part of the shear box after

sheared for 42 m under 196 kPa normal stress, shear speed = 3 mm/sec.

Figure 6.1 Location and plan of the Harihara debris slide–debris flow (from Sassa et al. 1998).

Figure 6.2 Aerial oblique view of the Harihara debris slide–debris flow (from Sassa 1998).

Figure 6.3 Plan of the initial landslide in the Harihara debris slide–debris flow (from Sassa et al. 1998).

Figure 6.4 Longitudinal section along the moving path of the landslide mass in the Harihara debris slide–debris flow (from Sassa et al. 1998).

Figure 6.5 Ring-shear test results for the andesitic debris from the Harihara debris slide–debris flow (from Sassa et al. 1998).

The shear box was switched from the drained state to the undrained state immediately after the initiation of failure, and returned to the drained state after the steady state of shearing. $B_D = \Delta u / \Delta \sigma = 0.96$

a) Stress path, b) Time series data of normal stress, pore pressure and shear resistance, c) Time series data of shear displacement, sample height and shear speed.

Figure 6.6 Excess pore pressure ratio and shear resistance change with shear displacement in the undrained period in the test of Fig. 6.5.

Figure 6.7 Test results for the andesitic debris (from Sassa et al. 1998).

The shear box was maintained in the drained state after the initiation of failure. It then was changed to the undrained state after the shear-resistance value had almost stabilized. $B_D = \Delta u / \Delta \sigma = 0.96$

a) Stress path, b) Time series data of stress.

Figure 6.8 Shear resistance and sample height change with shear displacement in the drained period in the test for the Harihara debris slide–debris flow of Fig. 6.7.

Figure 6.9 Photo of section through the shear zone after the test of Fig. 6.7 (from Sassa et al. 1998).

Pins show the border between the shear zone and less-disturbed zones. The shear zone was very silty. The total shear displacement was 113 m.

Figure 6.10 Results of grain size distribution analysis on the original andesitic sample from the Harihara debris slide–debris flow and the sample at the shear zone in the shear box after shear for 113 m.

Table 2.1 The most important features of the DPRI Ver.5 and Ver.6 ring shear apparatuses.

	Ver.5	Ver.6
Shear box		
-inner diameter (mm)	120	250
-outer diameter (mm)	180	350
Maximal normal stress (MPa)	1.0	2.0
Maximal shear speed (cm/sec)	10	214
Resolution of gap control system (mm)	0.001	0.001
Maximum data acquisition rate (readings/sec)	200	200
Maximum frequency of cyclic-loading (Hz)	5	5
Possibility of undrained test	Yes	Yes
Possibility of simulation of monitored seismic wave records by normal stress and shear stress	Yes	Yes
Automatic safeguard and alarm system for mishandling	Yes	Yes

Table 3.1 Classification and index properties of the employed samples.

Classification property	T-sample	S-sample	O-sample
Mean grain size, D_{50} (mm)	0.18	0.16	0.80
Effective grain size, D_{10} (mm)	0.11	0.09	0.28
Uniformity coefficient, U_c	1.7	2.1	4.7
Maximum void ratio, e_{max}	0.98	1.30	1.17*
Minimum void ratio, e_{min}	0.61	0.71	0.66*
Specific gravity, Gs	2.64	2.64	2.61
Residual friction angle, ϕ (degree)	32.8	32.8	34.5

* Not standard test result.

** Based on the normal-consolidated constant-speed ring shear test.

Table 4.1 Relative density and compression index C_c of test samples in the drained ring shear tests and the undrained ring shear tests.

Test type	Sample	D_{ri}(%)	C_c	D_r(%)
Drained Ring Shear Test	T-sample	21.6	0.037	39.7
	S- sample	40.7	0.047	60.8
	O- sample (loose)	2.94	0.066	87.1
	O- sample (dense)	81.4	0.103	100.8
Undrained Ring Shear Test	T-sample	25.1		45.9
	S- sample	38.8		63.6
	O- sample (loose)	2.94		93.5
	O- sample (dense)	81.4		98.0

Table 4.2 Sample relative densities and amplitude of cyclic-loading for the consolidated undrained cyclic-loading ring shear tests.

Test No.	D_{ri}(%)	D_r(%)	ϕ (°)	K_c	$\Delta\sigma$ (kPa)	$\Delta\tau$ (kPa)
T-F(0.1)-25°	32.7	43.2	32.8	0.128	48.5	104.1
S-F(0.1)-25°	51.6	67.8	32.8	0.128	48.5	104.1
O-F(0.1)-25°	22.8	111.1	34.5	0.157	59.7	128.1
O-F(0.5)-25°	22.8	117.6	34.5	0.157	59.7	128.1
O-F(0.02)-25°	22.8	115.4	34.5	0.157	59.7	128.1
O(Dense)-F(0.1)-25° (K/K_c = 1.5)	111.2	119.8	34.5	0.157	59.7	128.1
O(Dense)-F(0.1)-25°(K/K_c = 2)	111.2	119.8	34.5	0.157	79.6	170.8

Table 5.1 Physical properties of the test sample of the Osaka-group coarse sandy soil.

Specific gravity, G_s	2.60
Maximum void ratio, e_{max}	1.57*
Minimum void ratio, e_{min}	0.90*
Uniformity coefficient, U_c	75
Average grain size, D_{50}	0.50 mm

*: Not standard test result.

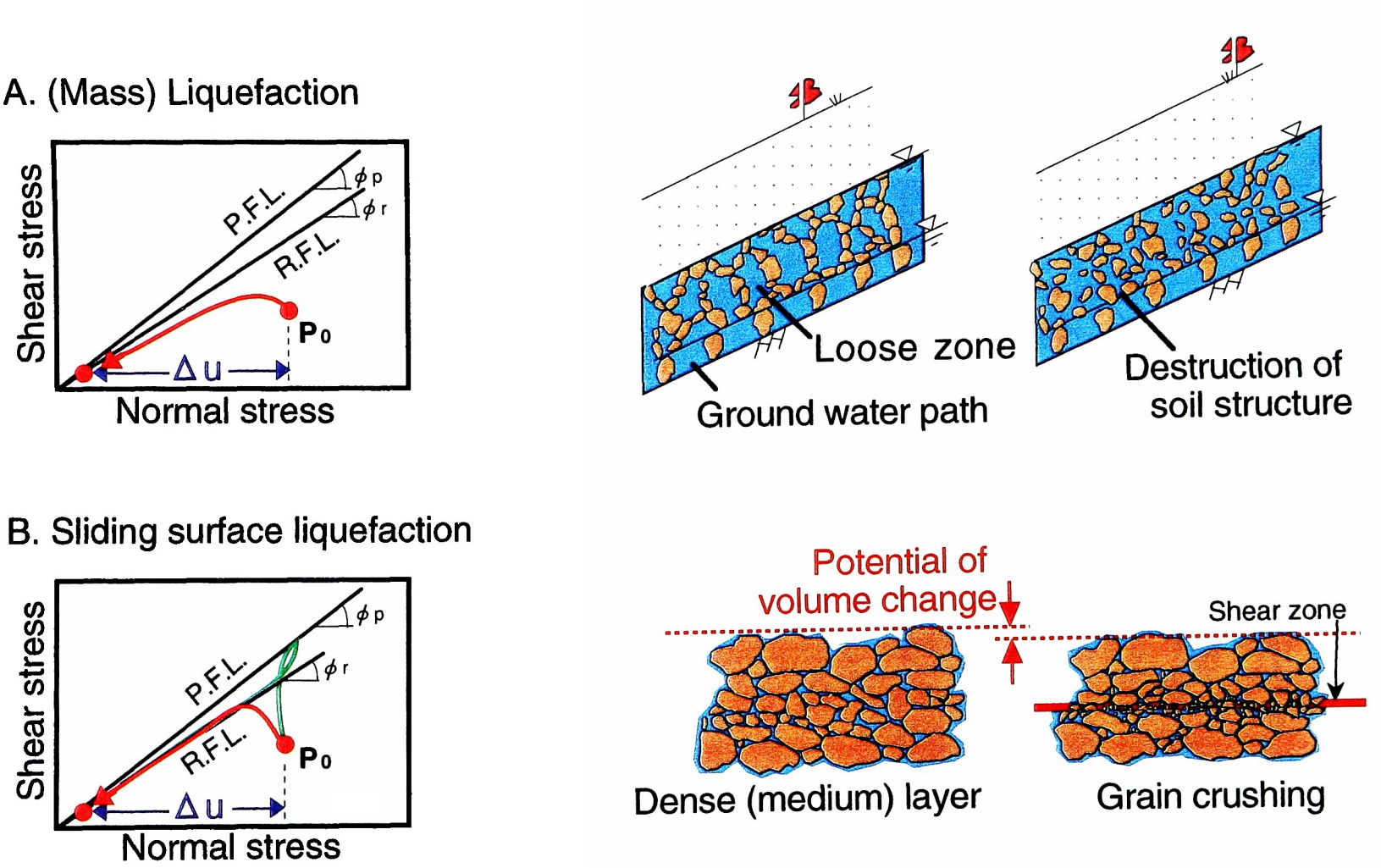

Figure 1.1 Stress path and illustration of (mass) liquefaction and "sliding surface liquefaction" (modified from Sassa et al. 1996).

P.F.L.: Peak failure line; R.F.L.: Residual failure line

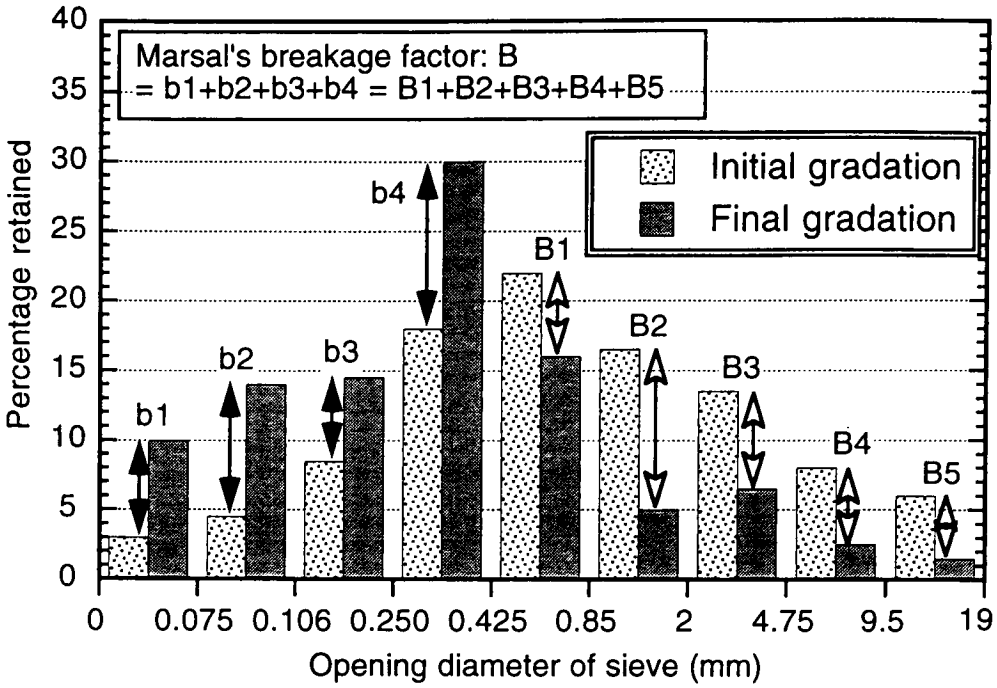

Figure 1.2 Definition of Marsal's breakage factor, *B*. It is a sum of the difference having the same sign based on the grain size distribution analysis results of original sample and tested sample (modified from Vankov et al. 1998).

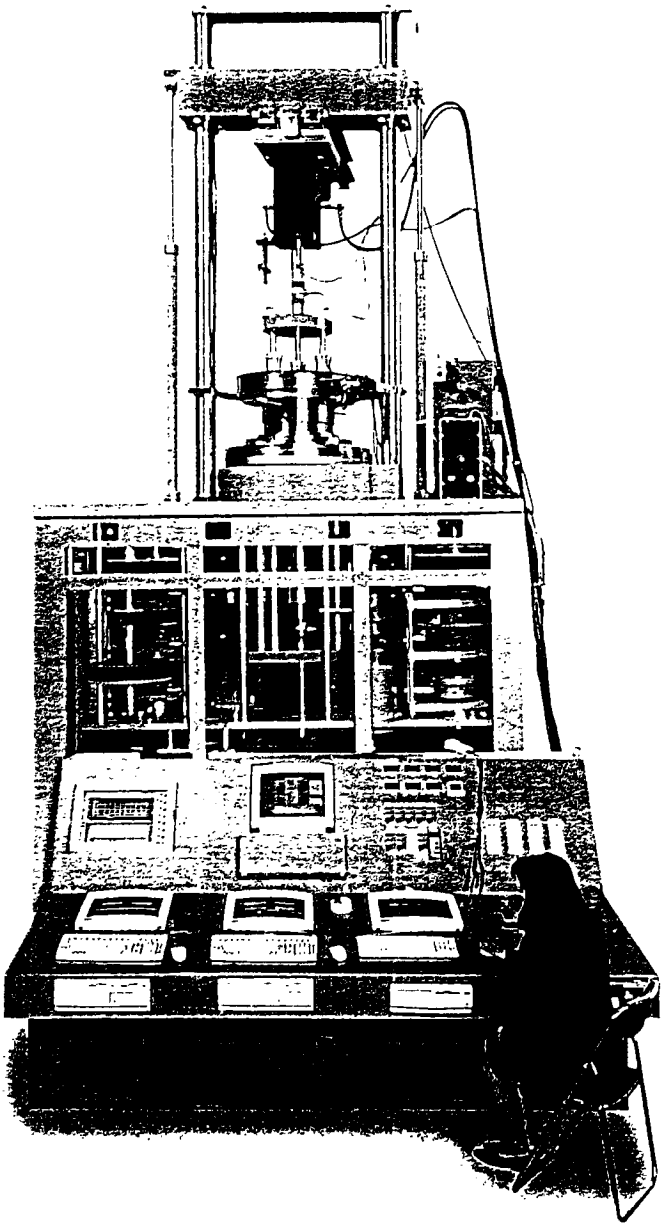

Figure 2.1 Photograph of the DPRI Ver.6 ring shear apparatus.

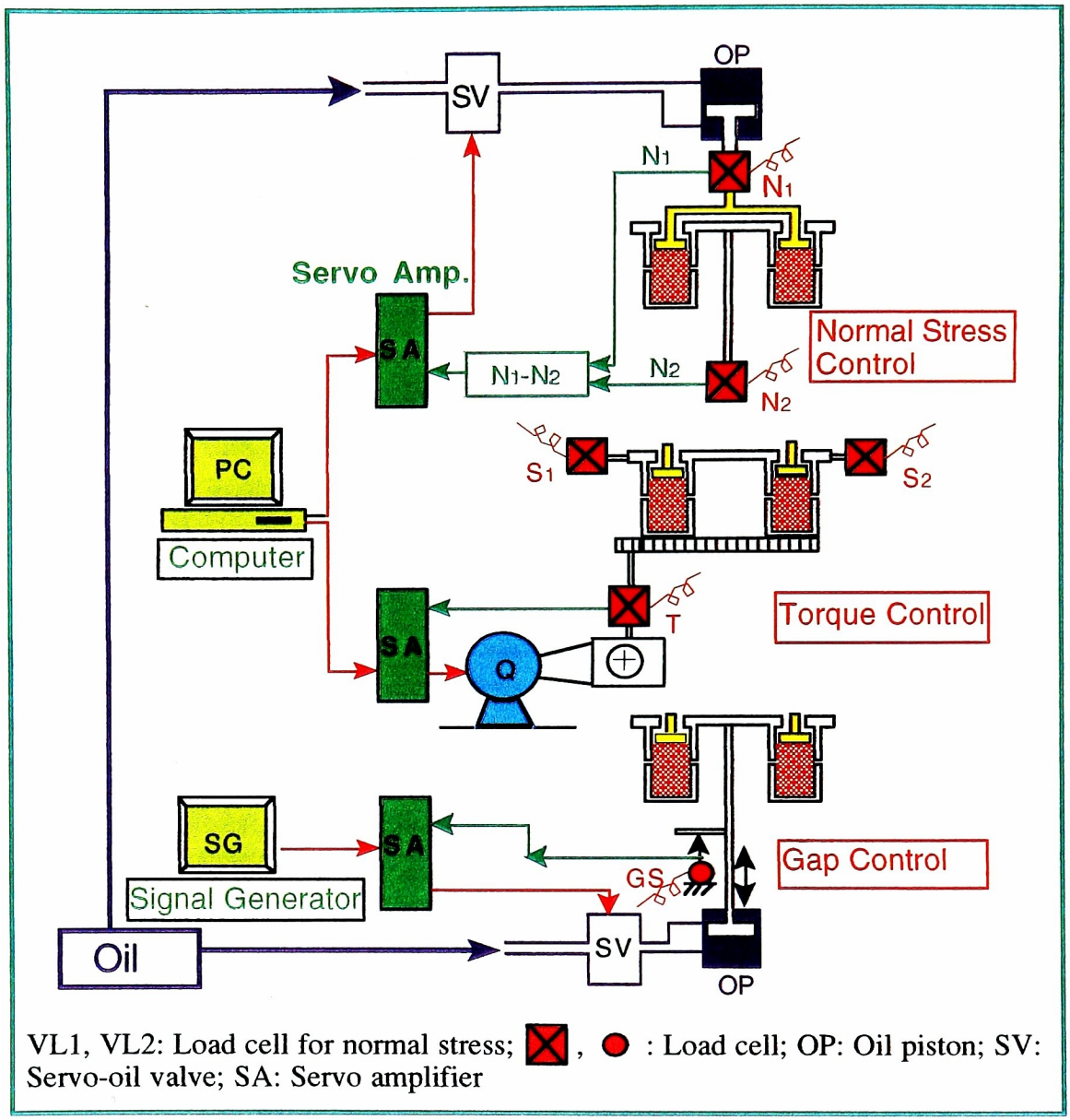

VL1, VL2: Load cell for normal stress; ⊠ , ● : Load cell; OP: Oil piston; SV: Servo-oil valve; SA: Servo amplifier

Figure 2.2 Electronic control system for the ring shear apparatus.

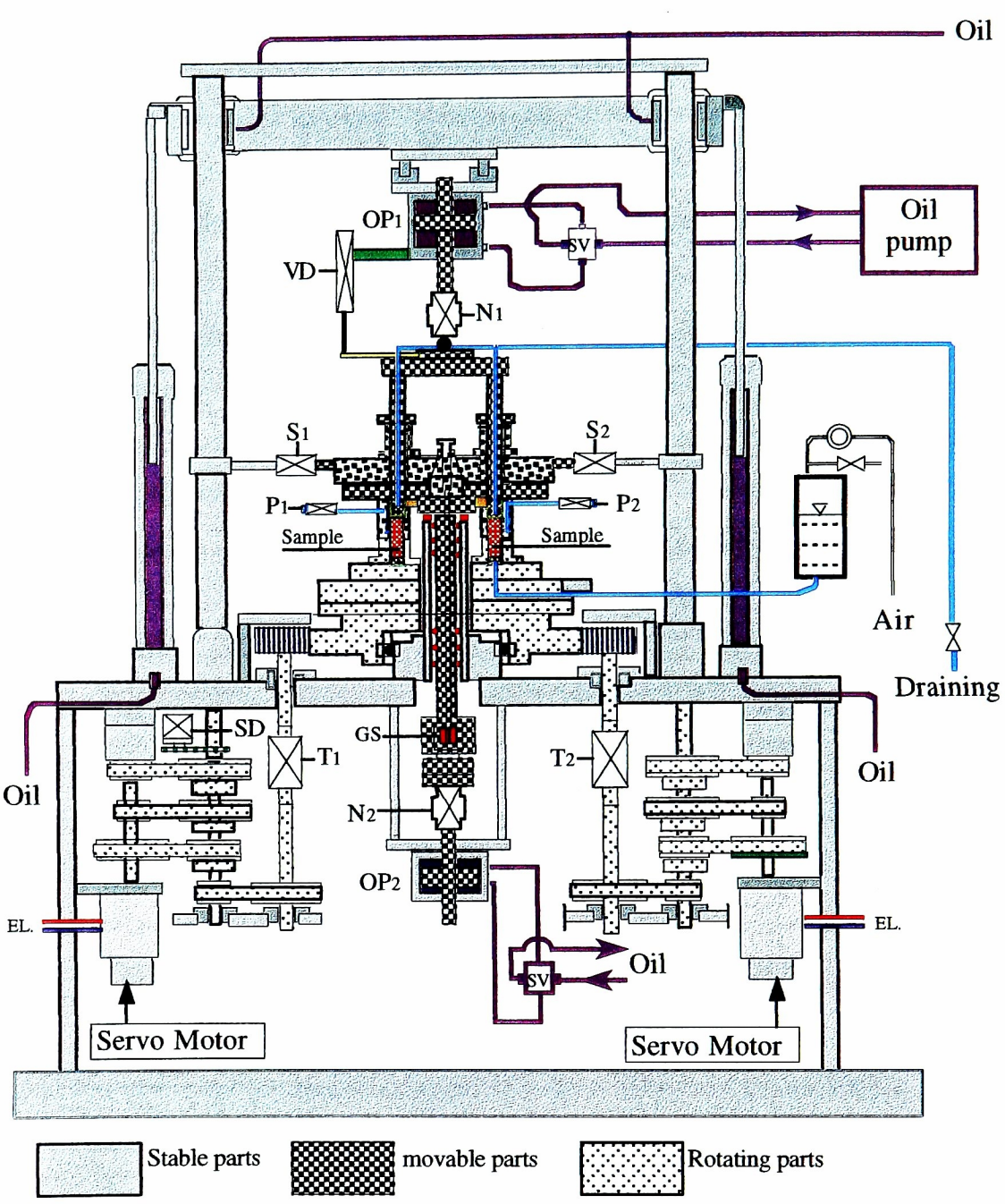

N_1, N_2: Load cell for normal stress; S_1, S_2: Load cell for shear resistance; P_1, P_2: Pore-pressure transducer; GS: gap sensor; OP1, OP2: Oil piston; VD: Vertical displacement meter; SD: Shear displacement meter; T_1, T_2: Load cell for Torque

Figure 2.3 Schematic structure of the DPRI Ver.6 ring shear apparatus.

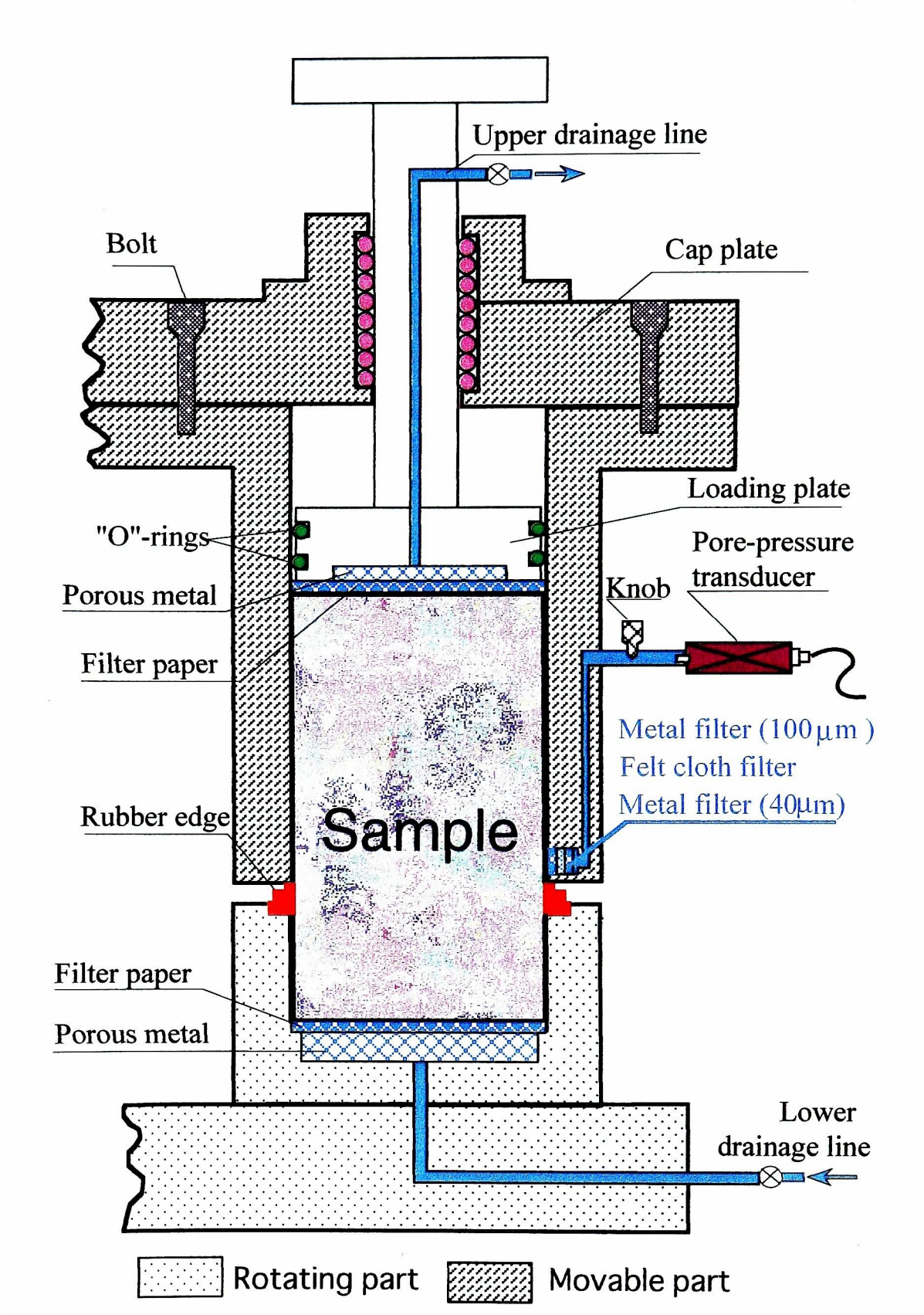

Figure 2.4 A half section of the undrained shear box and the pore pressure measurement.

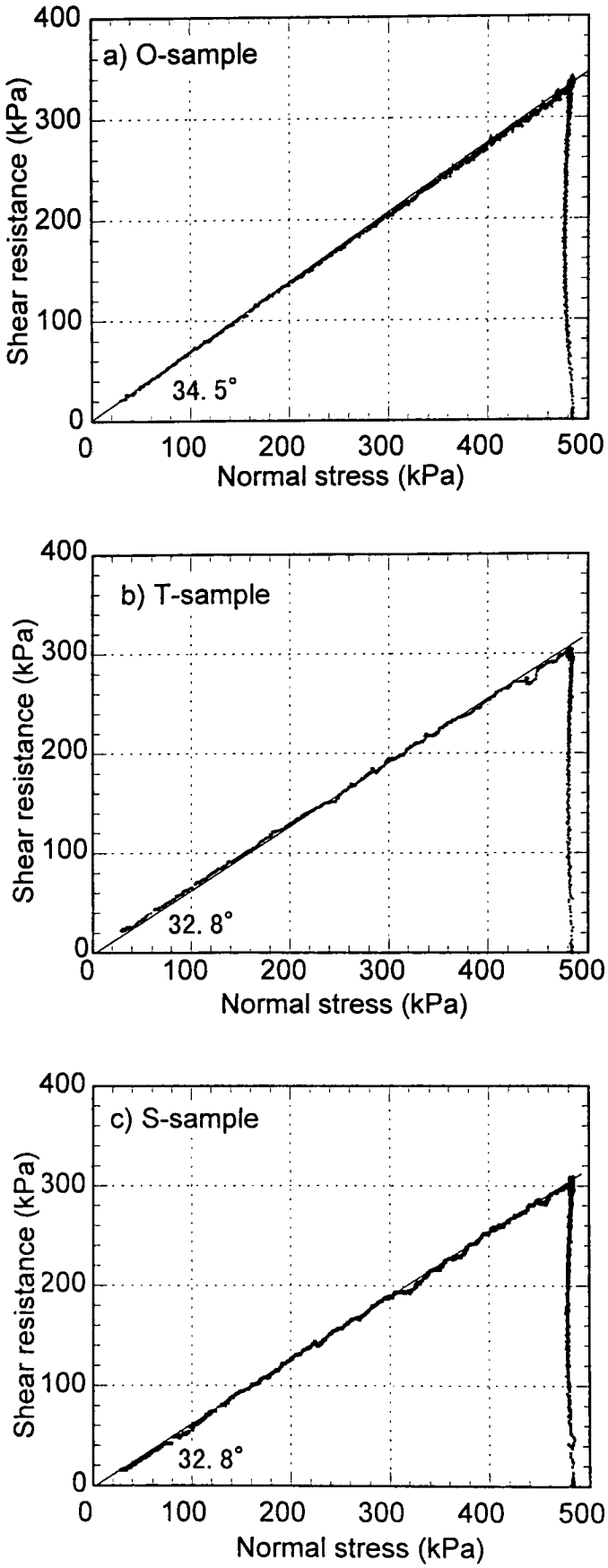

Figure 3.1 Ring shear test results for residual friction angle on three samples (shear speed = 3 mm/sec). a) O-sample, D_r = 117.6%; b) T-sample, D_r = 34.8% and c) S-sample, D_r = 59.3%.

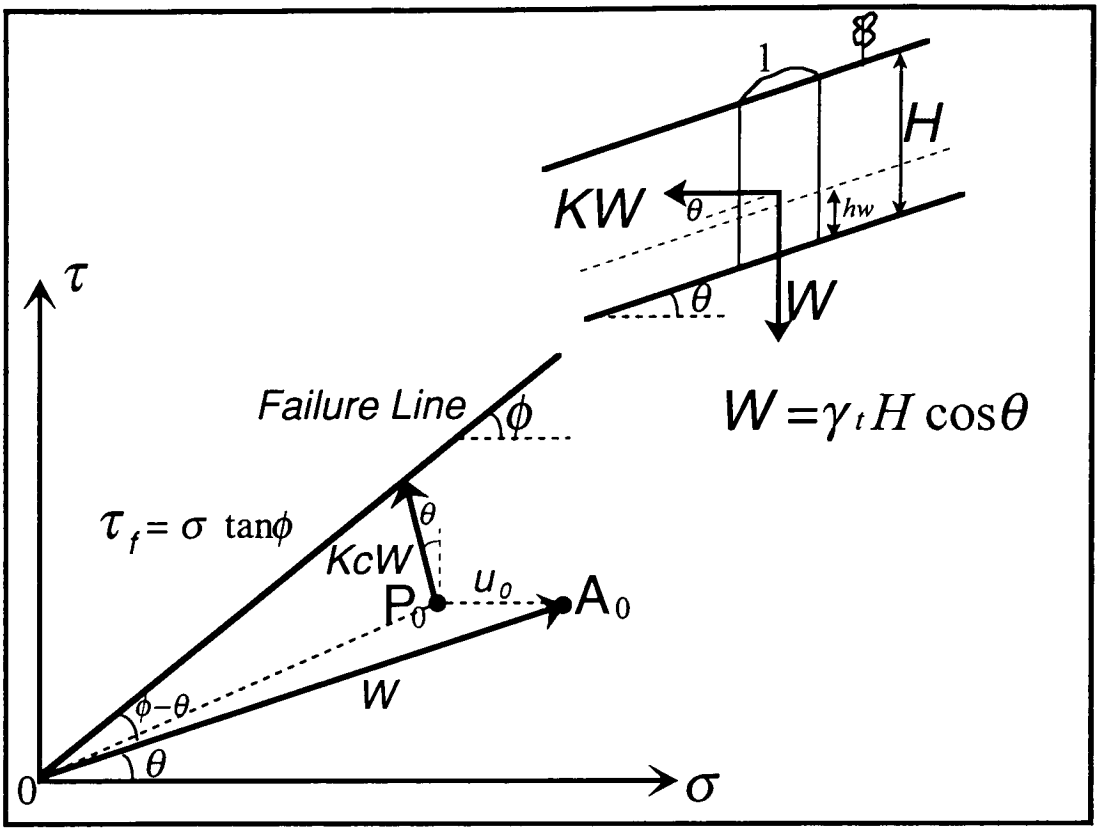

Figure 4.1 Schematic diagram of the cyclic-loading ring shear tests.

A_0: Initial stress state in dry condition. $\sigma_0 = W\cos\theta$, $\tau_0 = W\sin\theta$;

P_0. Initial stress state when initial pore pressure, u_0, exists;

Critical stress increment K_cW: $\Delta\sigma_c = -K_cW\sin\theta$, $\Delta\tau_c = K_cW\cos\theta$.

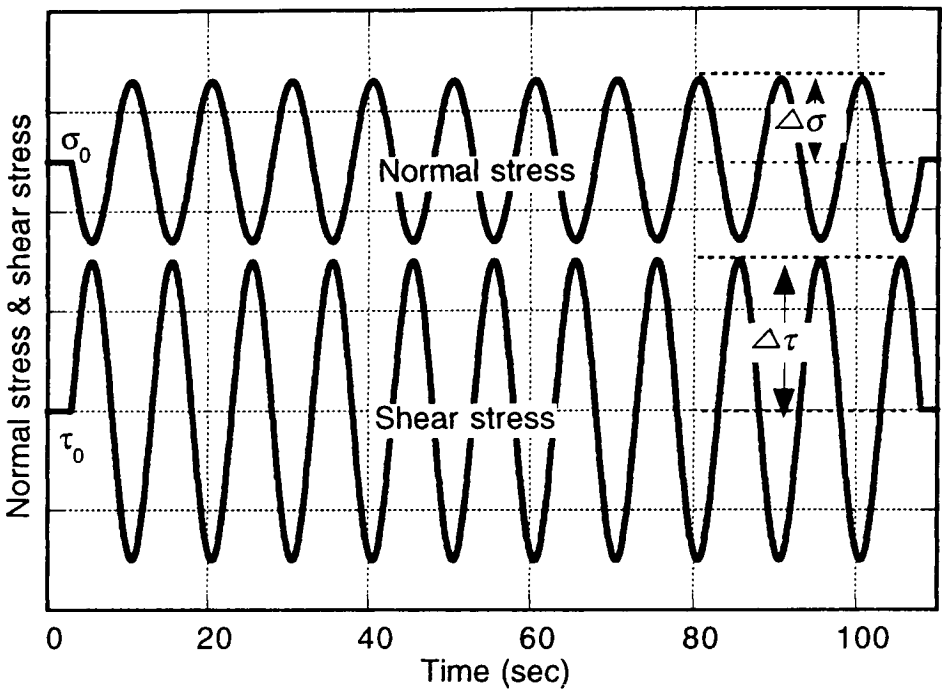

Figure 4.2 Stress pattern used in the cyclic-loading tests (case of frequency = 0.1 Hz).

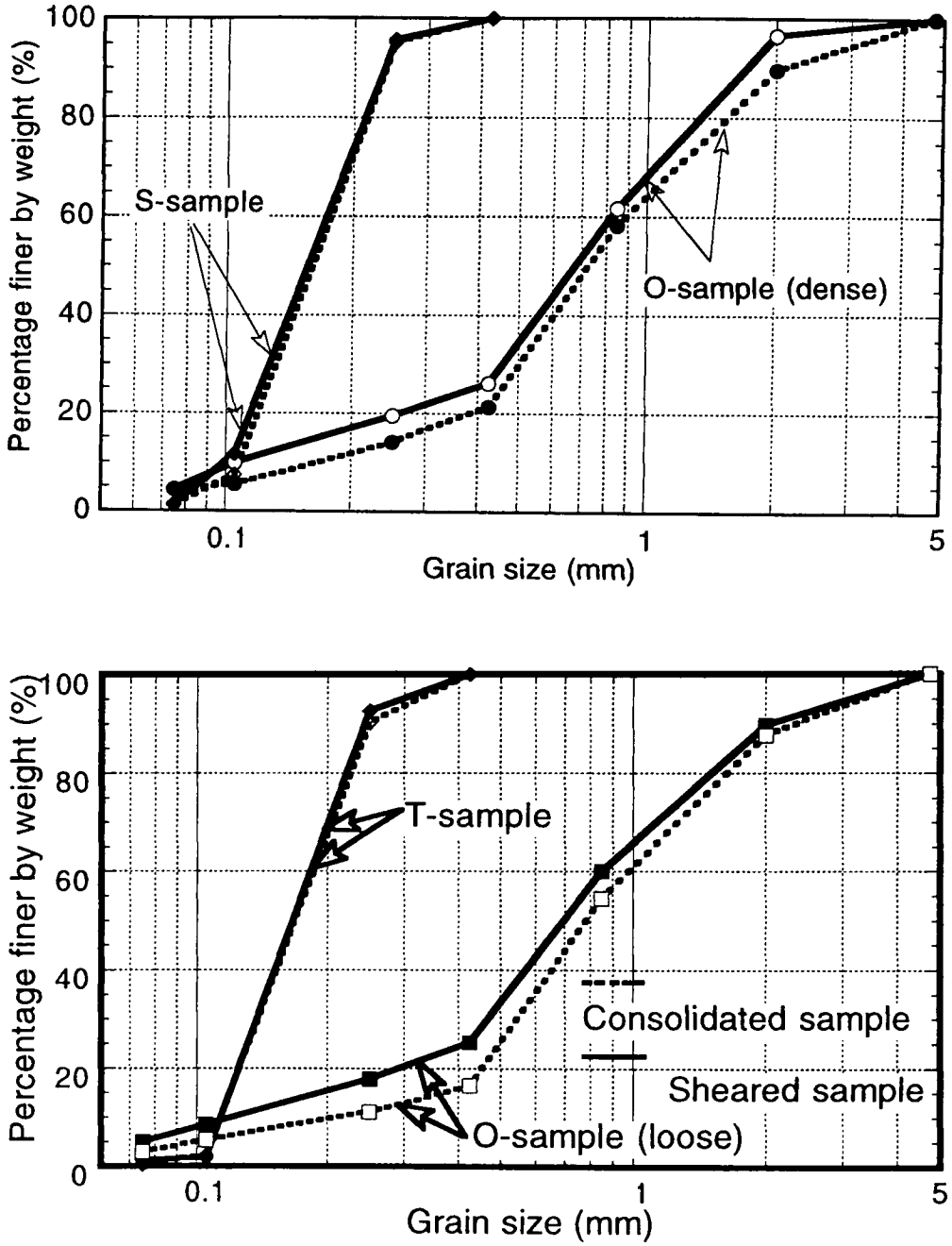

Figure 4.3 Grain-size distribution of samples after consolidation and samples taken from shear zone after shear finished.

Dotted line: sample after consolidation; solid line: sample from shear zone after shearing.

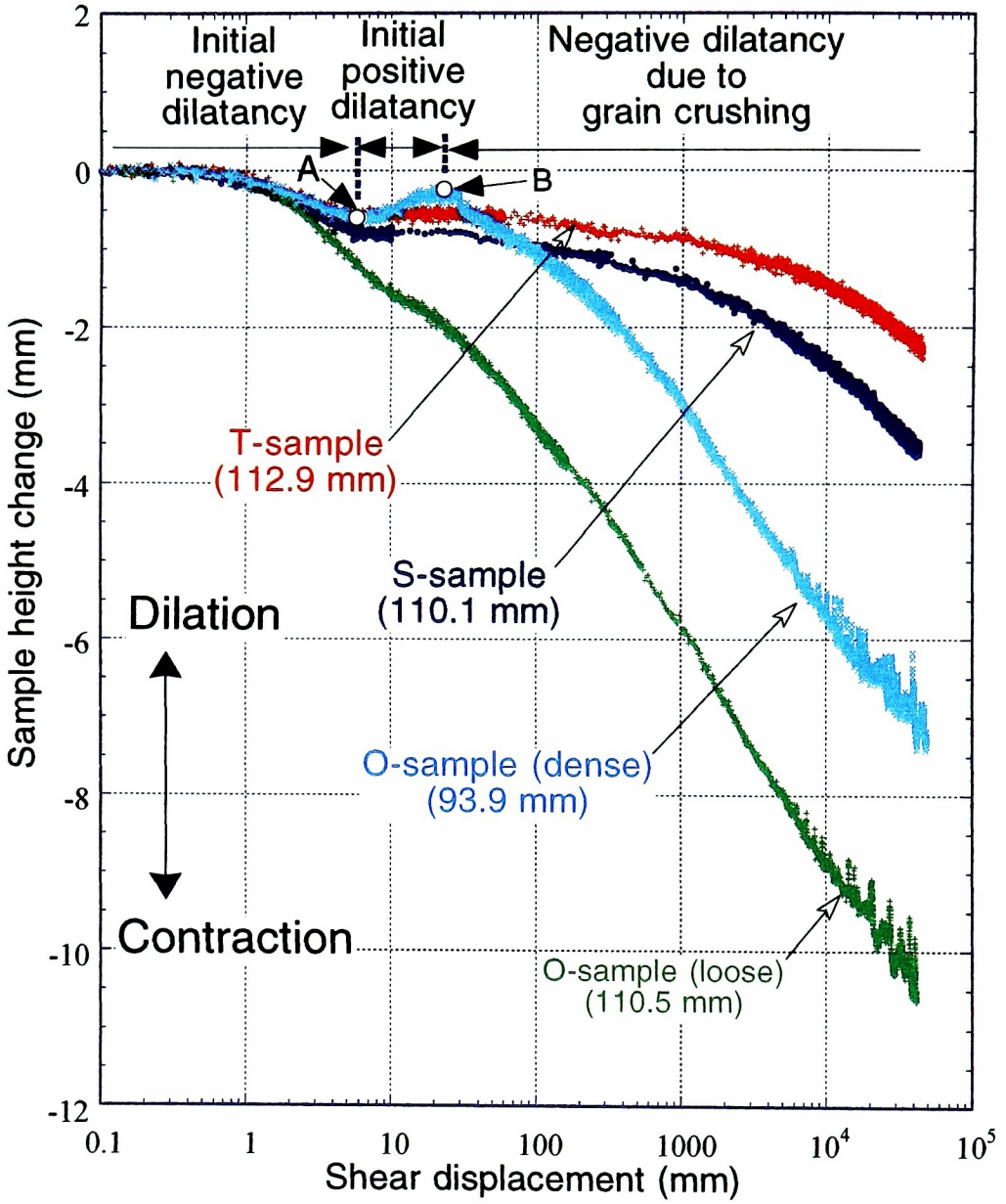

Figure 4.4 Sample height change during consolidated drained constant speed ring shear tests. D_r for T-sample was 39.7%, for S-sample was 60.8%, for O-sample (loose) was 87.1% and for O-sample (dense) was 100.8%. The numbers in bracket show the sample height at the beginning of shearing.

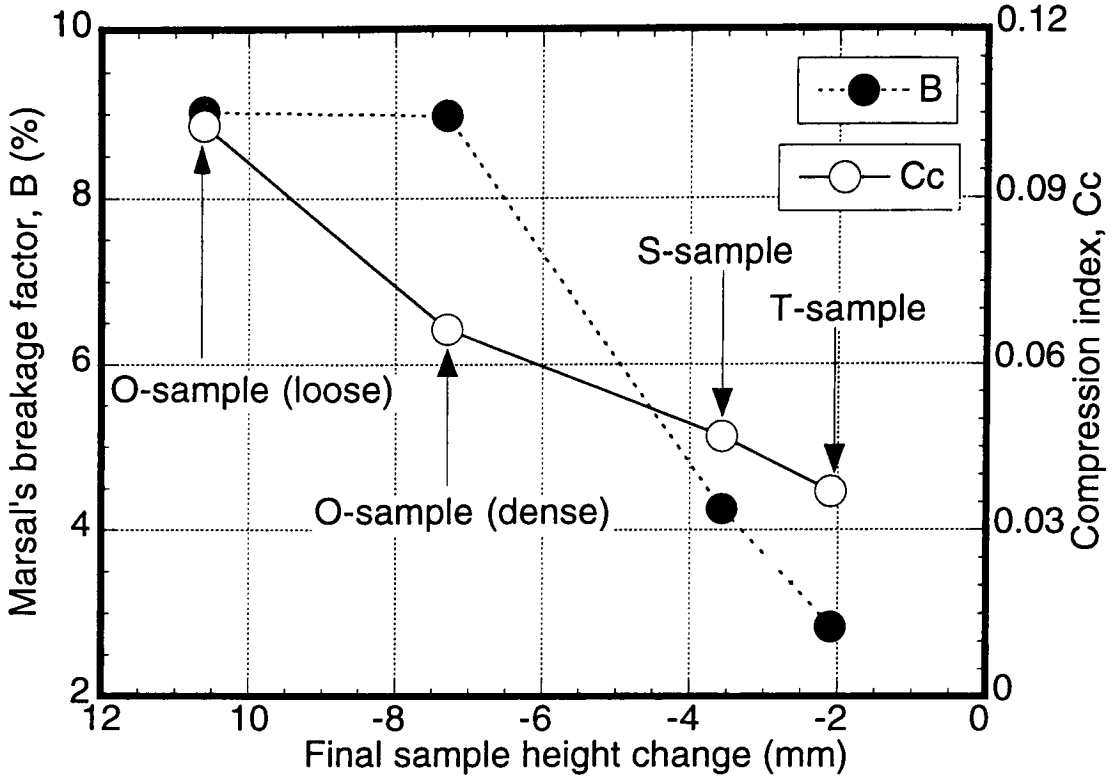

Figure 4.5 Relationships between final sample height change and Marsal's breakage factors, B, as well as the compression index, C_c of samples at a certain relative density.

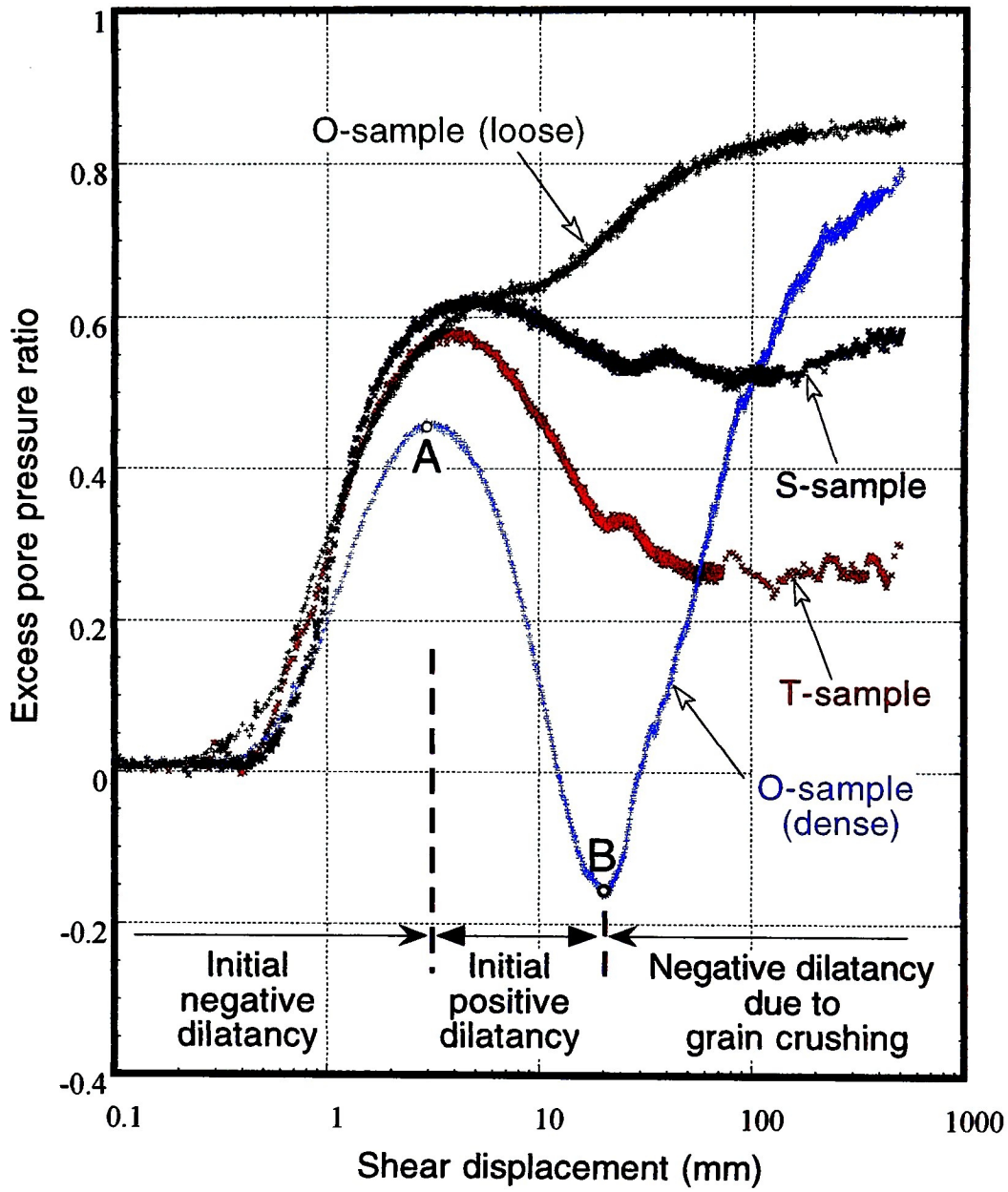

Figure 4.6 Excess pore pressure ratio of various samples in consolidated undrained constant speed ring shear test.

Shear speed = 3 mm/sec. D_r for T-sample was 45.9%, for S-sample was 63.6%, for O-sample (loose) was 93.5% and for O-sample (dense) was 98.0%.

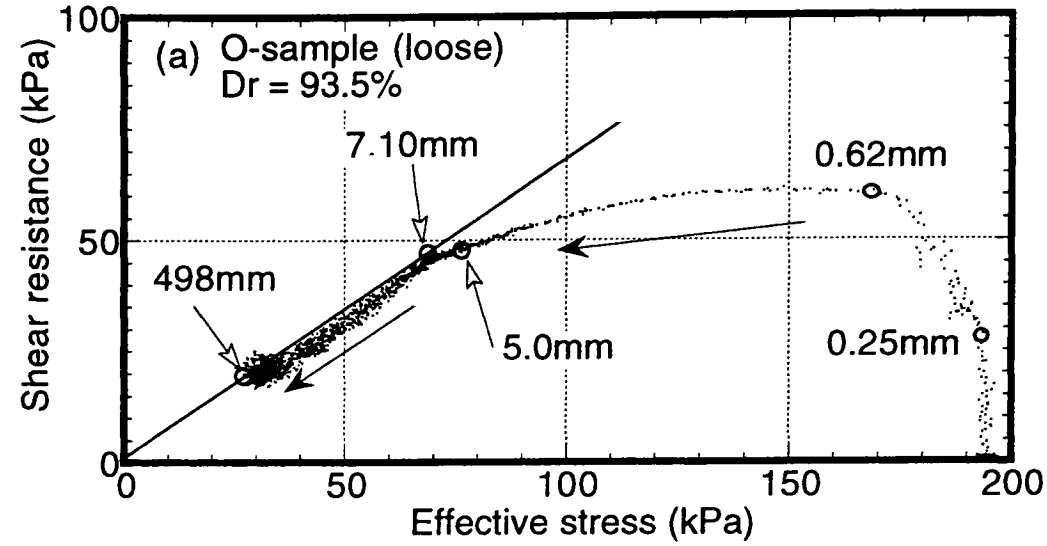
(a) O-sample (loose)
Dr = 93.5%
7.10mm
0.62mm
498mm
5.0mm
0.25mm
Shear resistance (kPa)
Effective stress (kPa)
0
50
100
150
200

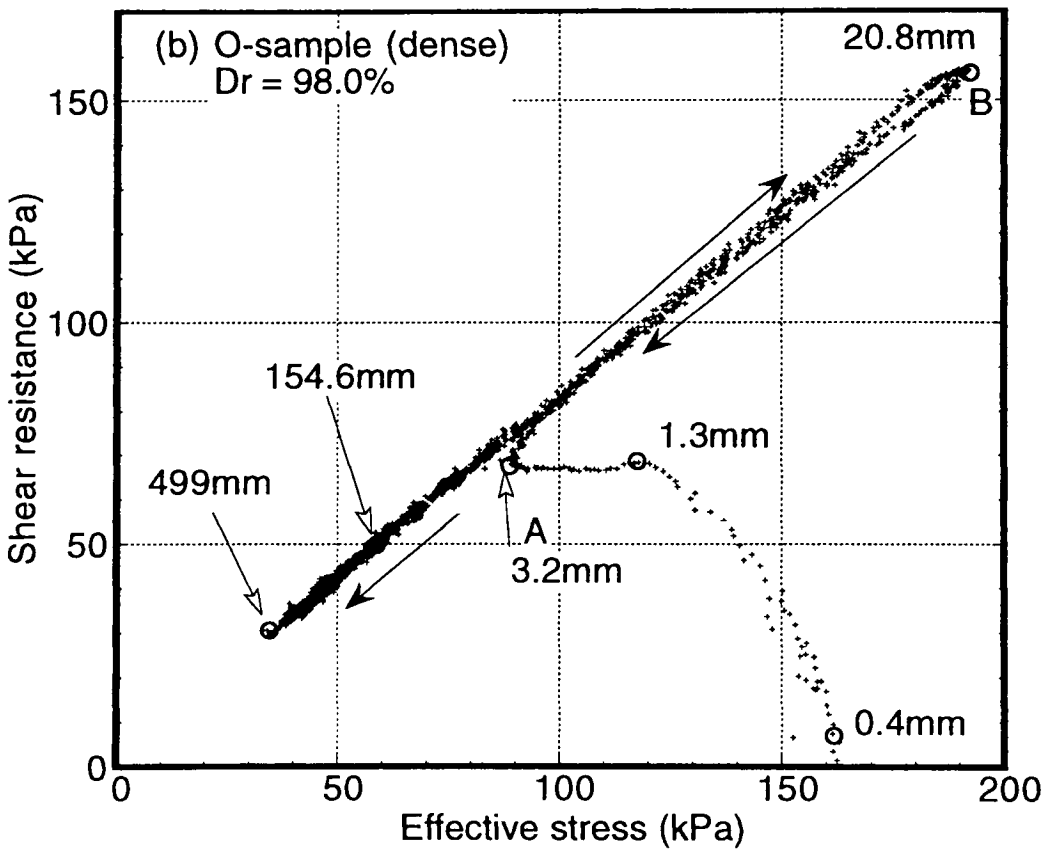
(b) O-sample (dense)
Dr = 98.0%
20.8mm
B
154.6mm
1.3mm
499mm
A
3.2mm
0.4mm
Shear resistance (kPa)
Effective stress (kPa)
0
50
100
150
200

Fig. 4.7 (a) and (b)

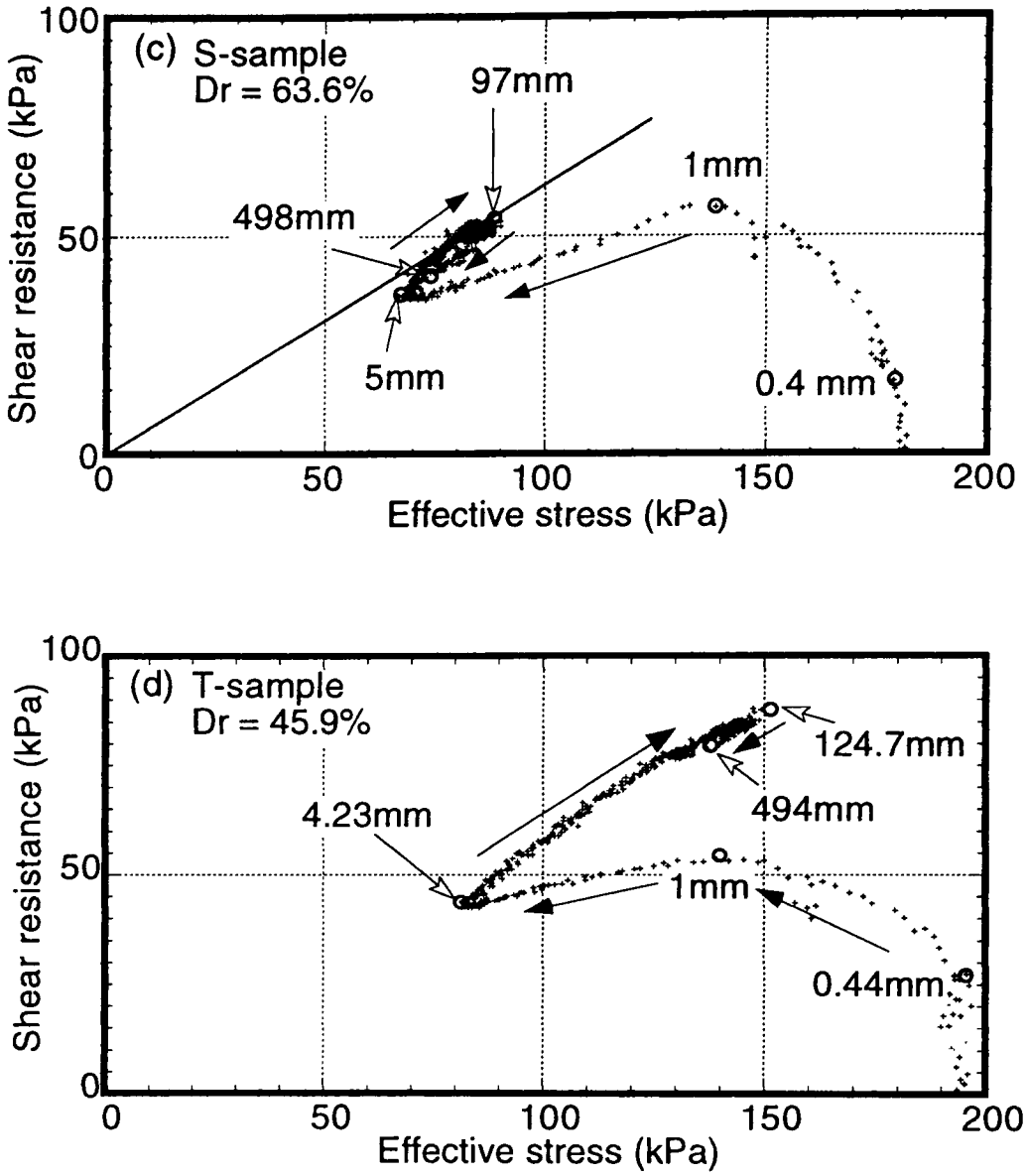

Figure 4.7 Stress path of various samples in consolidated undrained constant speed ring shear test.

Shear speed = 3 mm/sec. (a) O-sample (loose), (b) O-sample(dense), (c) T-sample and (d) S-sample.

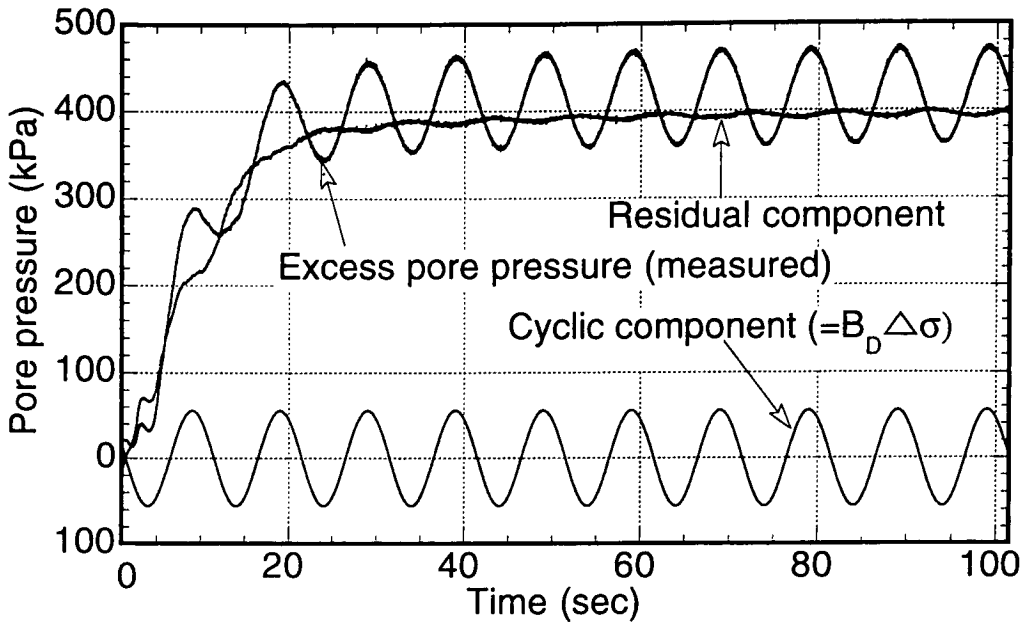

Residual excess pore pressure ratio =

$$\frac{\text{(Residual component of excess pore pressure)}}{\text{(The initial effective stress)}}$$

Figure 4.8 Process showing pore pressure divided to cyclic component and residual component, and the definition of "residual excess pore pressure ratio" (with the data of O-F(0.1)-25°).

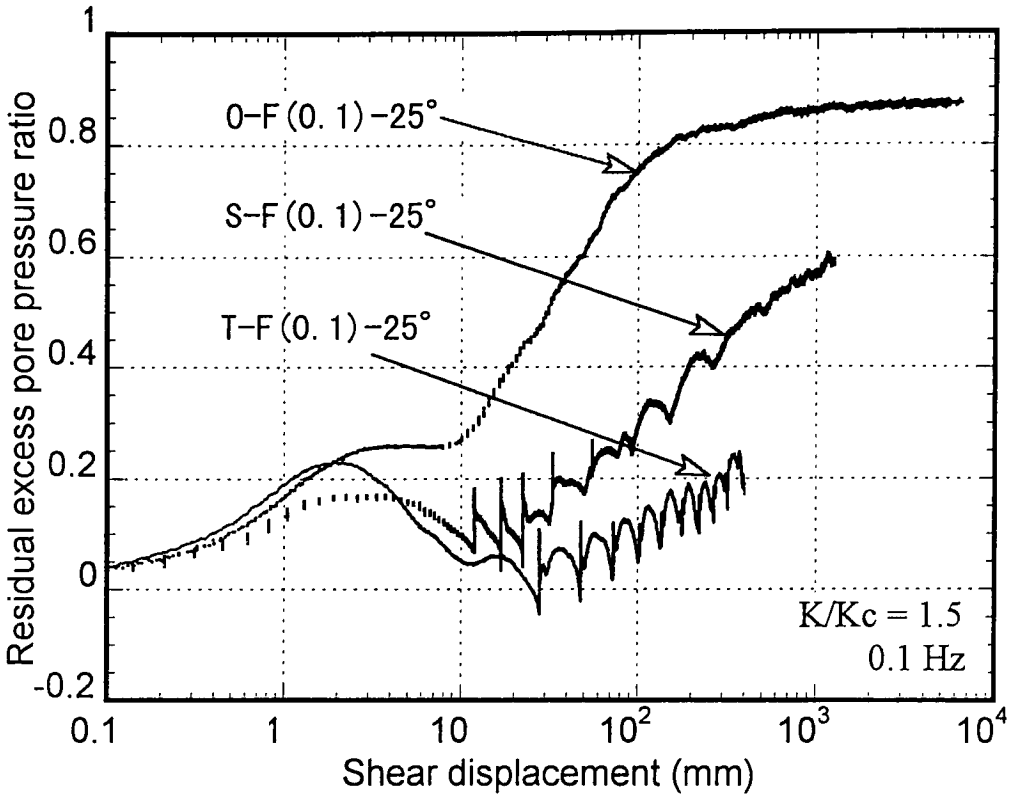

Figure 4.9 Residual excess pore pressure ratio generated in the consolidated undrained cyclic-loading tests on O-sample (loose), T-sample and S-sample at K/K_c = 1.5 with cyclic frequency = 0.1 Hz.

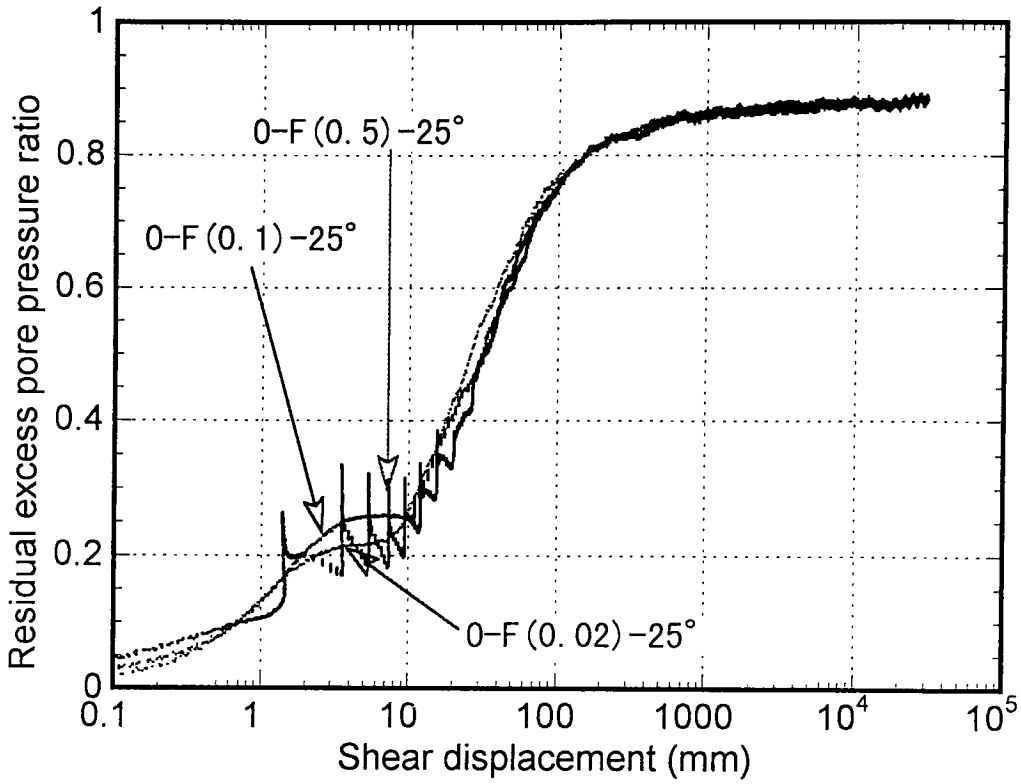

Figure 4.10 Residual excess pore pressure ratio generated in the undrained cyclic-loading tests on O-sample (loose) at frequencies of 0.02 Hz, 0.1 Hz and 0.5 Hz at $K/K_c = 1.5$.

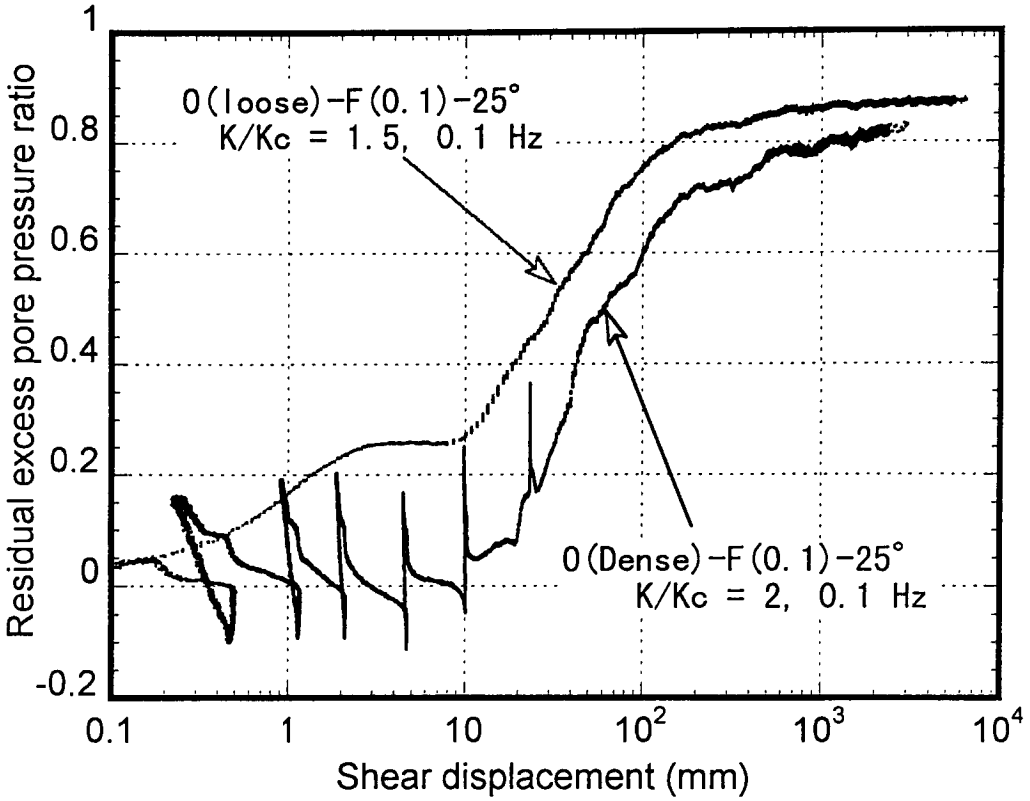

Figure 4.11 Residual excess pore pressure ratio generated in the consolidated undrained cyclic-loading tests on loose O-sample (loose) at K/K_c = 1.5, 0.1 Hz and O-sample (dense) at K/K_c = 2.0, 0.1 Hz.

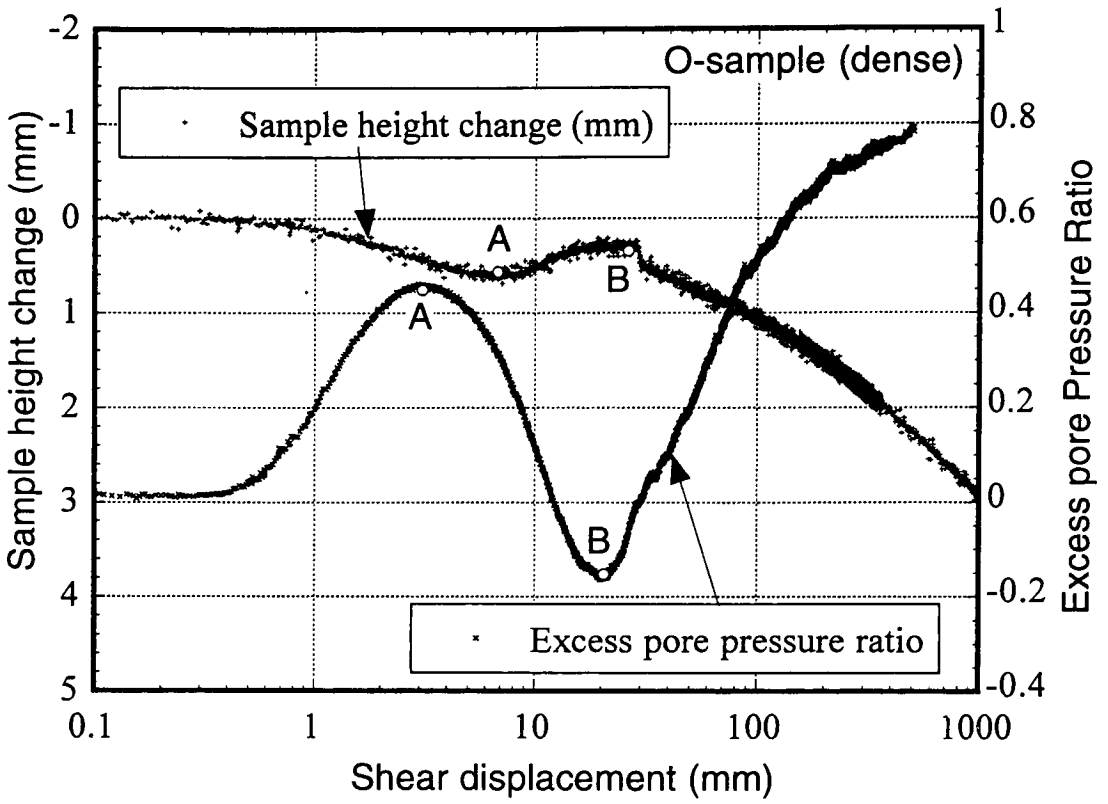

Figure 4.12 Comparison of sample height change in the consolidated drained ring shear test and excess pore pressure ratio in the consolidated undrained ring shear test on O-sample (dense).

Figure 5.1 Photo of the Nikawa landslide (Taken by K. Sassa, 1995.1.21).

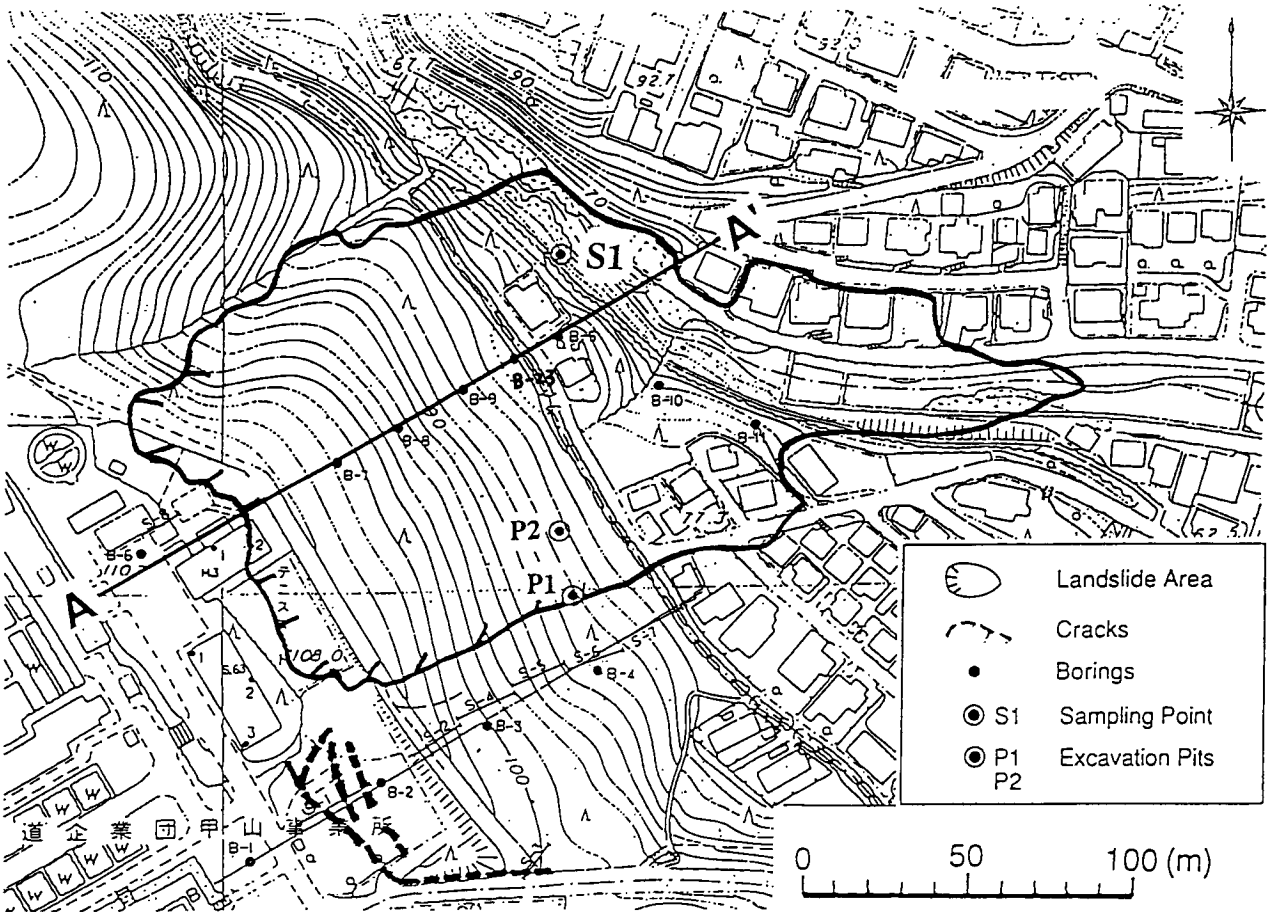

Figure 5.2 Plan of the slope before the Nikawa landslide occurred and the outline of the landslide area (from Sassa et al. 1996).

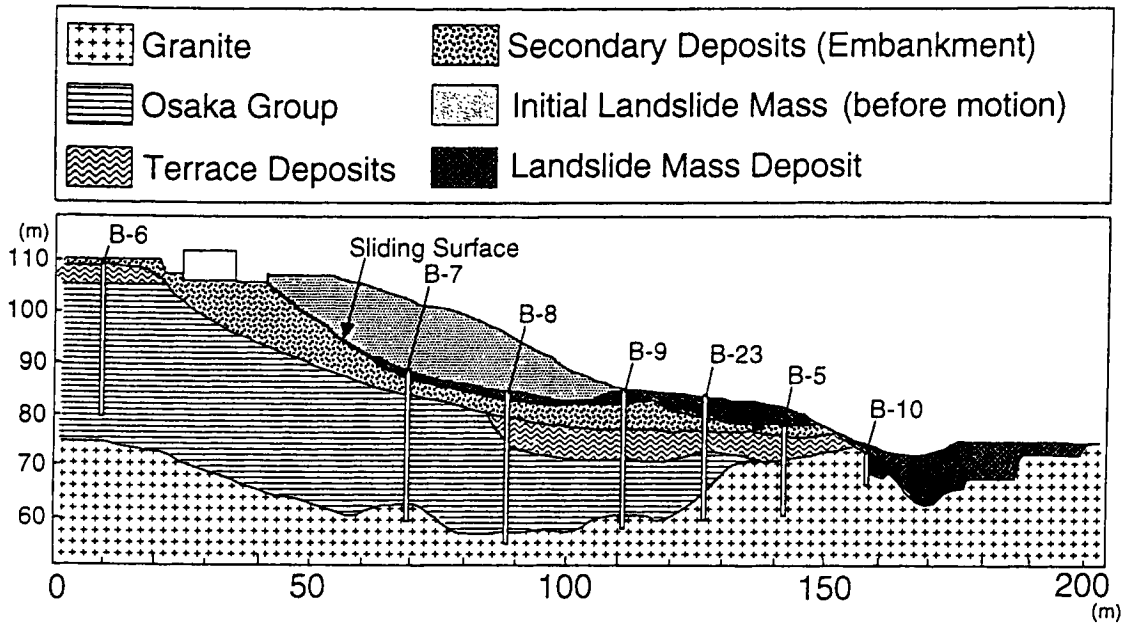

Figure 5.3 Geological section of the Nikawa landslide along A-A' line in Fig. 5.2 (from Sassa et al. 1995).

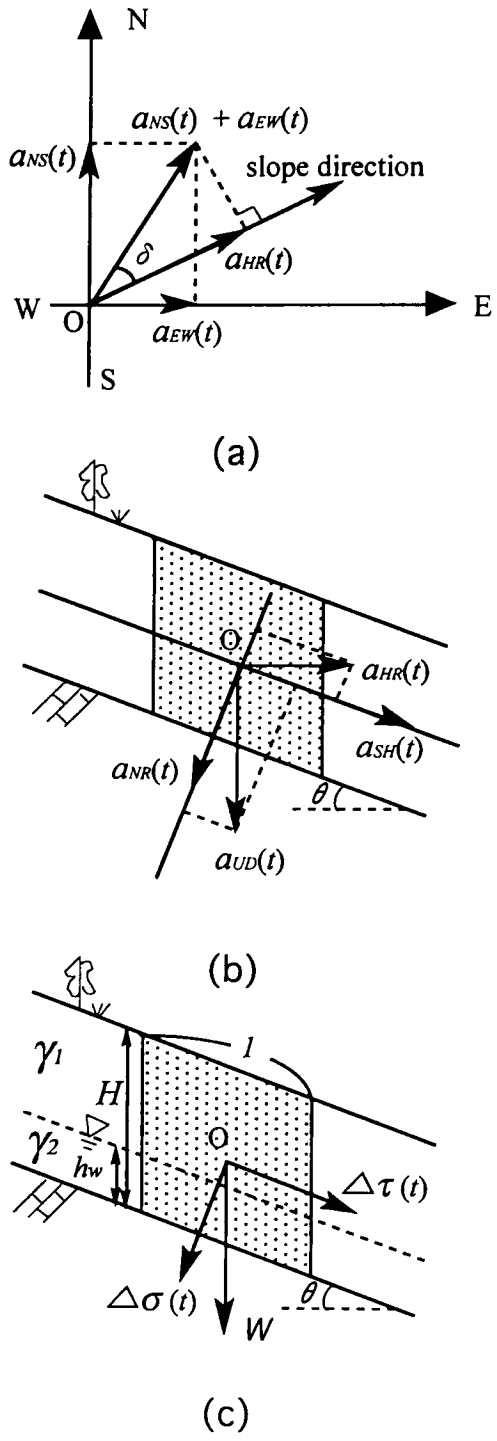

Figure 5. 4 The synthesizing procedure from seismic loading to normal stress and shear stress.

(a): Transfer the horizontal (EW and NS) components to the horizontal slope direction.

(b): Transfer the horizontal component along the slope direction and the vertical component (UD) to the component along the sliding surface.

(c): Sum up the initial stress (W) and the increments of normal stress ($\Delta\sigma$) and shear stress ($\Delta\tau$) acting on the sliding surface by multiplying acceleration and mass of the soil columns.

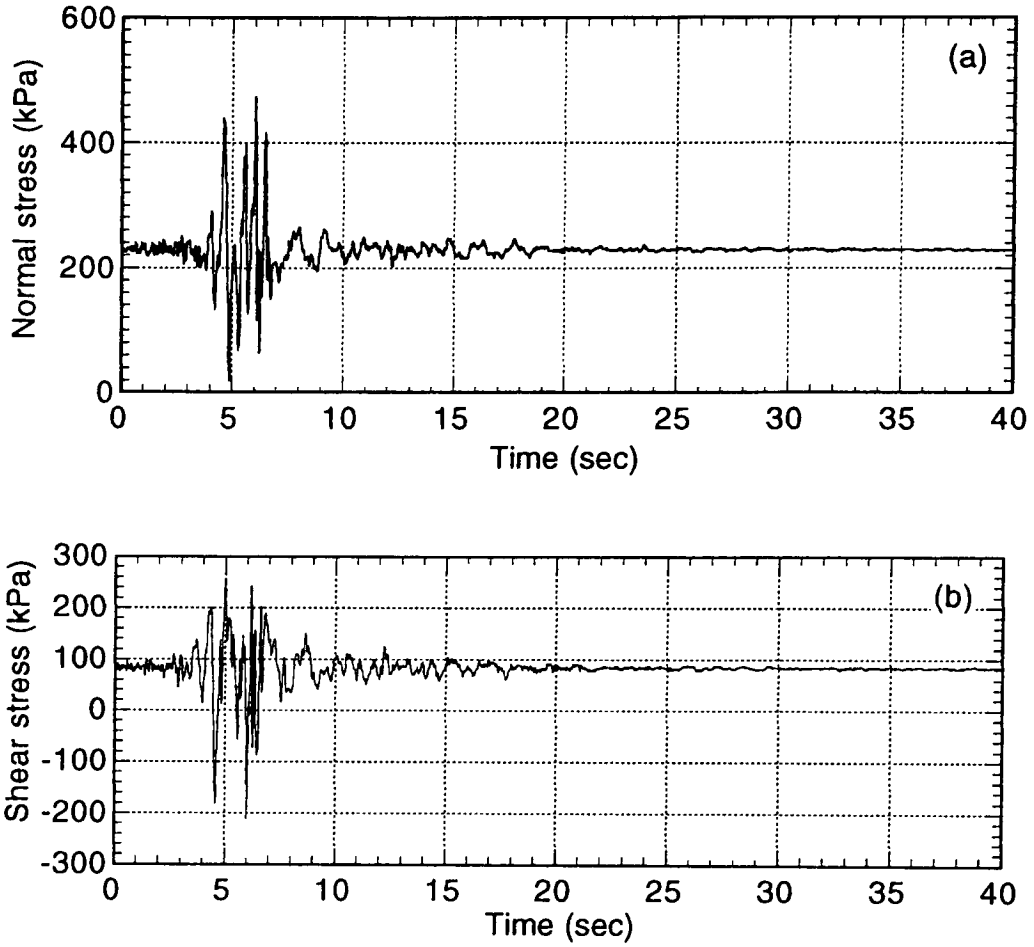

Figure 5.5 Loading stresses on the sample of the simulation test on the Nikawa landslide.

(a): Normal stress, (b): Shear stress

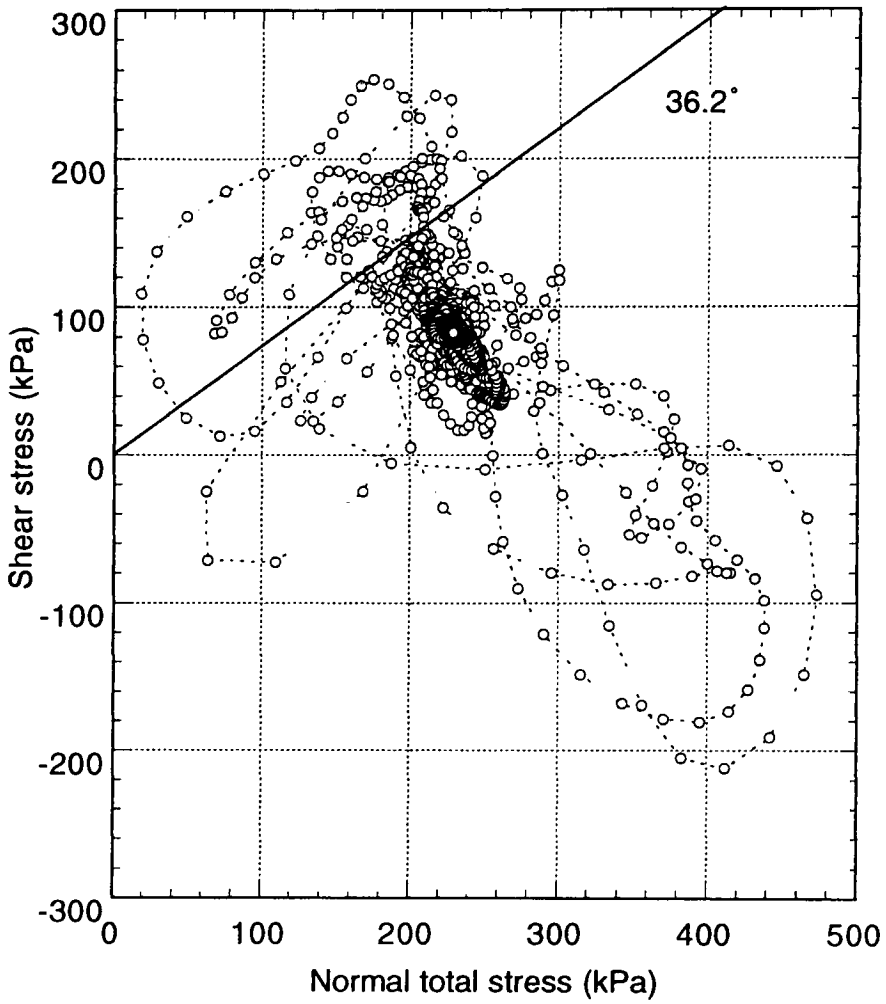

Figure 5.6 Stress path of the control signal in the simulation test on the Nikawa landslide.

The residual failure line obtained from the geotechnical simulation test.

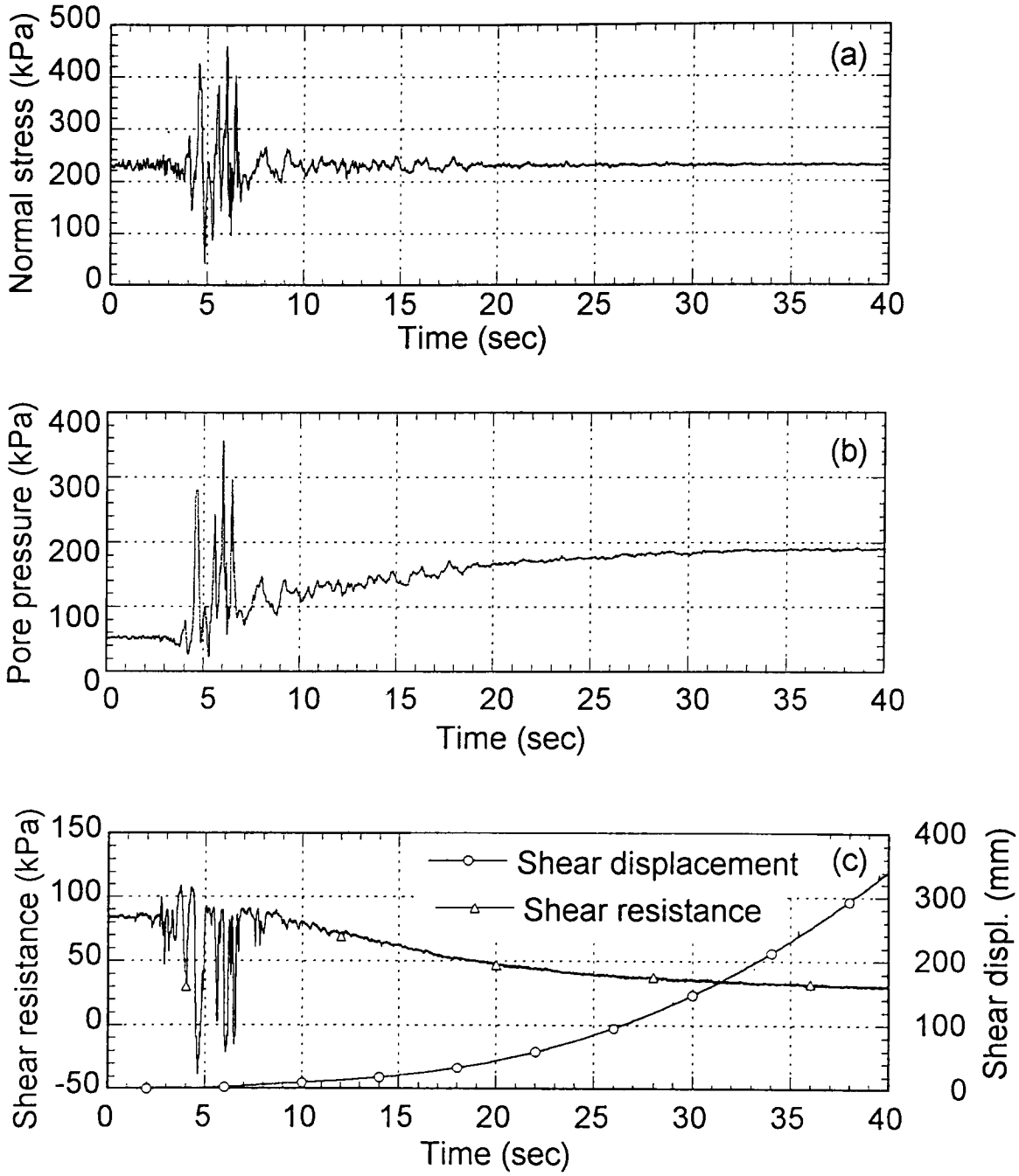

Figure 5.7 Time-series data of the simulation test on the Nikawa landslide.

B_D = 0.97, D_r = 147.2 percent

(a): Normal stress; (b): Pore pressure; (c): Shear resistance and shear displacement

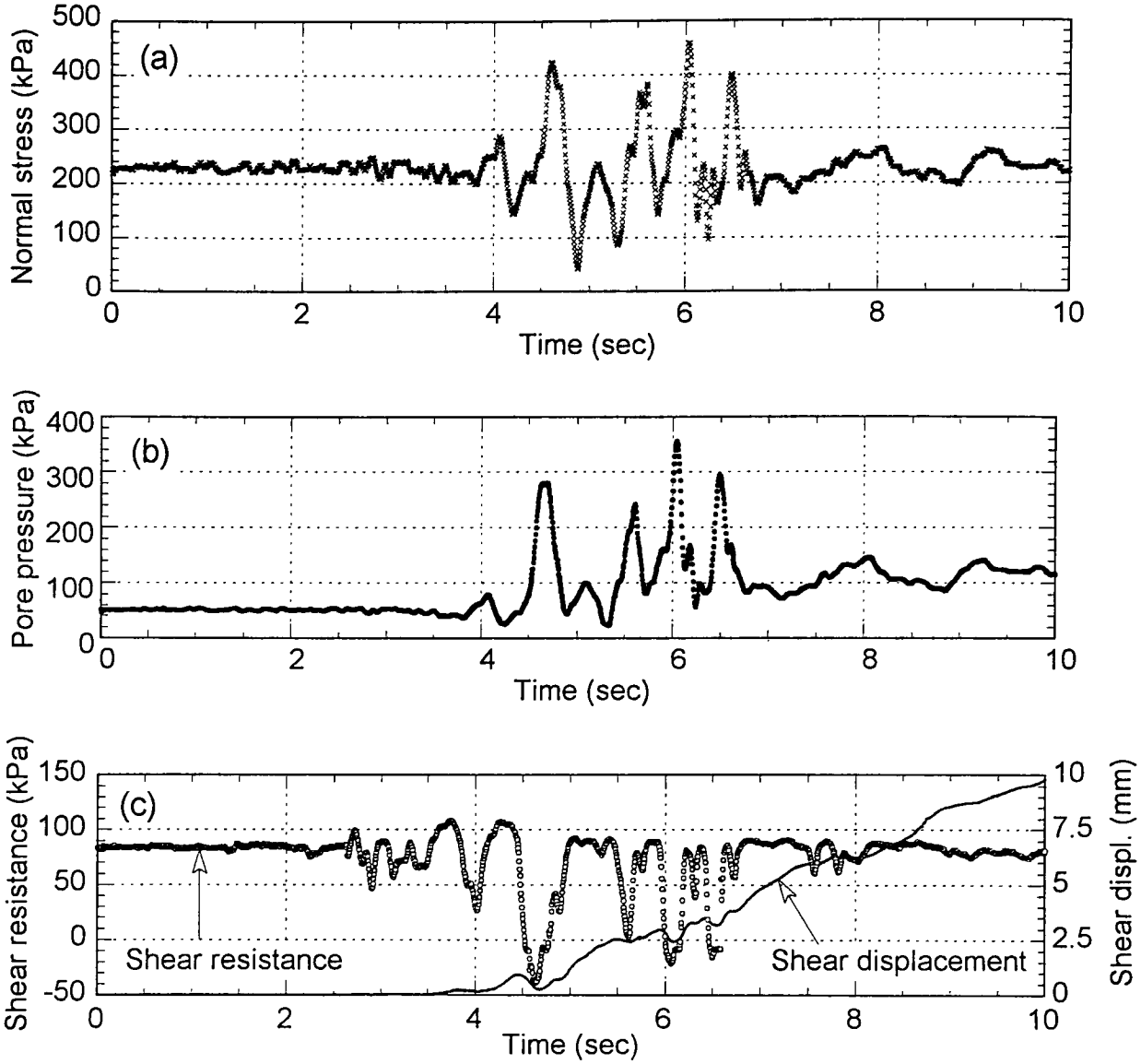

Figure 5.8 Time series data during the main shock in the simulation test on the Nikawa landslide.

B_D = 0.97, D_r = 147.2 percent

(a): Normal stress; (b): Pore pressure; (c): Shear resistance and shear displacement

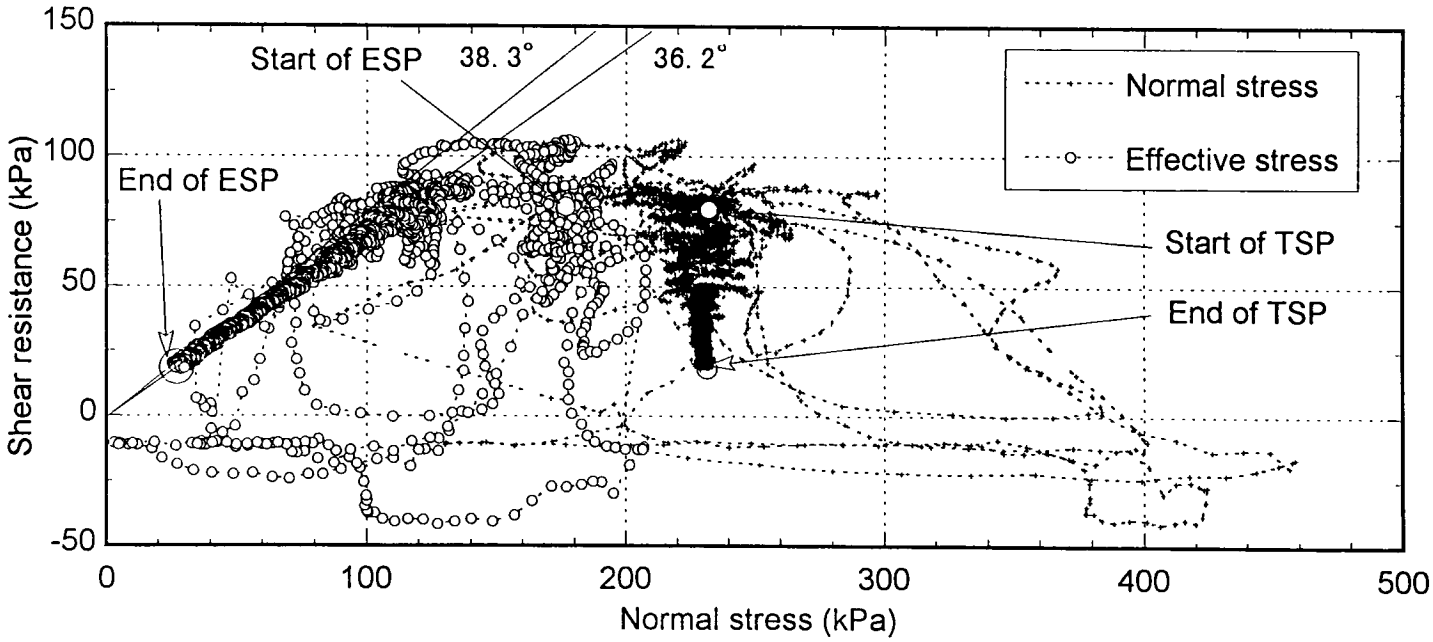

Figure 5.9 The stress path for the simulation test on the Nikawa landslide.

ESP: Effective stress path, TSP: Total stress path

B_D = 0.97, D_r = 147.2 percent

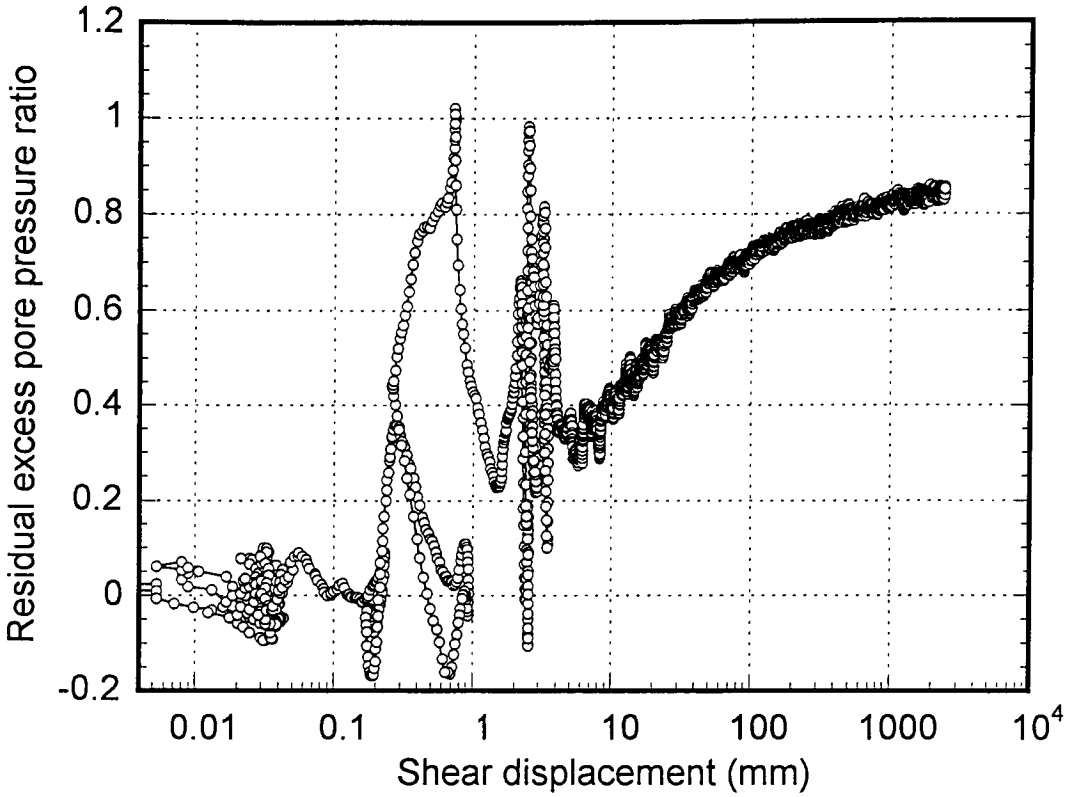

Figure 5.10 The relation of residual excess pore pressure ratio with the shear displacement in the simulation test on the Nikawa landslide.

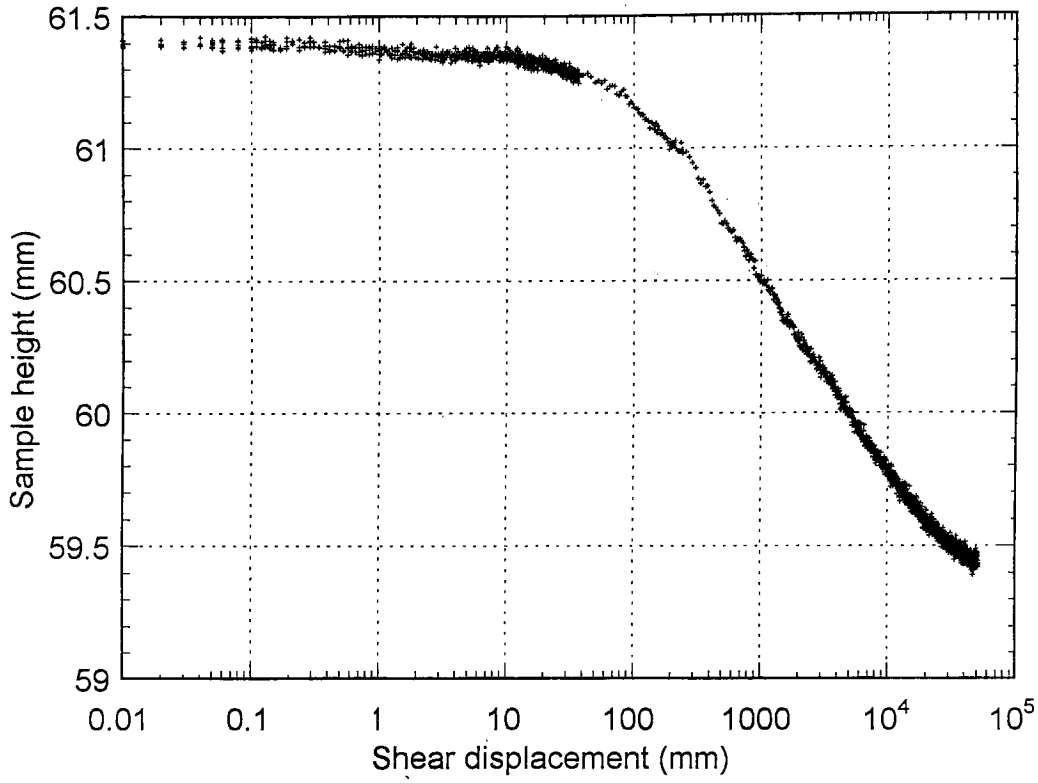

Figure 5.11 Sample height change with the shear displacement of Osaka-group coarse sandy soil taken from the Nikawa landslide under the drained ring shear test. Normal stress = 196 kPa, shear speed = 3 mm/sec. Initial relative density = 152.8 percent

Figure 5.12 Photograph of the sample after sheared for 42 m in the drained test.
A trench cut in the shear box. Pins show the upper and lower boundary of the grain-crushing zone

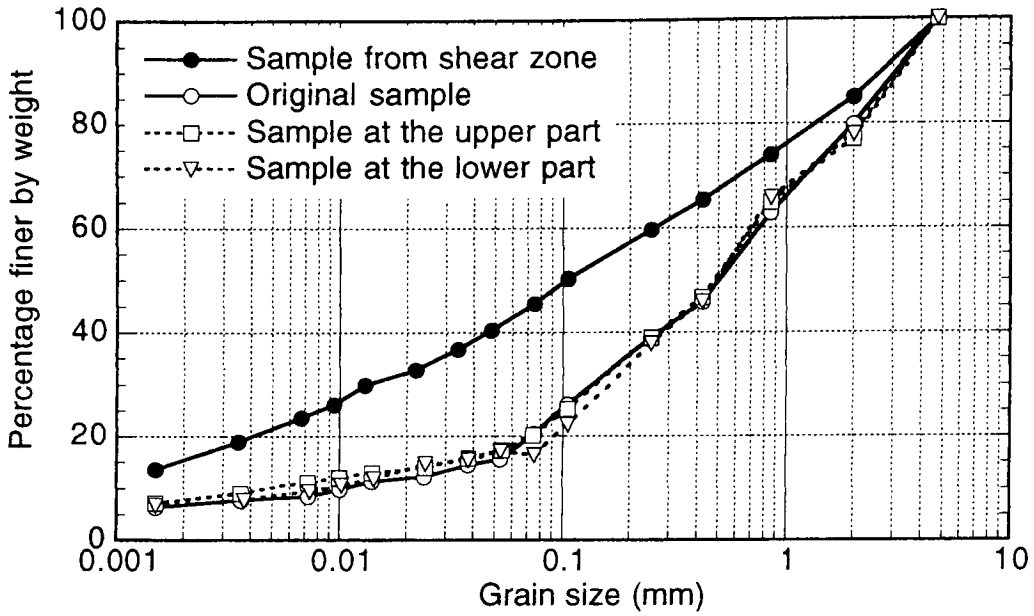

Figure 5.13 Grain size distribution analysis results for the original sample, sample at the shear zone, at the upper part and the lower part of the shear box after sheared for 42 m under 196 kPa normal stress, shear speed = 3 mm/sec.

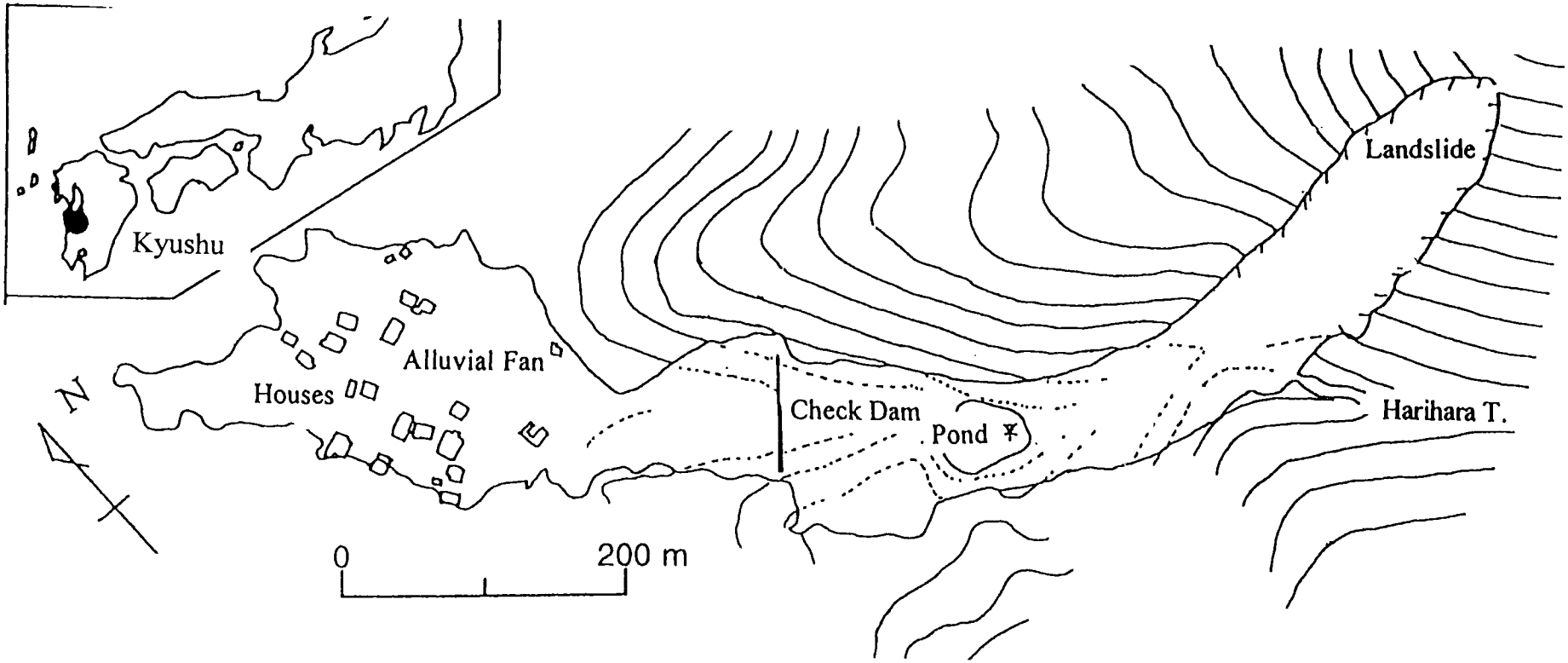

Figure 6.1 Location and plan of the Harihara debris slide–debris flow (from Sassa et al. 1998).

Figure 6.2 Aerial oblique view of the Harihara debris slide–debris flow (from Sassa 1998).

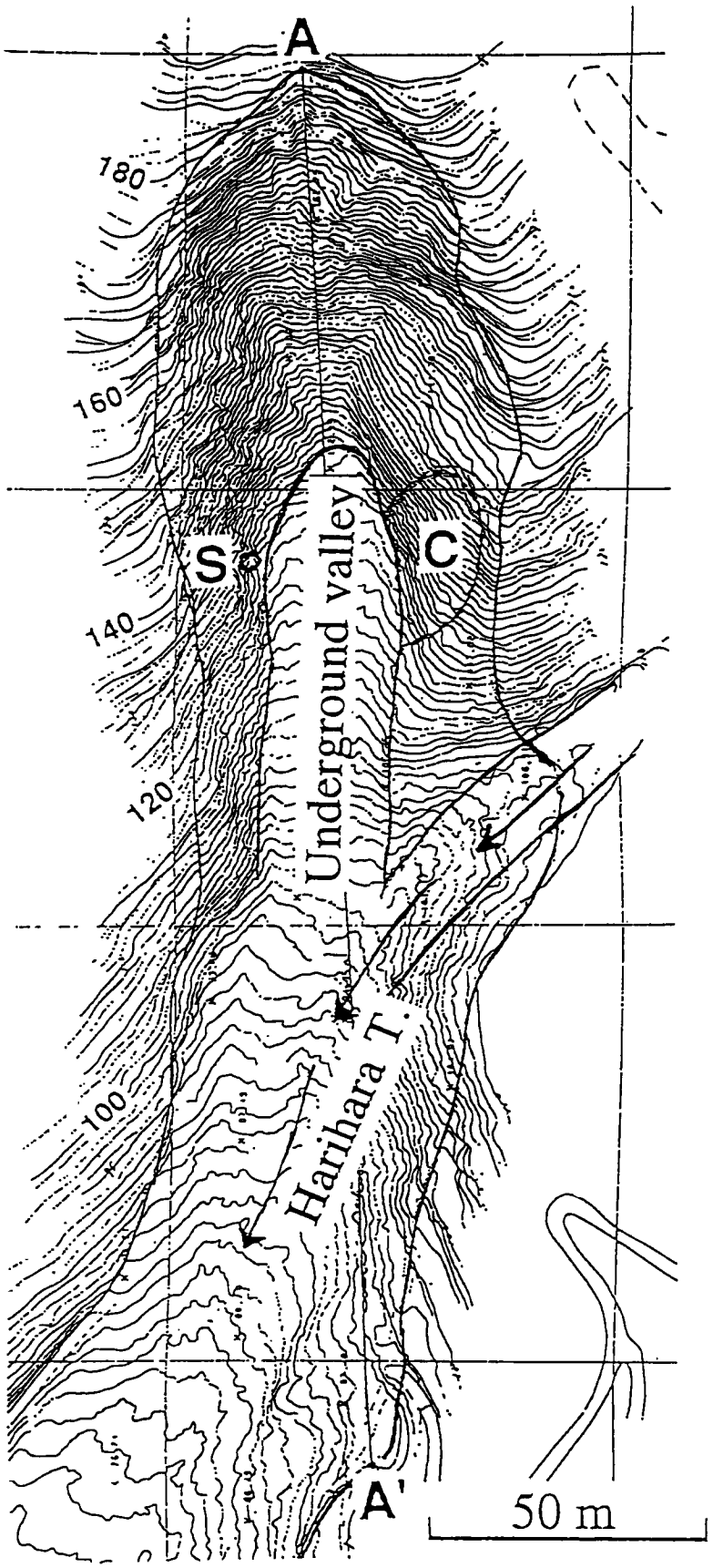

Figure 6.3 Plan of the initial landslide in the Harihara debris slide–debris flow (from Sassa et al. 1998).

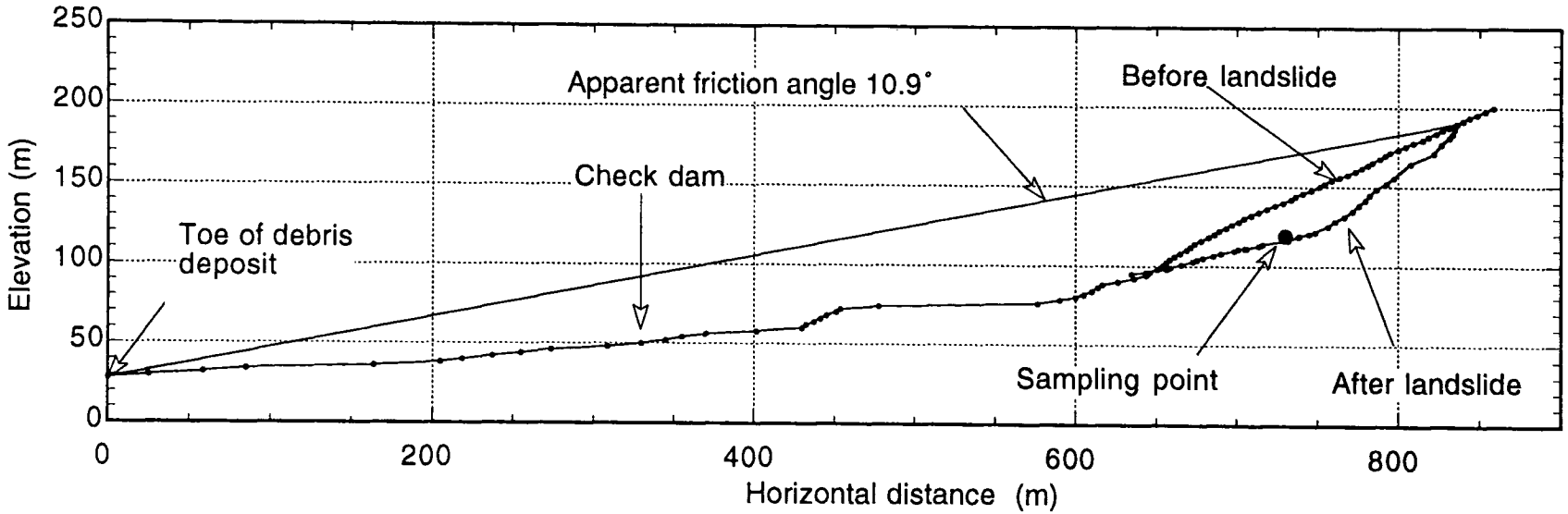

Figure 6.4 Longitudinal section along the moving path of the landslide mass in the Harihara debris slide–debris flow (from Sassa et al. 1998).

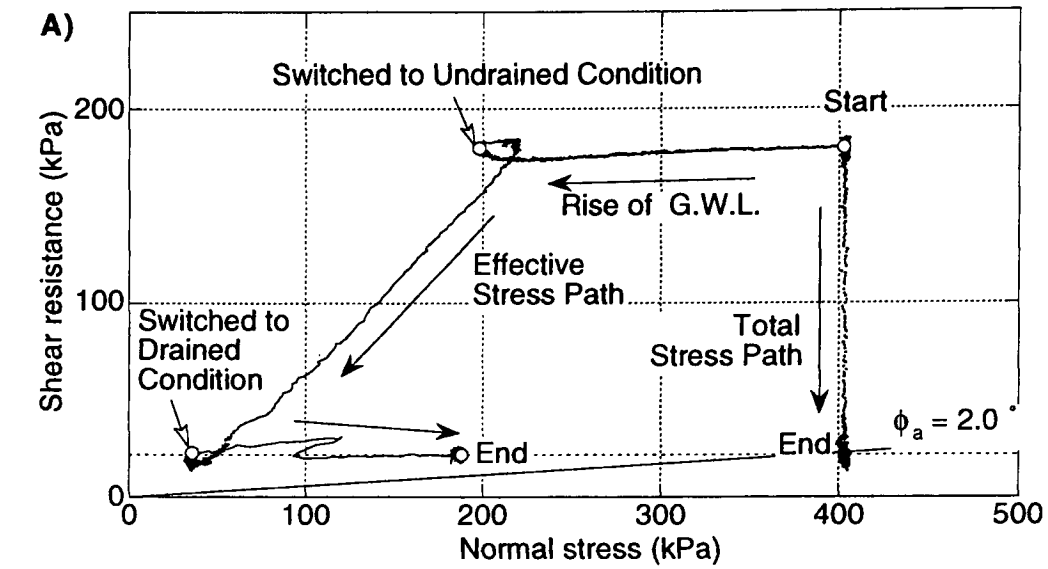
A)
Switched to Undrained Condition
Start
Rise of G.W.L.
Effective
Stress Path
Switched to
Drained
Condition
Total
Stress Path
End
End
$\phi_a = 2.0^\circ$
Shear resistance (kPa)
Normal stress (kPa)
0
100
200
300
400
500

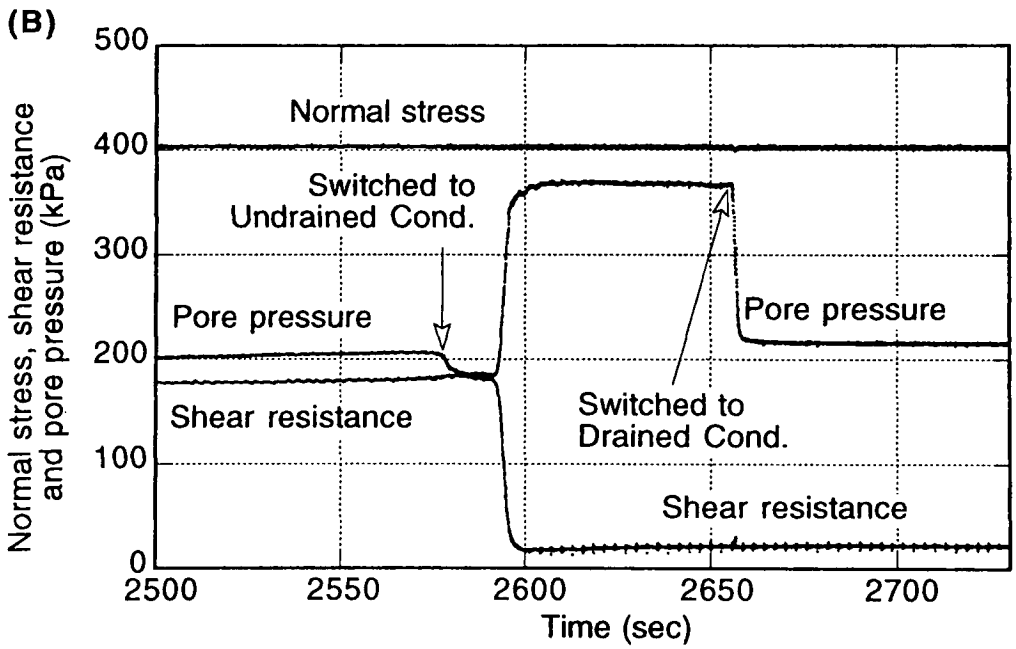
(B)
Normal stress
Switched to
Undrained Cond.
Pore pressure
Pore pressure
Shear resistance
Switched to
Drained Cond.
Shear resistance
Normal stress, shear resistance
and pore pressure (kPa)
Time (sec)
0
100
200
300
400
500
2500
2550
2600
2650
2700

Fig. 6.5 (a) and (b)

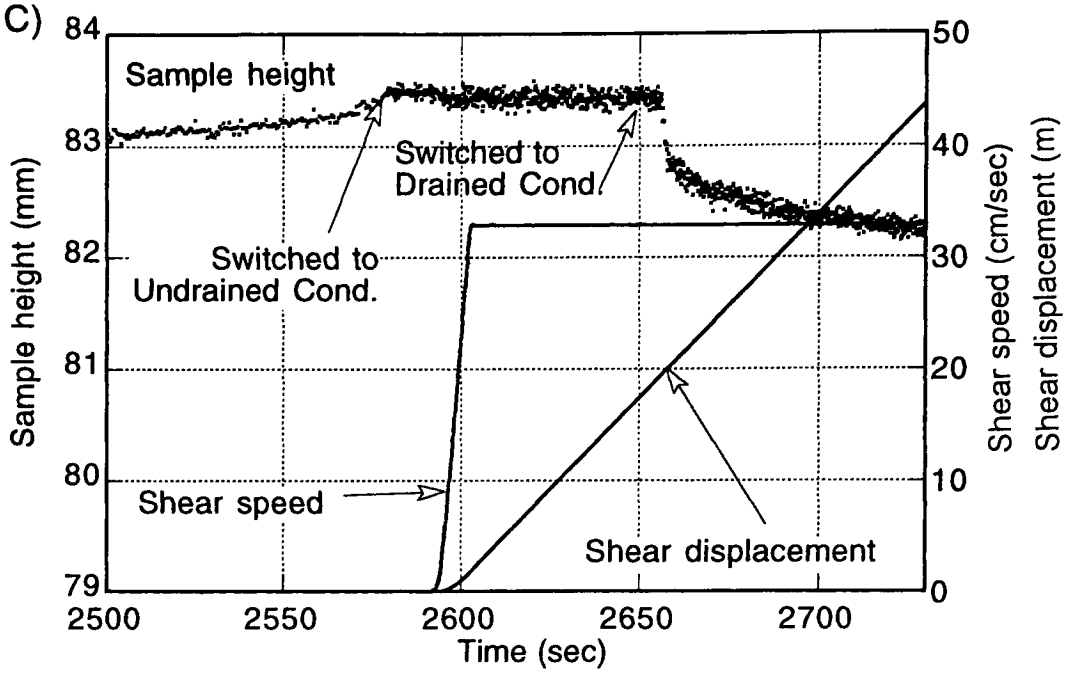

Figure 6.5 Ring-shear test results for the andesitic debris from the Harihara debris slide–debris flow (from Sassa et al. 1998).

The shear box was switched from the drained state to the undrained state immediately after the initiation of failure, and returned to the drained state after the steady state of shearing. $B_D = \Delta u / \Delta\sigma = 0.96$

a) Stress path, b) Time series data of normal stress, pore pressure and shear resistance, c) Time series data of shear displacement, sample height and shear speed.

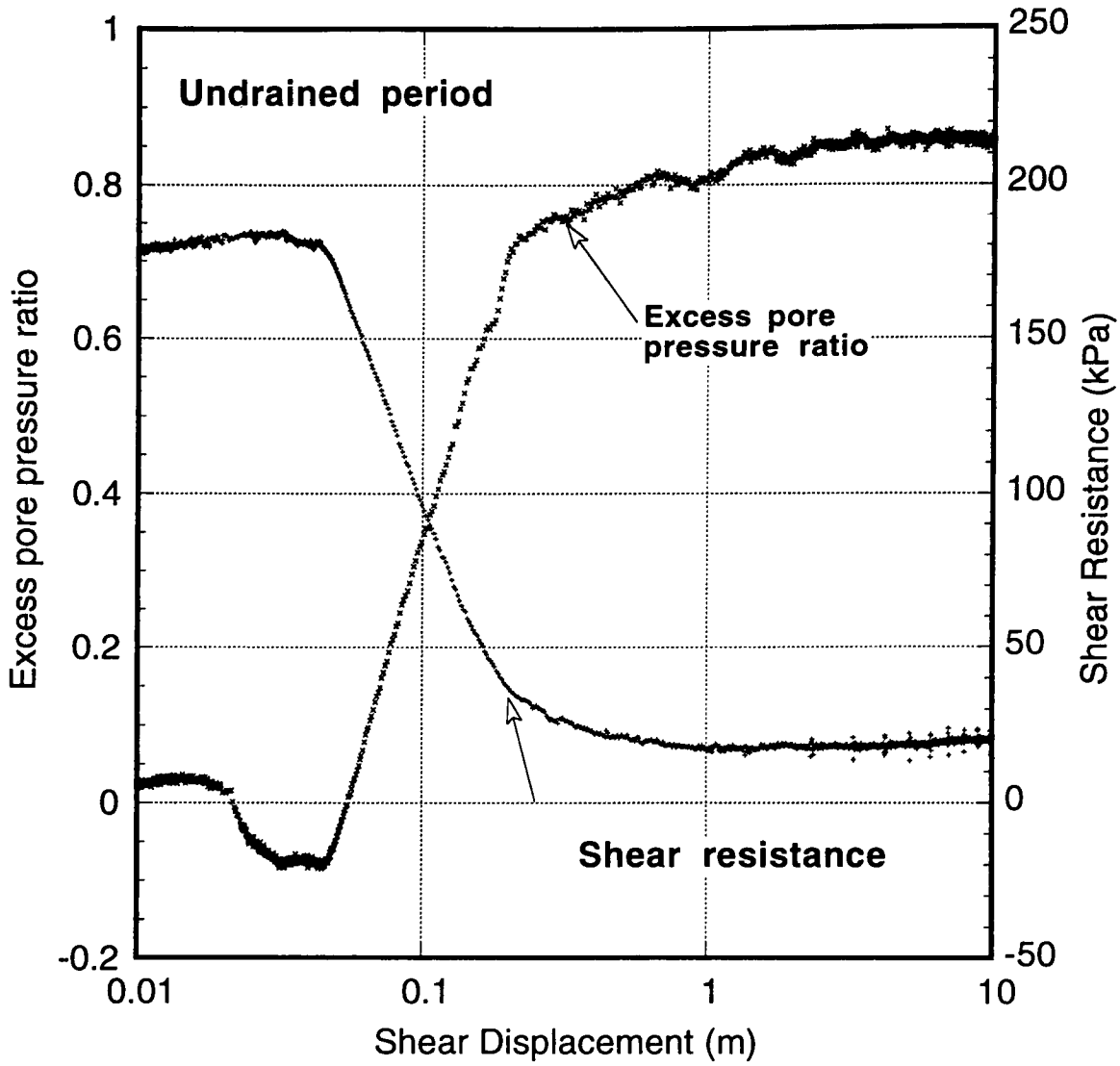

Figure 6.6 Excess pore pressure ratio and shear resistance change with shear displacement in the undrained period in the test of Fig. 6.5.

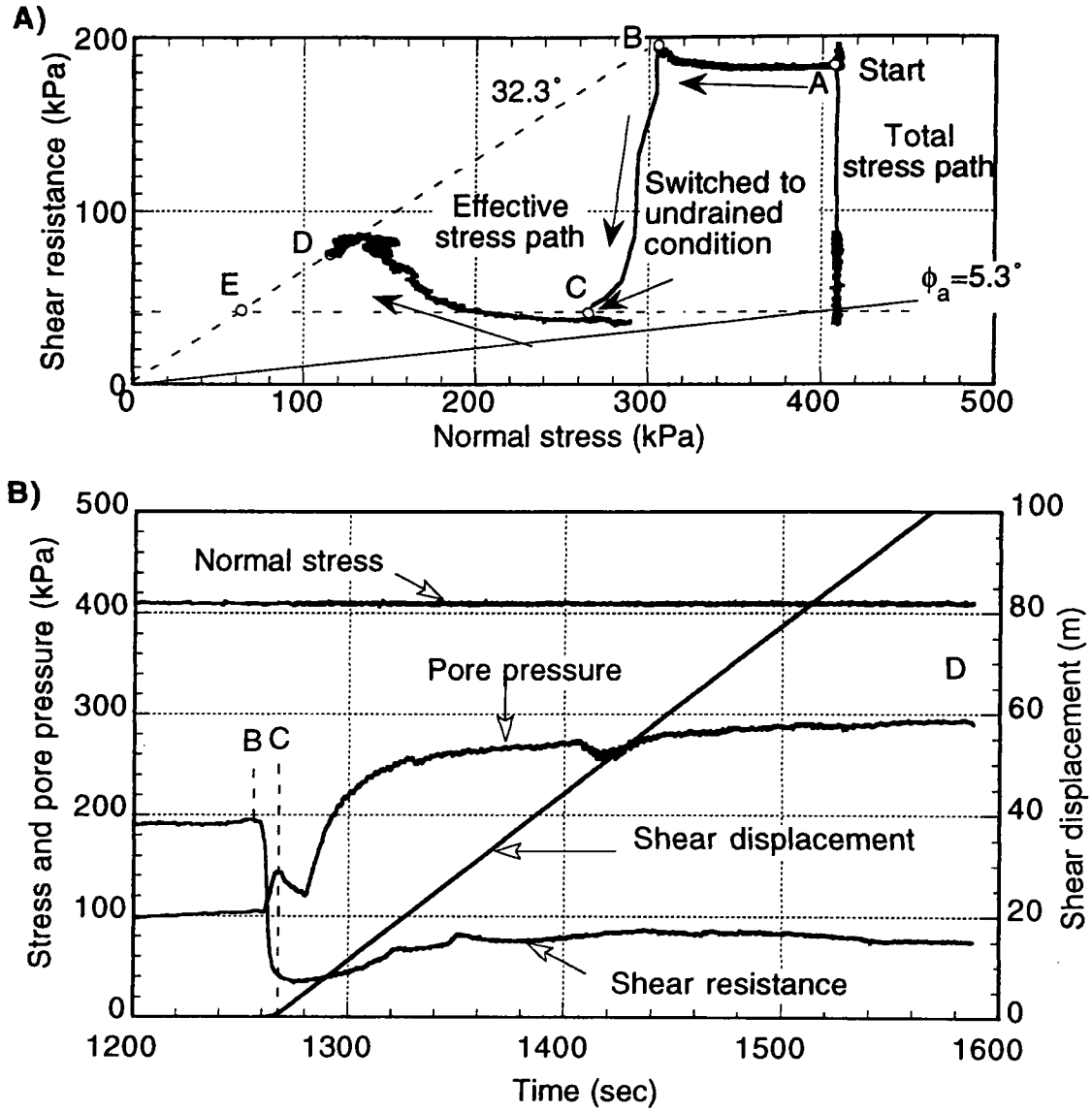

Figure 6.7 Test results for the andesitic debris (from Sassa et al. 1998).

The shear box was maintained in the drained state after the initiation of failure. It then was changed to the undrained state after the shear-resistance value had almost stabilized. $B_D = \Delta u / \Delta\sigma = 0.96$

a) Stress path, b) Time series data of stress.

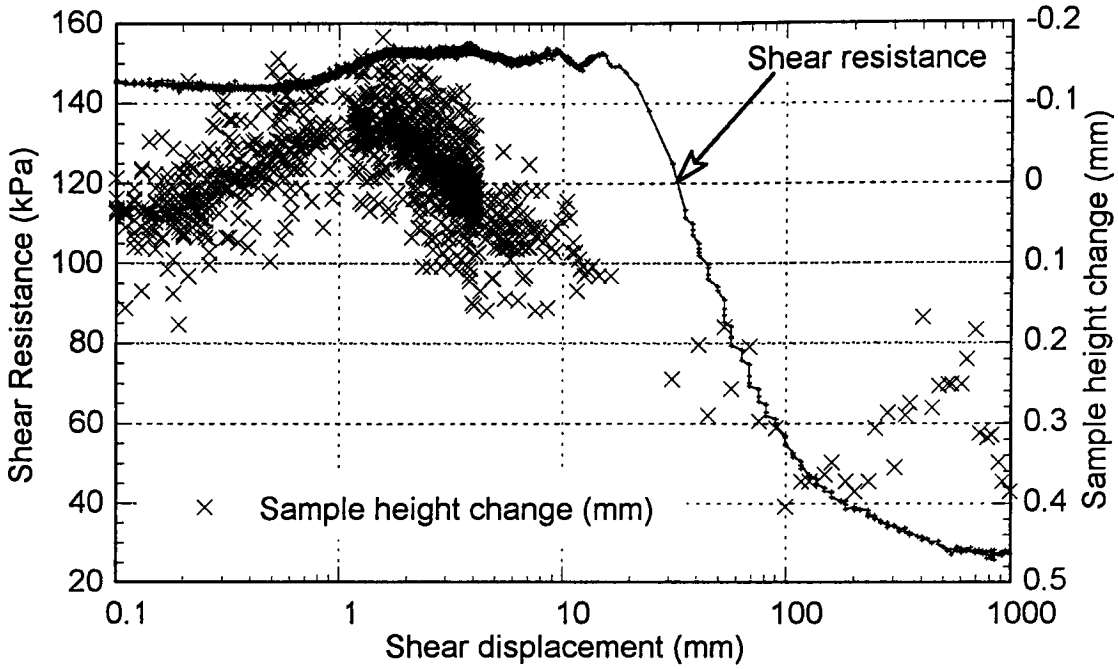

Figure 6.8 Shear resistance and sample height change with shear displacement in the drained period in the test for the Harihara debris slide–debris flow of Fig. 6.7.

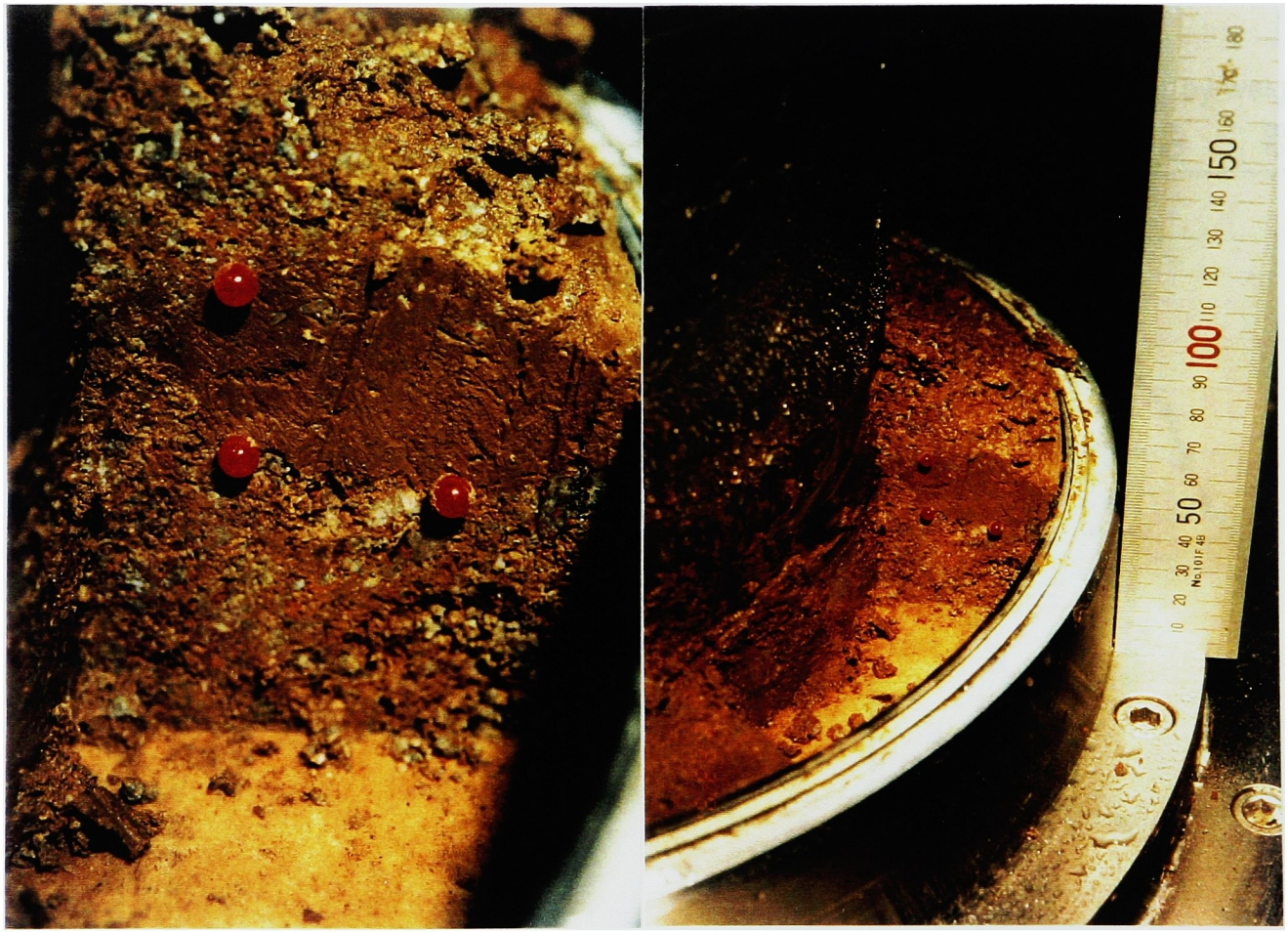

Figure 6.9 Photo of section through the shear zone after the test of Fig. 6.7 (from Sassa et al. 1998).
Pins show the border between the shear zone and less-disturbed zones. The shear zone was very silty. The total shear displacement was 113 m.

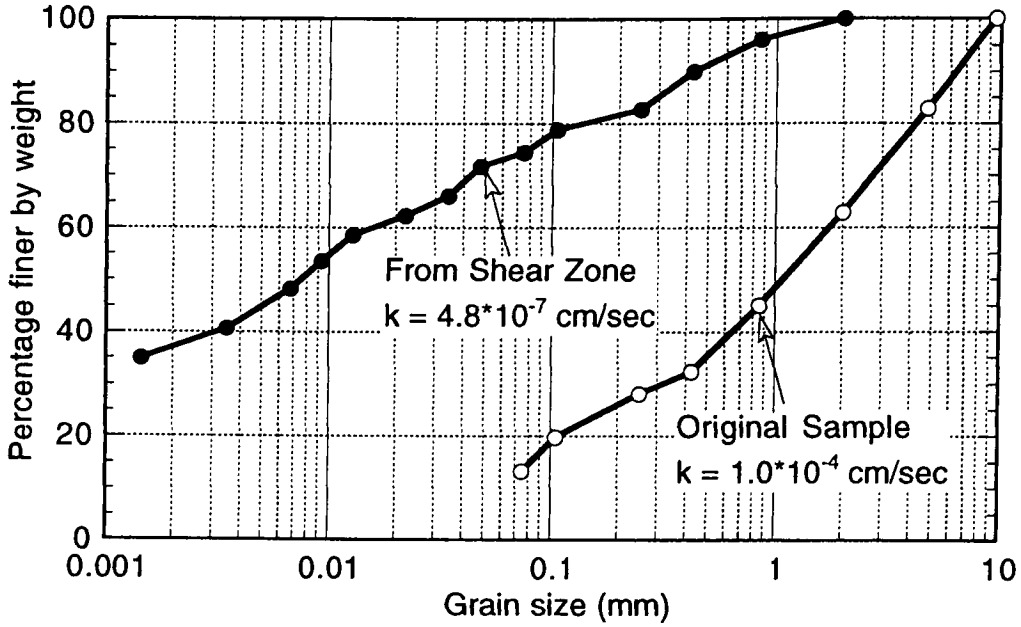

Figure 6.10 Results of grain size distribution analysis on the original andesitic sample from the Harihara debris slide–debris flow and the sample at the shear zone in the shear box after shear for 113 m.

Appendix

Time series data and stress path of the consolidated undrained cyclic loading ring shear tests

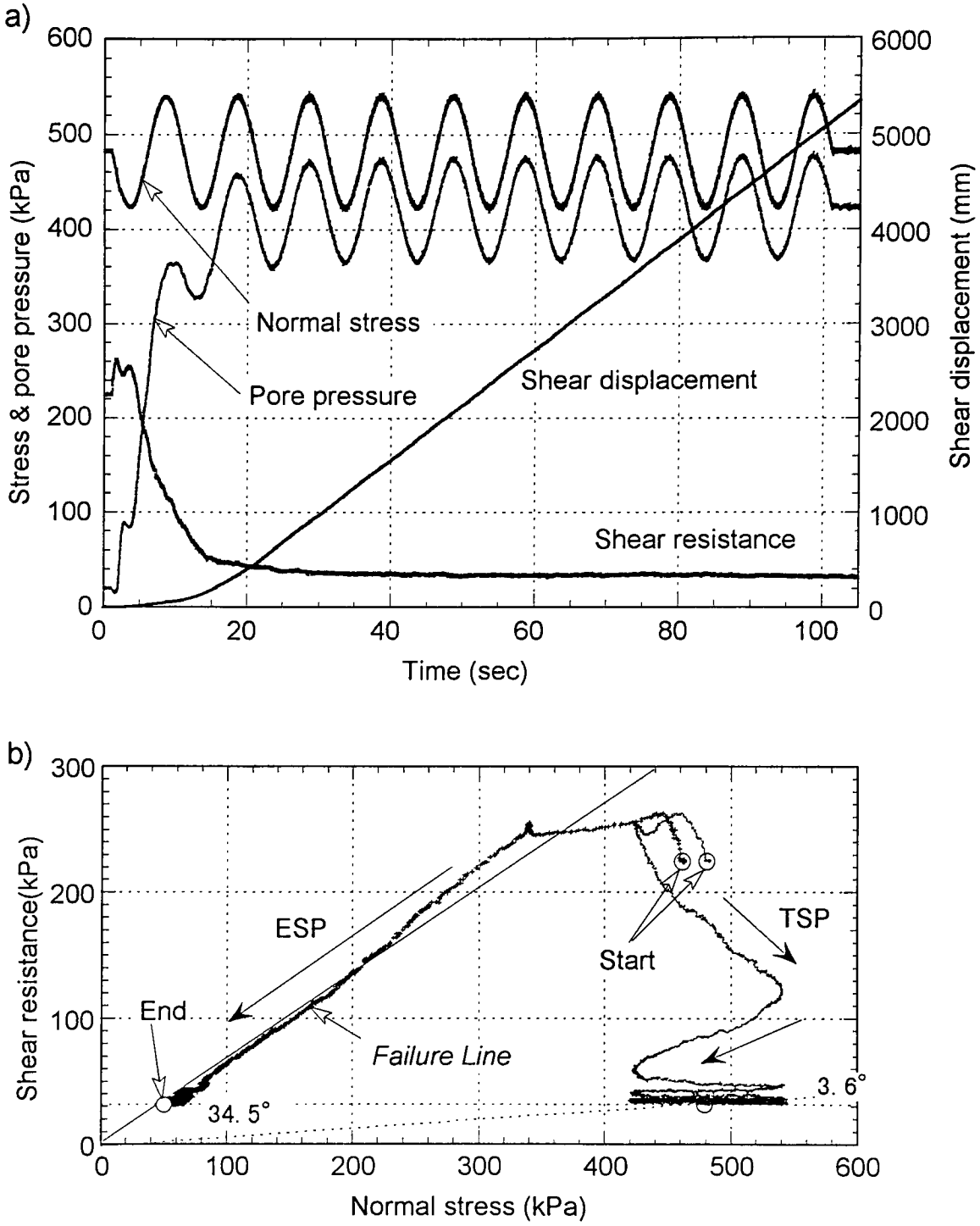

Fig. A-1 Time series data (a) and stress path (b) of O-F(0.1)-25°

TSP: Total stress path, ESP: Effective stress path.

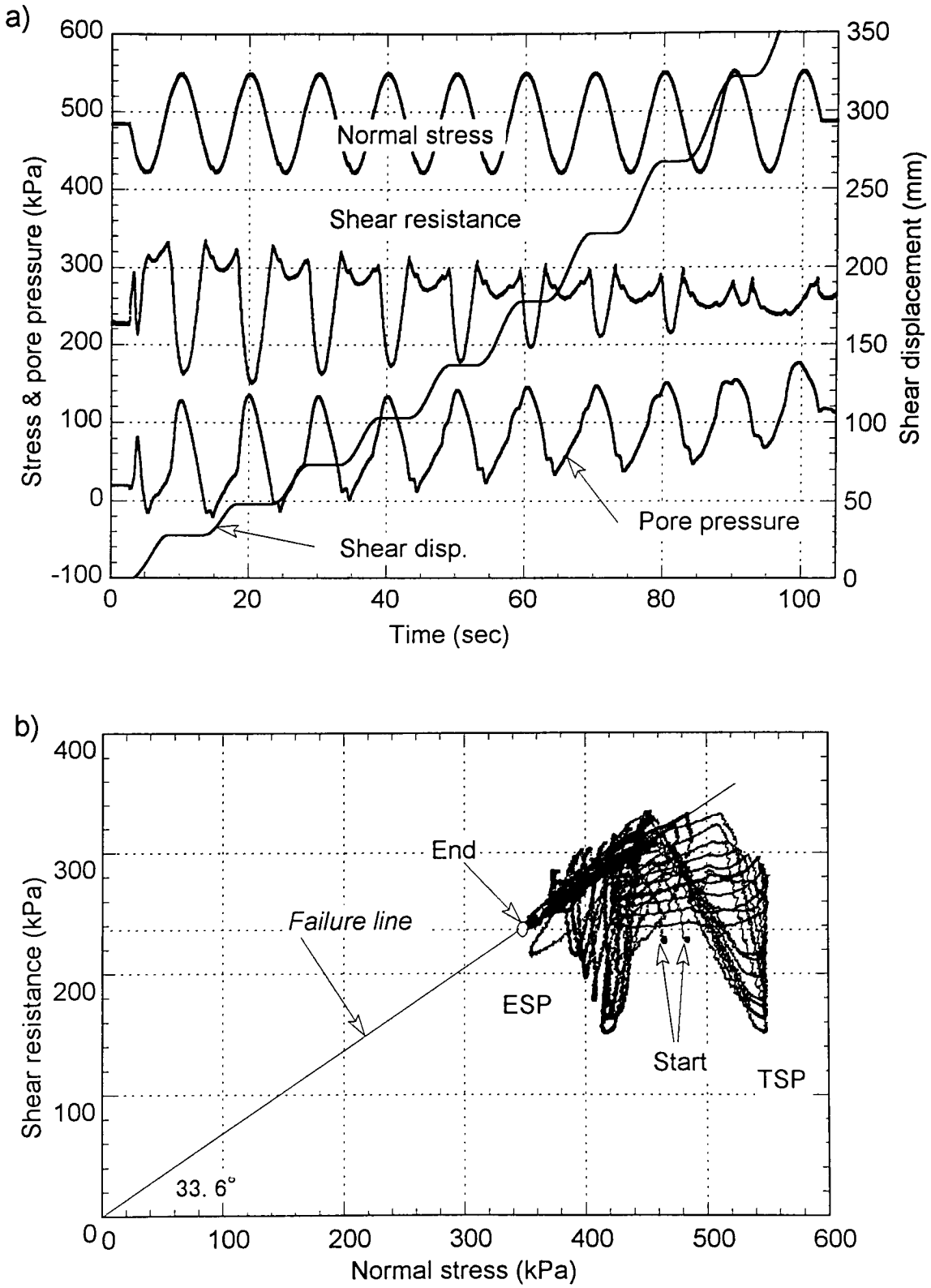

Fig. A-2 Time series data (a) and stress path (b) of T-F(0.1)-25°

TSP: Total stress path, ESP: Effective stress path.

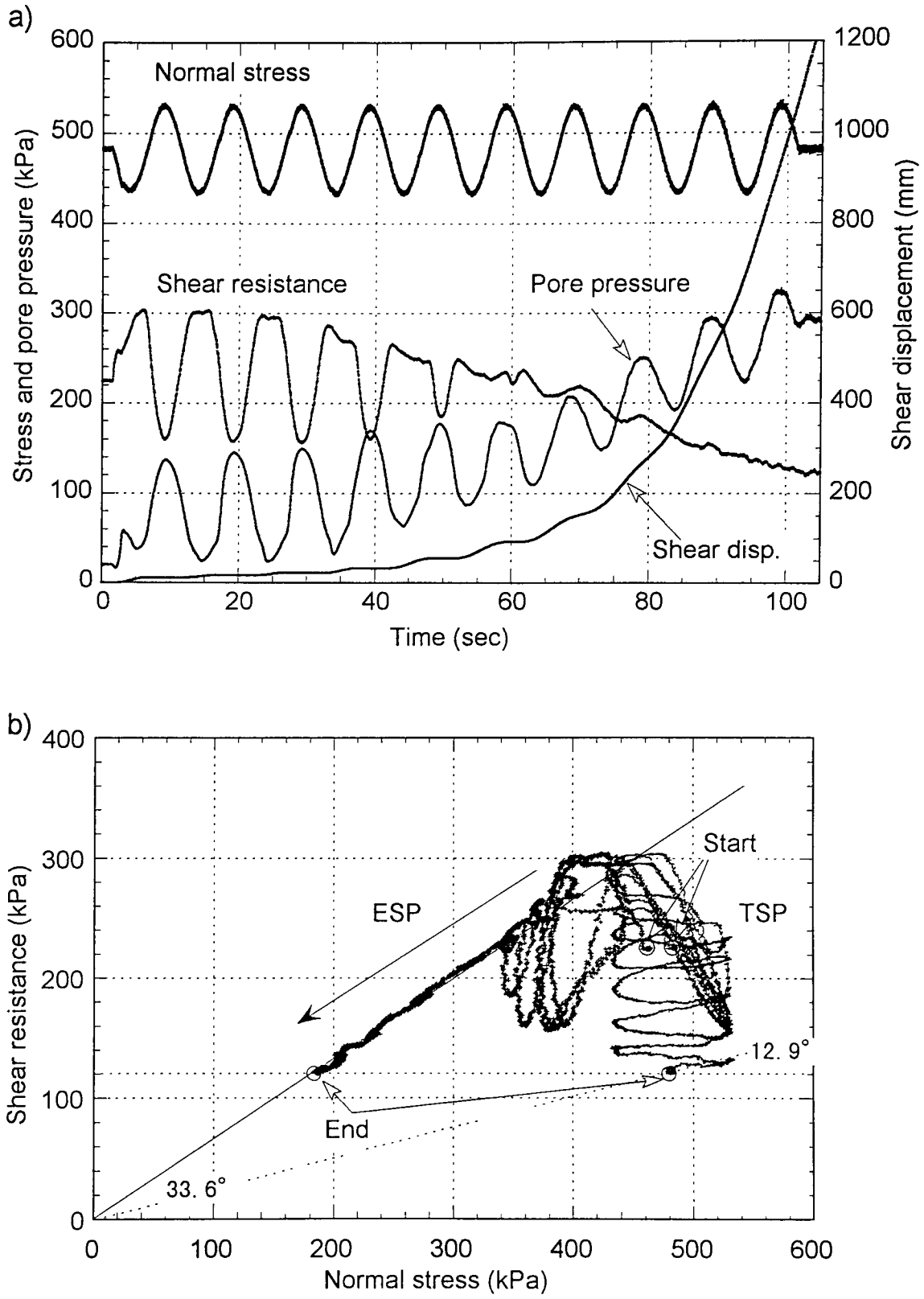

Fig. A-3 Time series data (a) and stress path (b) of S-F(0.1)-25°

TSP: Total stress path, ESP: Effective stress path.

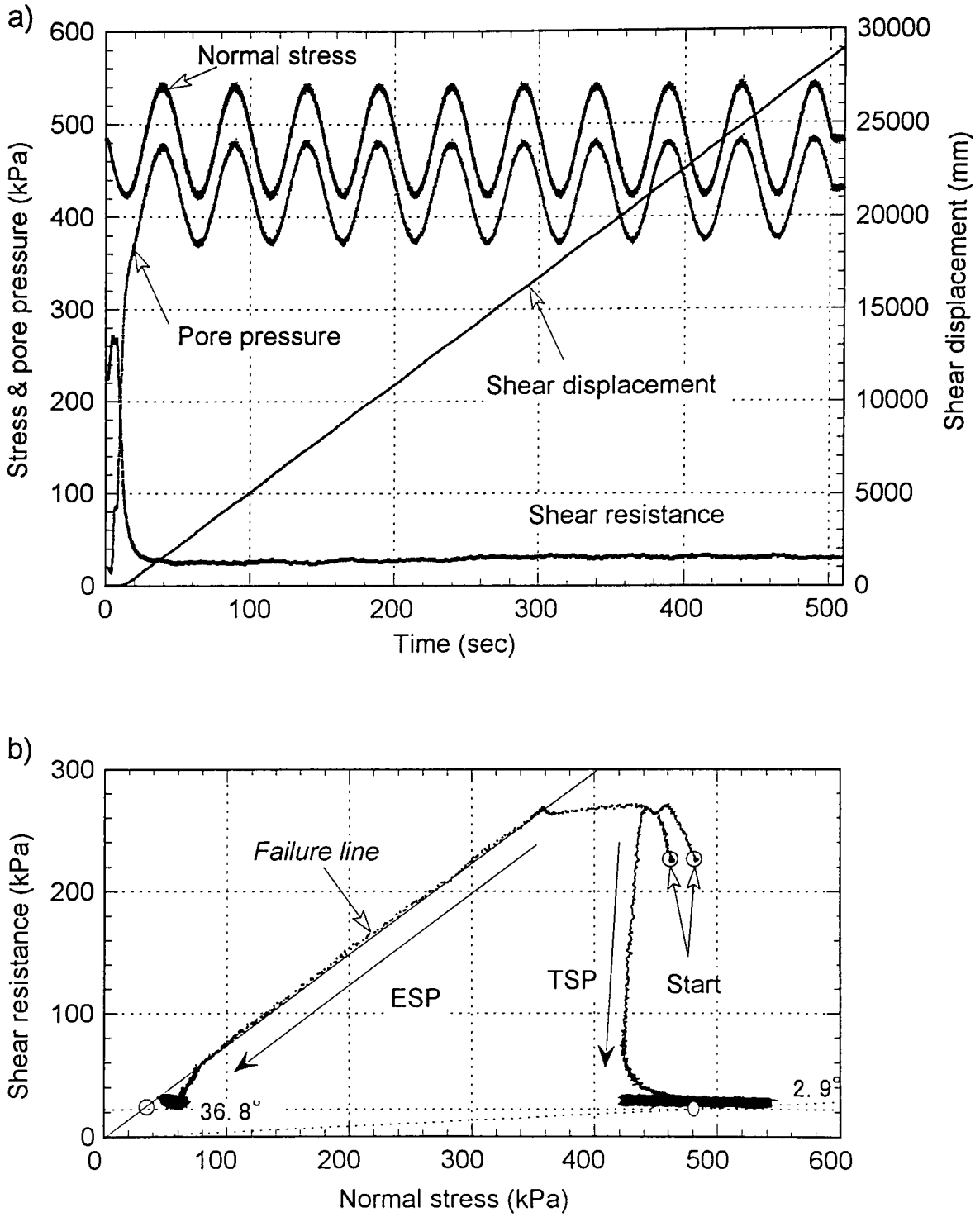

Fig. A-4 Time sereis data (a) and stress path (b) of 0-F(0.02)-25°

TSP: Total stress path, ESP: Effective stress path.

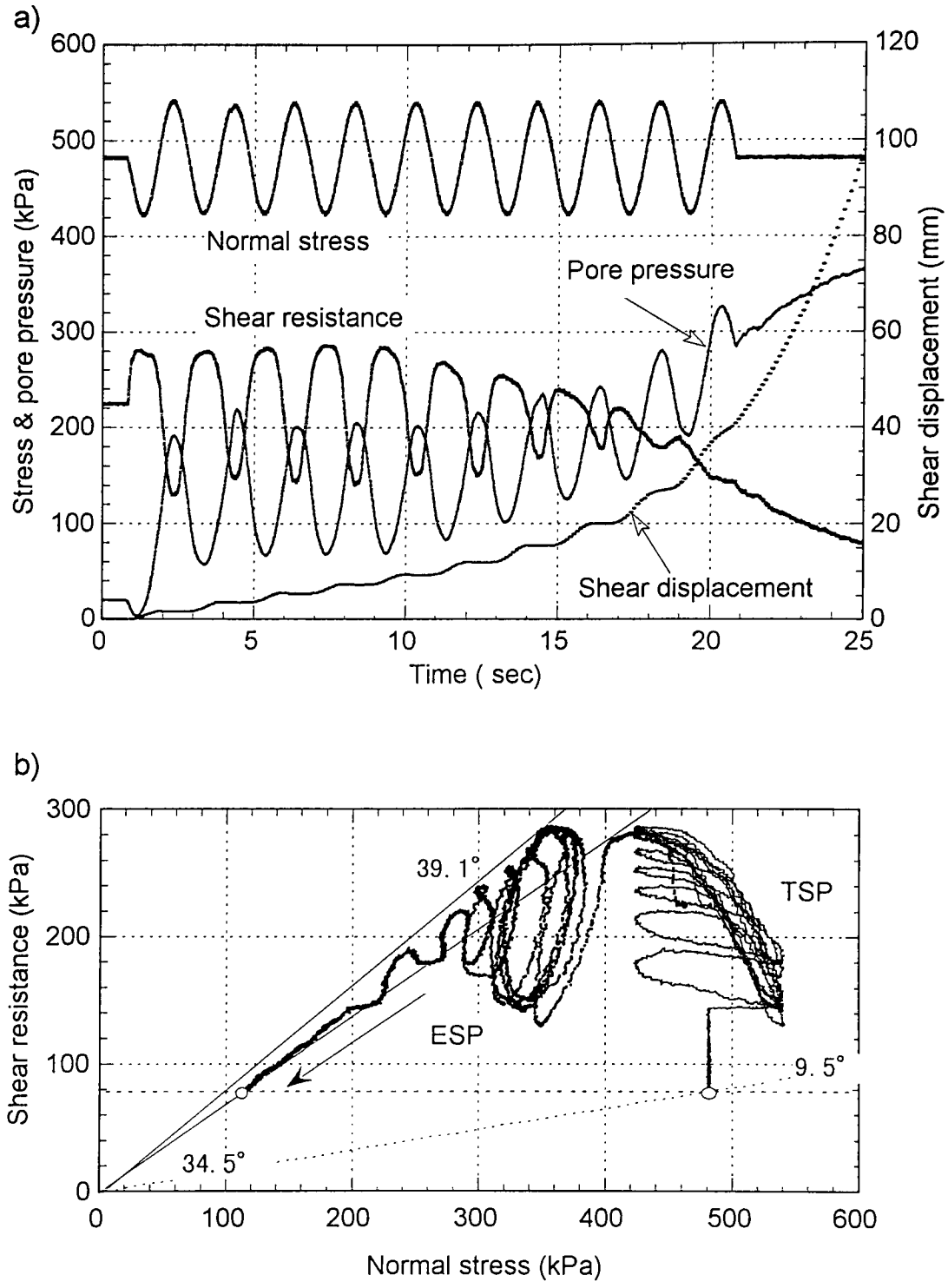

Fig. A-5 Time series data (a) and stress path (b) of 0-F(0.5)-25°

TSP: Total stress path, ESP: Effective stress path.

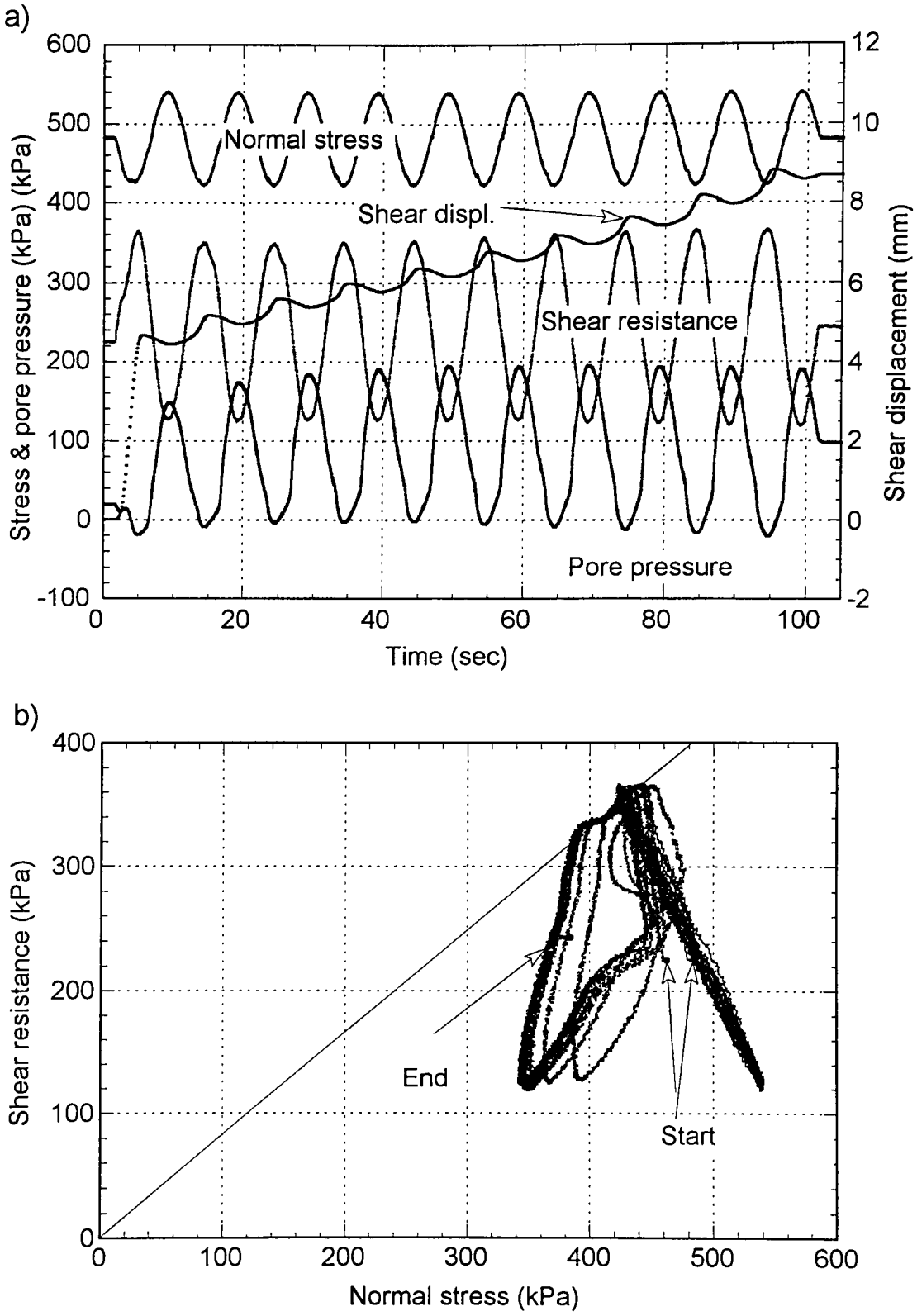

Fig. A-6 Time series data (a) and stress path (b) of 0(Dense) -F(0.1)-25° at K/Kc = 1.5.

TSP: Total stress path, ESP: Effective stress path.

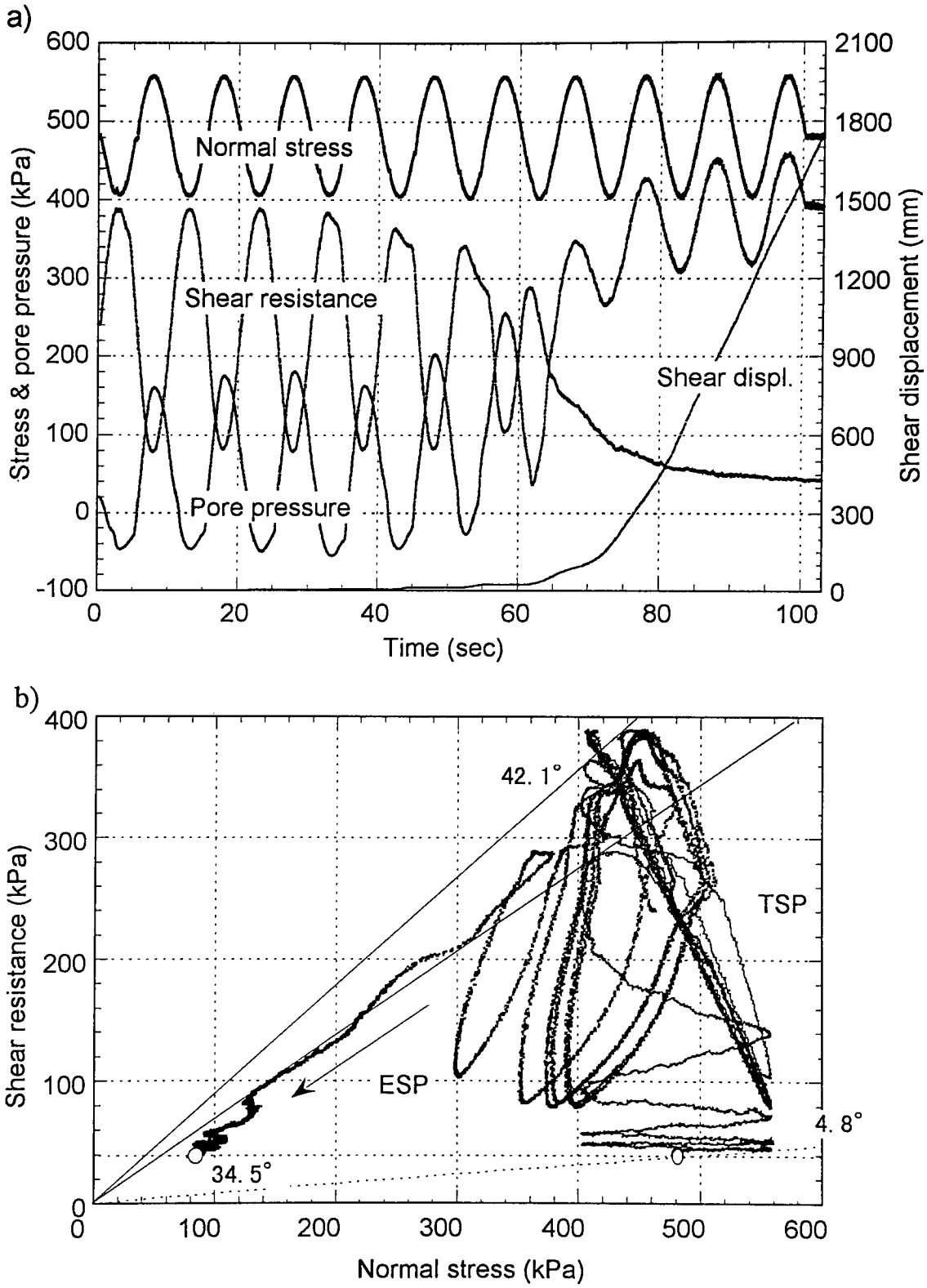

Fig. A-7 Time series data (a) and stress path (b) of 0(Dense) -F(0.1)-25° at K/Kc = 2.0.

TSP: Total stress path, ESP: Effective stress path.